

LASER INTERFEROMETER GRAVITATIONAL WAVE OBSERVATORY  
-LIGO-

CALIFORNIA INSTITUTE OF TECHNOLOGY  
MASSACHUSETTS INSTITUTE OF TECHNOLOGY

<b>Technical Note</b>	<b>LIGO-T-980666-00-D</b>	<b>January 27, 1999</b>
-----------------------	---------------------------	-------------------------

<p style="text-align: center;"><b>The BIG BOOK of LIGO Lock Acquisition Design</b></p>
--

<p style="text-align: center;">Brent Ware ware@ligo.caltech.edu</p>
---

This is an internal working note  
of the LIGO Project.

<b>California Institute of Technology</b>	<b>Massachusetts Institute of Technology</b>
<b>LIGO Project - MS 18-34</b>	<b>LIGO Project - MS 20B-145</b>
<b>Pasadena CA 91125</b>	<b>Cambridge, MA 01239</b>
Phone (626) 395-2966	Phone (617) 253-4824
Fax (626) 304-9834	Fax (617) 253-7014
e-mail: info@ligo.caltech.edu	e-mail: info@ligo.mit.edu
WWW: <a href="http://www.ligo.caltech.edu/">http://www.ligo.caltech.edu/</a>	

file /home/ware/docs/isc/ugla.ps and ugla\_2up.ps

## Abstract

A summary of what I think I know about LSC lock acquisition.

## 1 Lock Acquisition

Lock acquisition is the process by which the six pendulum-mounted masses which comprise a recycled Fabry-Perot interferometer are constrained from their initial condition of swinging about wildly due to ground motion ('wildly', here, means tens of microns), which give a signal only in the brief moments when their random juxtaposition fulfills the resonance conditions of the (varying) laser frequency, and using feedback to stop their motion within that ephemeral resonance condition.

The design criteria by which this is done are constrained by several considerations, not all of which are independent of the others. The feedback control system which is optimal for the low-noise gravitational detection mode operation of the interferometer is not suitable for lock acquisition, so a different set of controllers must be designed.

## 2 Design Considerations

There are several constraints of the interferometer which unavoidably affect the properties of the lock acquisition controller design. Among these are:

- Parameters – optics, stacks, pendula, etc. – which are optimized for gravity wave detection
- seismically-induced motion
- internal modes of optics
- physical limits on actuator/sensors

Within these constraints, the design of the acquisition mode must meet the requirements of

- Short mean time to lock
- Robustness against seismically-induced motion
- Stability

### 2.1 Acquisition time

The overriding concern of the lock acquisition system is to acquire lock within a reasonably short time. 'Reasonably short' is of course open to interpretation, but the Mean Time to Lock (MTTL) should be short enough that it does not hinder the operation of the interferometer, which I take to mean that MTTL is a small fraction of average time the IFO is locked. Paradoxically, this implies the importance of a short MTTL is most important in the initial days of LIGO when the IFO will almost certainly fall out of lock constantly and often. So lock acquisition must work reliably and robustly from the initial LIGO turn-on.

## 2.2 Acquisition states

Extensive simulation with the SMAC simulator (refs?) has shown that there is One True Path to lock acquisition [5]:

**State 1** Masses swinging wildly about, no resonant buildup.

**State 2** Sideband resonant within the recycled Michelson cavity.

**State 3** Sideband resonant within the recycled Michelson cavity and the carrier resonant within the in-line arm.

**State 4** Sideband resonant within the recycled Michelson cavity and the carrier resonant in both Fabry-Perot arms.

This sequence of events is shown in Fig. 1. This figure also shows two pseudo-lock resonant states, States 2sb and 3sb. Unless controllers are configured to acquire these states, there is no danger of the interferometer locking in either of these pseudo-states; their significance lies in the possibility of disrupting the acquisition sequence as the interferometer passes through these resonant conditions.

## 3 Design Software

SMAC uses linear transfer functions from sensors to actuators and non-linear controllers (e.g., polarity changes of signals) to time-simulate the LIGO lock acquisition. The linear controllers are Matlab .m files, containing poles and zeros, transformed in the proper manner. The non-linear controllers are Fortran (.f).

Because SMAC is a time-simulator, it is difficult to design a feedback control system using only SMAC using familiar frequency-domain techniques; its only avenue of doing frequency domain analysis is the slow and computationally expensive brute force method of imitating a network analyzer, running a sinusoid through the system for a number of cycles and comparing it to the response, over a sufficient range of frequencies and at a high enough resolution. In this mien, SMAC suffers the same deficiencies as a network analyzer; looking at low frequencies takes a corresponding longer time. Since many of the characteristics affecting the plant and controller have very low frequency components (below 1 Hz), this method, while useful for comparison, is not very efficient. In addition, the original creators of SMAC did not implement the ability to analyze the open-loop gain of the plant-controller system, only that of the plant.

In order to design the controllers, then, a Matlab pole-zero frequency model of the plant was developed which allowed rapid visual and analytical study of a particular controller design, which could then be implemented in SMAC and tested for lock acquisition.

When SMAC writes out the transfer function of the optical plant, it does not include the pendulum transfer function (Fig. 3 and Fig. 2). So the pole-zero model differs from SMAC in that SMAC applies forces directly to the masses (the controllers have a force/volt transfer function), while the model applies voltages (controllers are volt/volt).

Therefore none of the plant transfer functions in this document include the pendulum transfer function; it is put in by hand into the control transfer function so that the overall open loop gain turns out correctly. The pole-zero model controller transfer functions implicitly include the sensor and actuator transfer functions as they are not broken out separately; these must be deconvolved from the model and SMAC controllers in order to obtain the set of zeros, poles, and gains which will actually be implemented by the system as the acquisition mode controllers.

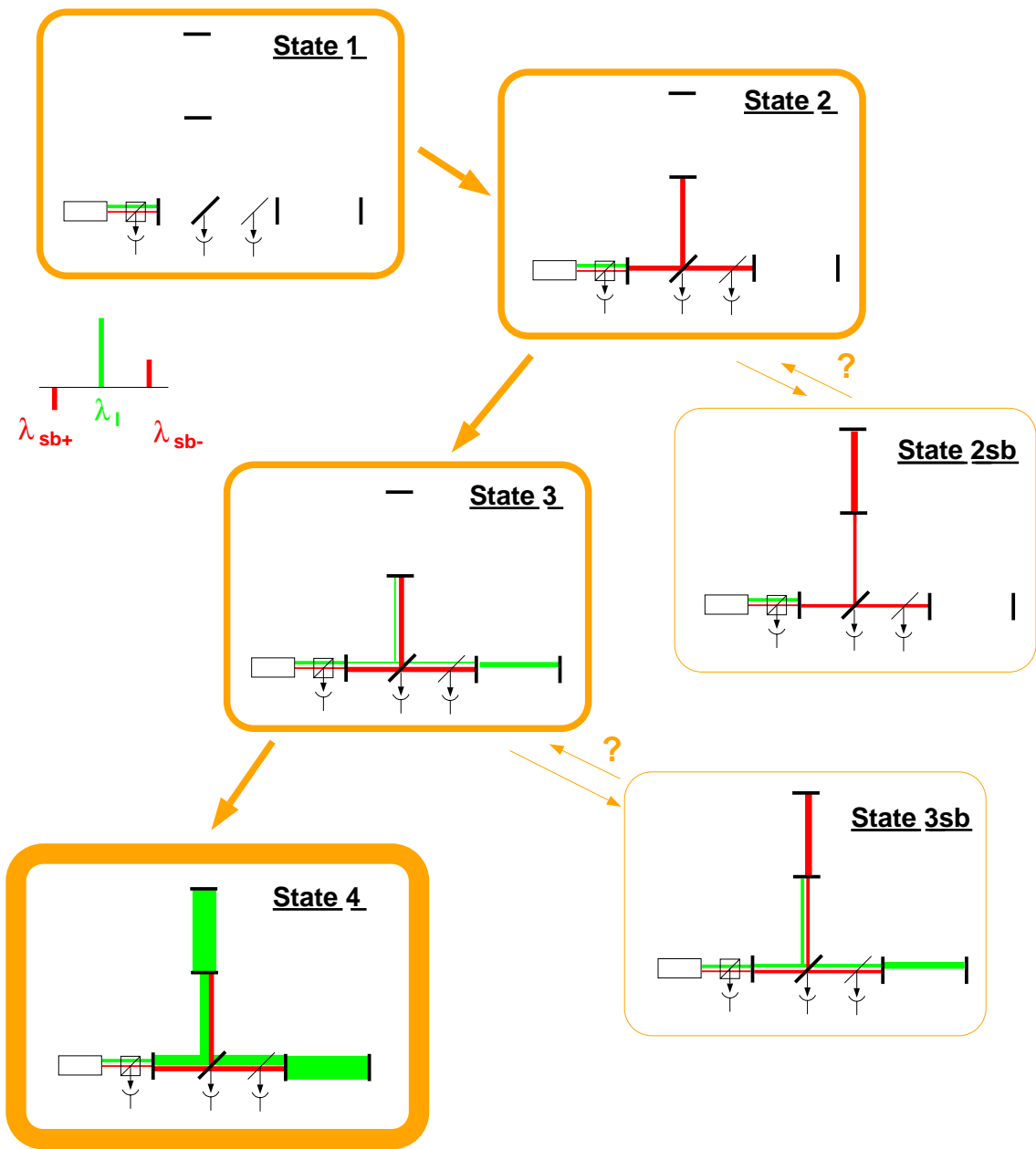


Figure 1: Acquisition locking sequence, definition of acquisition states.

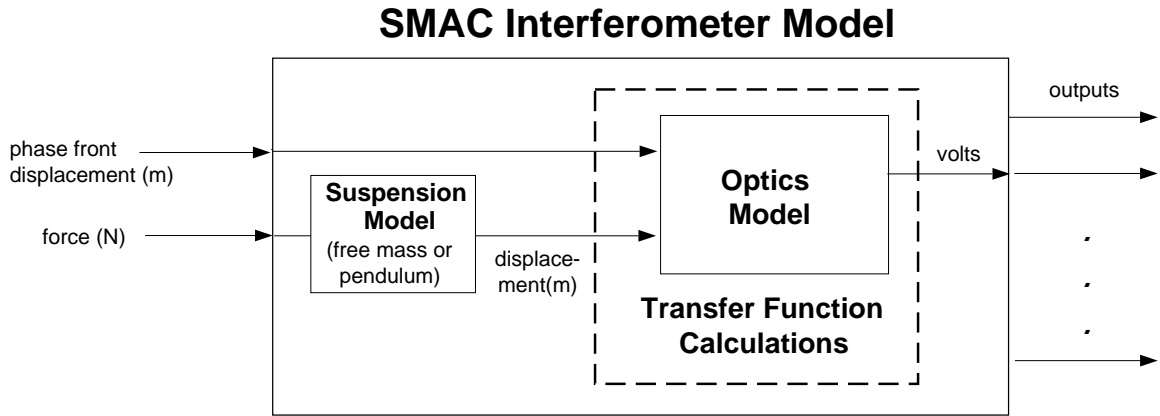


Figure 2: Block diagram of the SMAC IFO model (after SMAC Manual Figure 7, pg. 21). The Bode plots shown in this document modeled only the block inside the dotted line; therefore the pendulum transfer function is *not* part of the system transfer function, but *is* included in the open loop gain transfer functions.

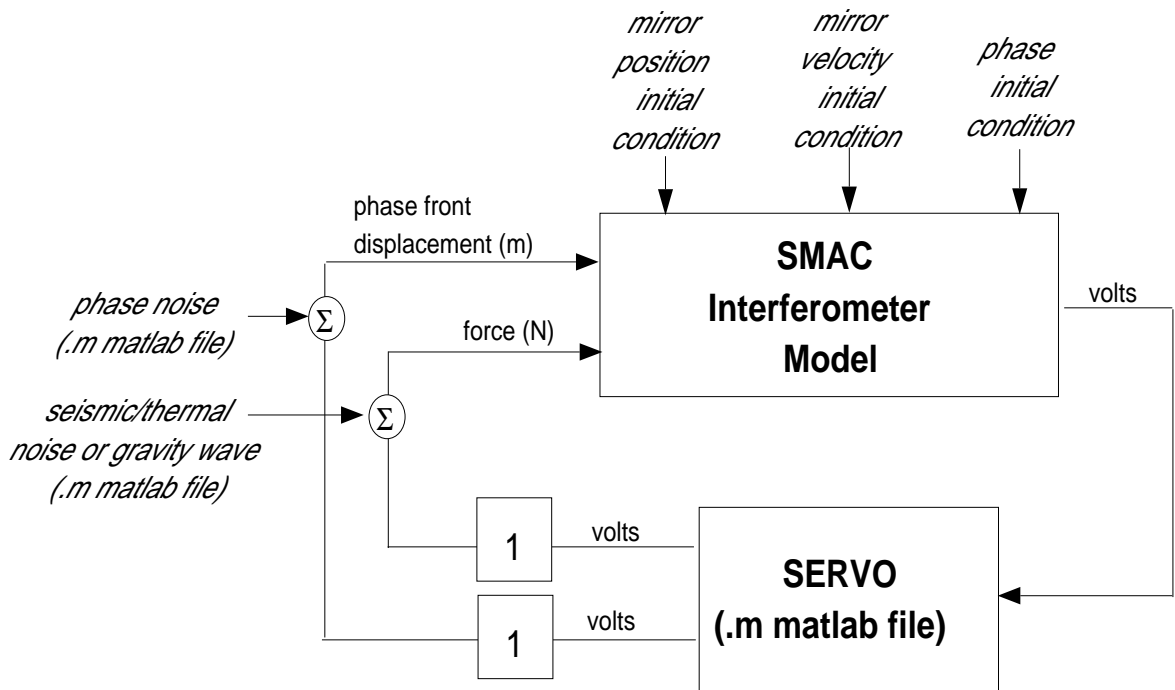


Figure 3: Block diagram of servo system including external inputs (after SMAC Manual Figure 3, pg. 15). This diagram shows that the sensor and actuator transfer functions are not explicitly included, and must be pulled out of the controller transfer functions.

## 4 Theory

Threshold velocity is defined as the velocity above which the feedback-controlled interferometer will not attain lock, and below which the controller will achieve lock in every instance. In a recycled Michelson Fabry-Perot interferometer, each degree of freedom can have a threshold velocity. This is a bit of slippery concept; if each time the cavity passes through a resonance, it receives a small restoring force, is there any limitation on the maximum threshold velocity, or is it simply a matter of waiting long enough. Should the definition be changed to “that velocity below which the controller will capture the resonance during the first passage through the fringe” ?

### 4.1 Measuring velocity

Cavity ringdown period [1] for a Fabry-Perot cavity:

$$\tau_{12} \simeq (\sqrt{2} - 1) \left[ \left( \frac{2L_0}{c} \right) \left( \frac{\lambda}{v} \right) \right]^{1/2} \begin{cases} L_0 = 4 \text{ km} \\ \lambda = 1.06 \text{ } \mu\text{m} \end{cases} \quad (1)$$

where  $\tau_{12}$  is the time between the first and second minima. Using LIGO parameters,

$$\tau_{12} \simeq \frac{2.2}{\sqrt{v}} \text{ ms} \quad (\text{velocity in } \mu\text{m/s}) \quad (2)$$

The actual relationship observed in SMAC simulations differs by 5% from the predicted value (Figs. 6, 7):

$$\tau_{12} \simeq \frac{2.1}{\sqrt{v}} \text{ ms} \quad (\text{velocity in } \mu\text{m/s}) \quad (3)$$

This was measured by looking at fringes on  $S_{AQ}$  (Fig. 4) and measuring not the zero-crossings (which are dependent on DC bias amongst other things as one can see from the figure below), but the relative minima, which should be equivalent. Then if  $\tau \propto 1/f$ ,  $f_{bw} \propto \sqrt{v_{thr}}$ . How does this depend on gain?

### 4.2 Acquisition time

Particles bouncing in a box, time spent with  $v < v_{thr}$  with  $x < x_{fr}$ . Maxwell-Boltzmann distribution?  $L_{box} = \lambda/2$ .  $x_{fr} = \lambda/2\mathcal{F}$ .

$$\tau_{lock} = x/v = \int_{-\lambda/4}^{\lambda/4} \int_{-v_{thr}}^{v_{thr}} \frac{x f(x)}{v f(v)} dv dx \quad ? \quad (4)$$

From Fig. 12, it appears that the velocity has a Rayleigh distribution

$$f(v) = Av e^{-(v-v_0)^2/2} \quad (5)$$

Ballpark: From measurements of ground motion at Livingston and Hanford [5], the worst case  $v_{rms} \sim 5 \lambda/s$ . If  $v_{thr} \simeq 1 \lambda/s$ , then  $P(v < v_{thr}) \approx 0.15$ , which implies a  $\tau_{lock}$  on the order of seconds. The relative ground motion of  $L_-$  is the driving consideration, as this motion is on the order of  $30 \mu\text{m}$  peak-to-peak. The motion of the  $l_{\pm}$  degrees of freedom is much less, on the order of nm, and so is much less of a concern. The requirement of  $v_{thr} \geq 1 \lambda/s$  is then the figure of merit here.

$$\tau_{lock} \sim \frac{\lambda/2}{v_{thr} P(v < v_{thr})} \quad (6)$$

From Figs. 9 and 10,  $v_{rms} \simeq 5 \lambda/s$ , and if  $v_{thr} \simeq 1 \lambda/s$ ,  $P(v < v_{thr}) \approx 0.15$ , which implies  $\tau_{lock}$  is on the order of a second.

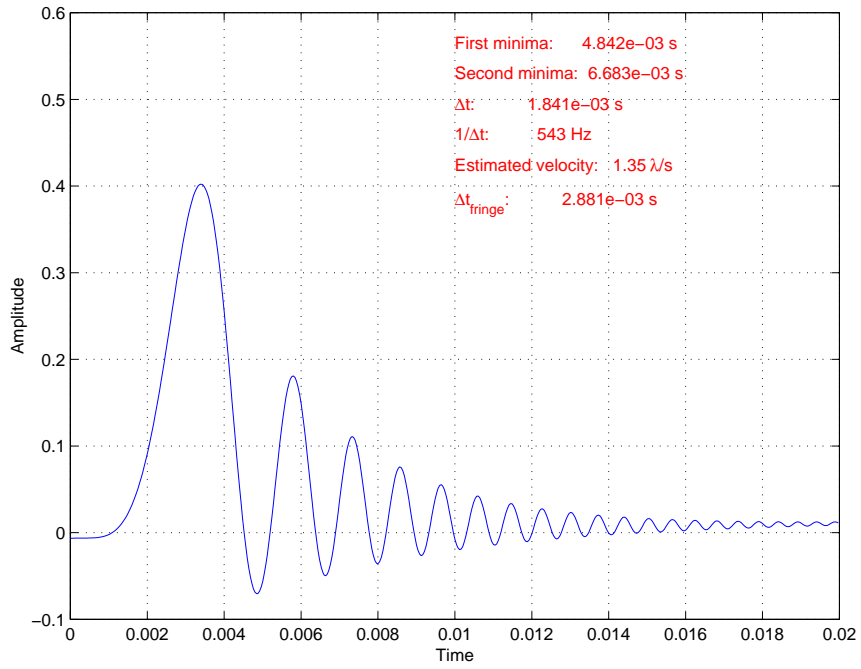


Figure 4: Representative fringe of recycled Michelson IFO, looking at  $S_{AQ}$ . ICs were  $\delta x_{M4} = -0.001 \lambda$ ,  $v_{M4} = 1.5 \lambda/s$ .

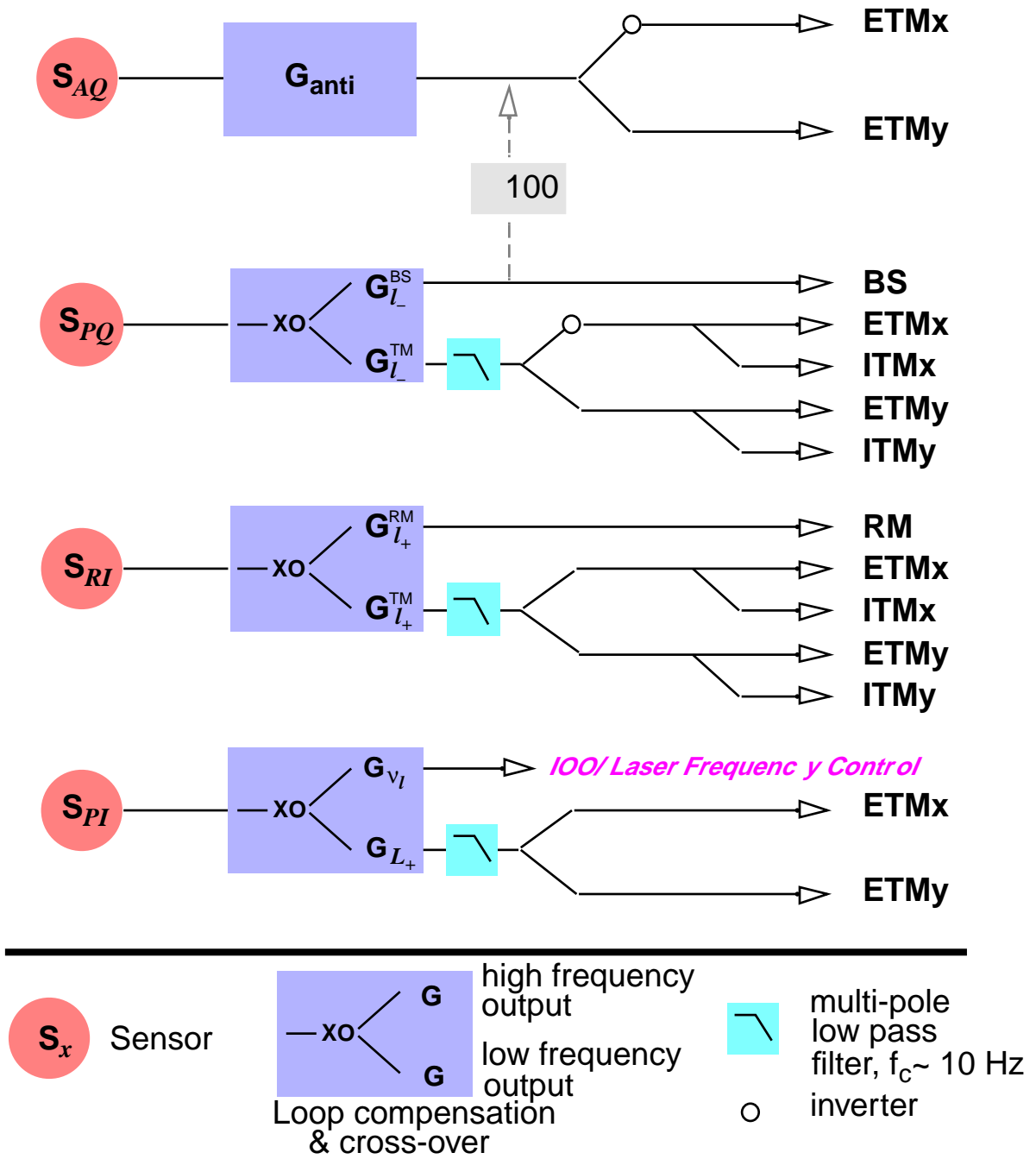


Figure 5: Sensor/actuator configuration –  $S_{PI}$  and  $S_{RI}$  are reversed from detection mode configuration because the amplitude of the fields on the pickoff is down by 30 dB in State 3, when  $l_+$  is needed but  $L_+$  is not.



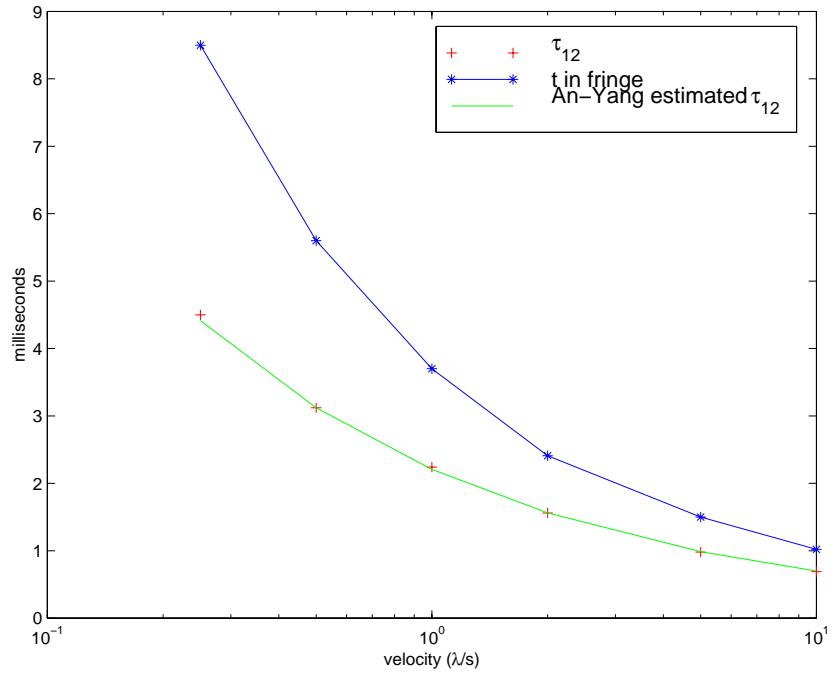


Figure 6: An-Yang calculated  $\tau$  and measured  $\tau$  of LIGO IFO.

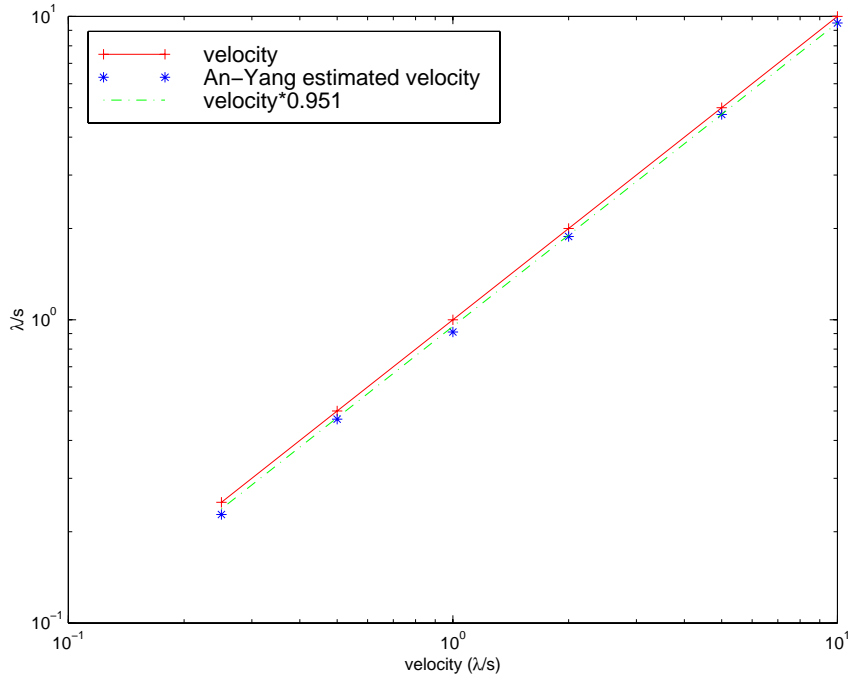


Figure 7: An-Yang calculated velocity and velocity fit of LIGO IFO.

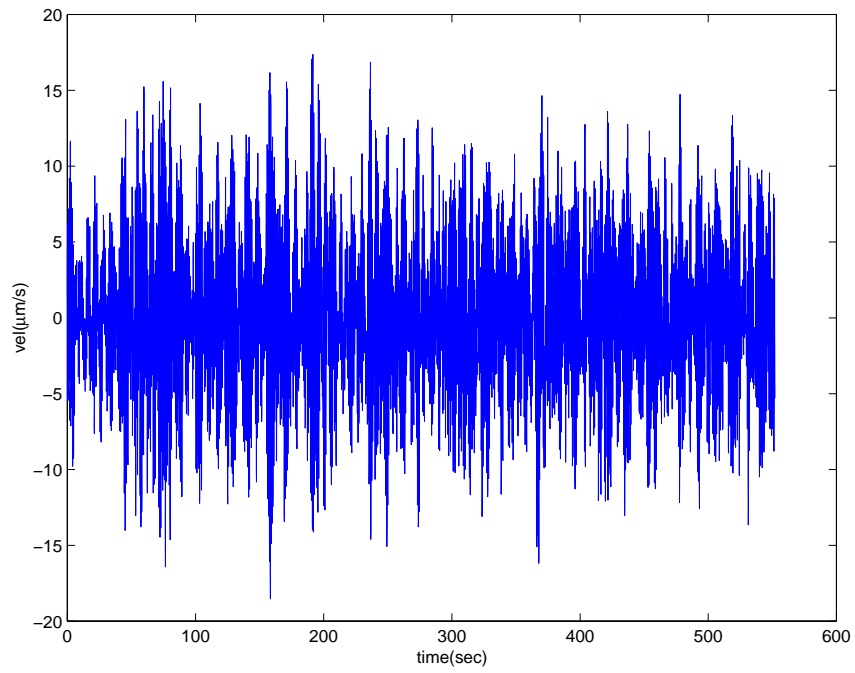


Figure 8: Typical ground motion,  $L_-$  mode, Louisiana [2].

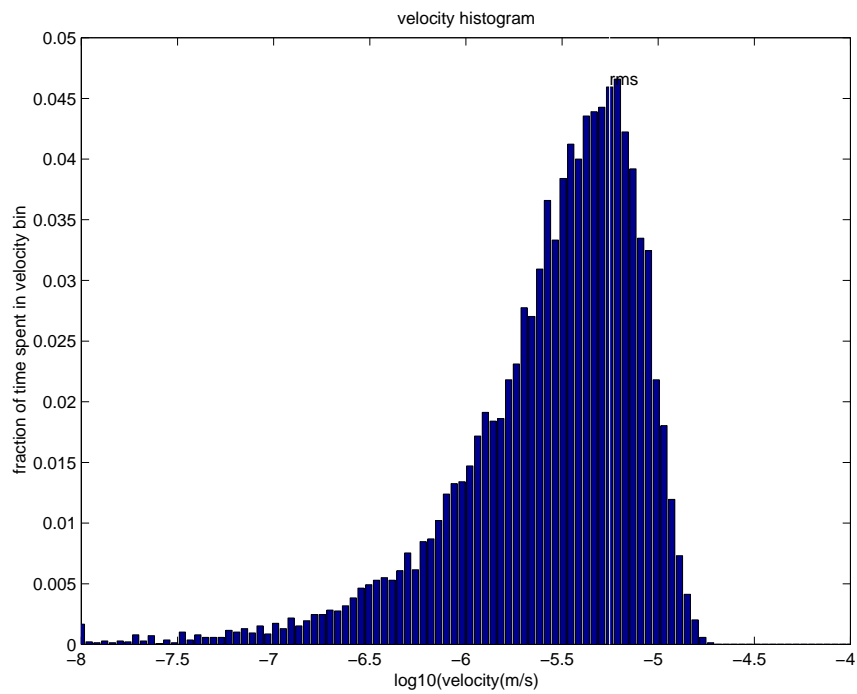


Figure 9: Velocity histogram – probability density [2].

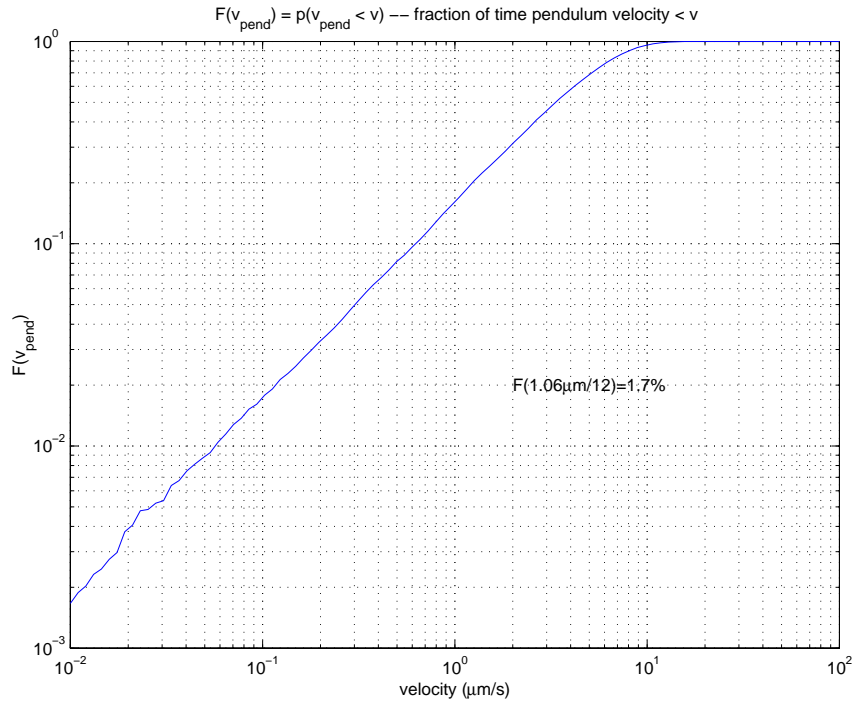


Figure 10: Velocity probability distribution function [2].

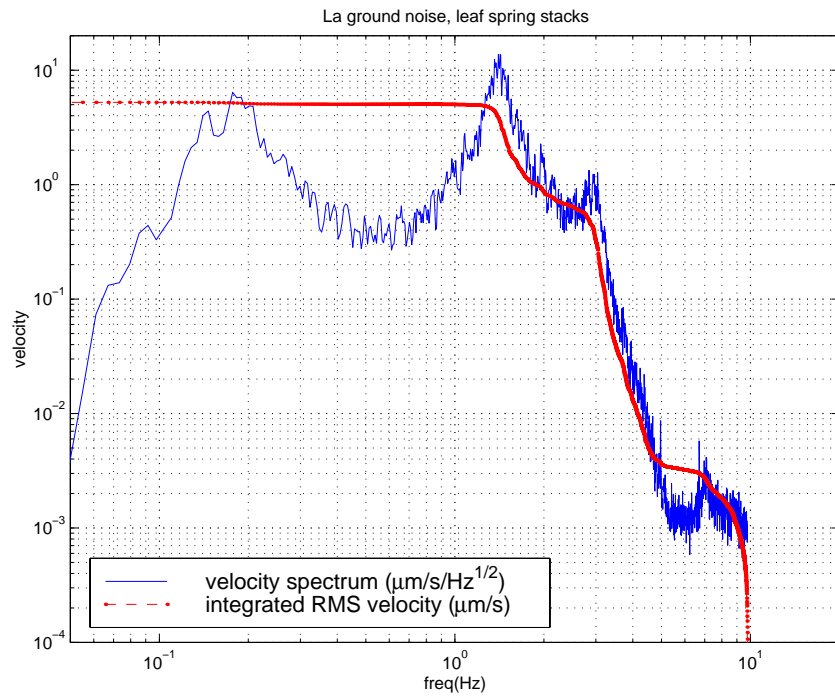


Figure 11: Velocity spectrum [2].

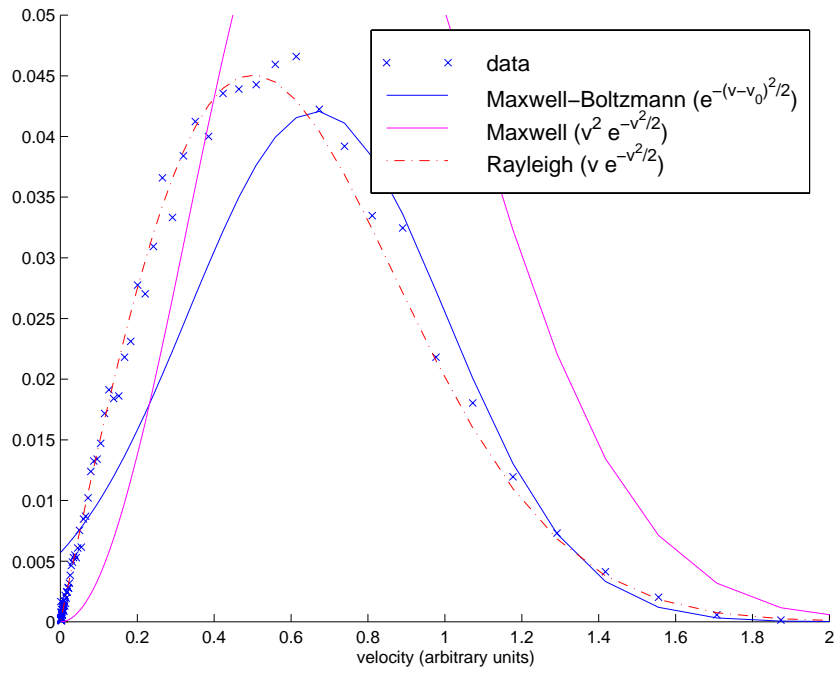


Figure 12: Fit to velocity probability density function.

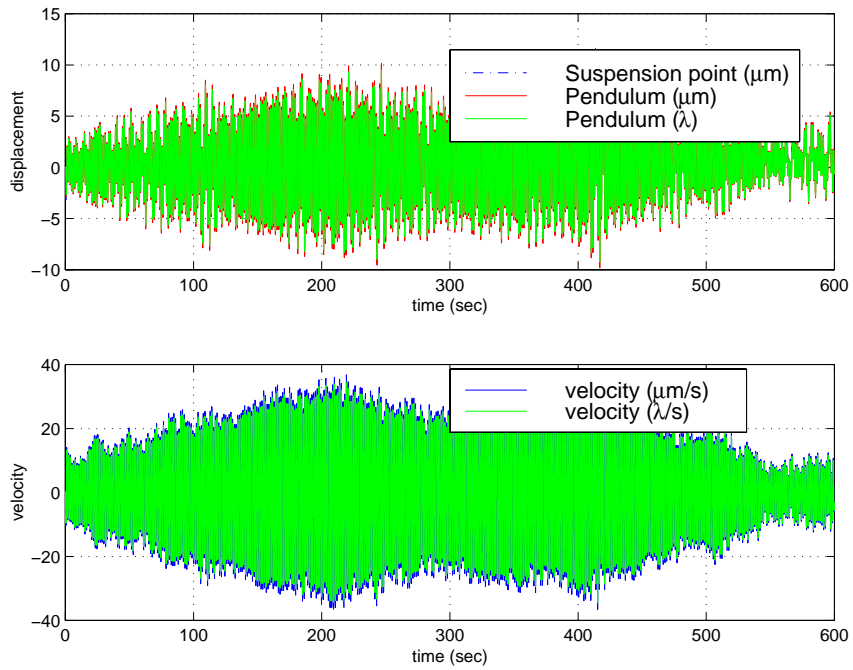


Figure 13: Time series of  $L_-$  displacement and velocity at the Livingston site.

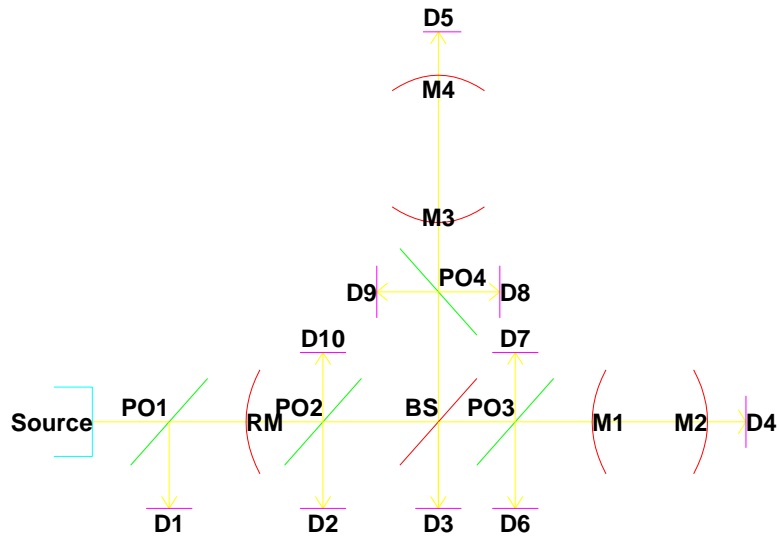


Figure 14: SMAC interferometer recycling configuration and notation.

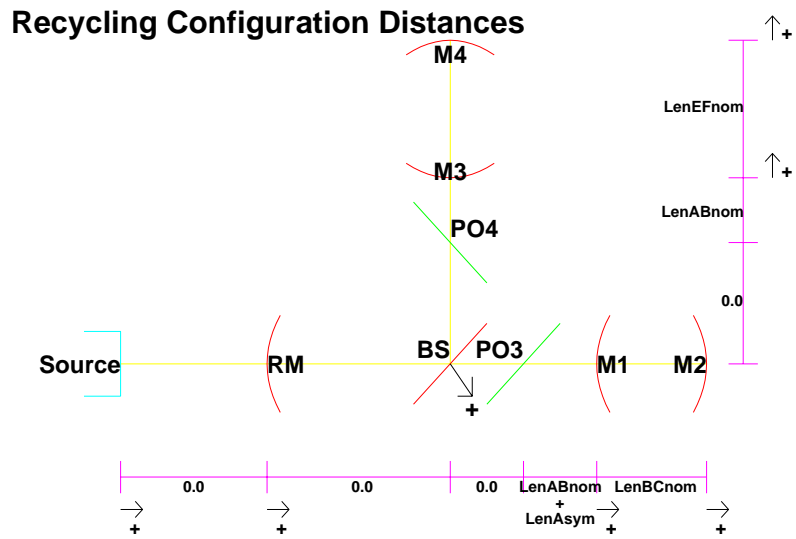


Figure 15: SMAC interferometer distance definitions.

## 5 Lengths

SMAC uses the DOFs:

$$\begin{array}{llll}
 \text{DM} = & (\delta M_4 - \delta M_2) & & L_- = (M_4 - M_3) - (M_2 - M_1) \\
 \text{CM} = & (\delta M_4 + \delta M_2) & \text{instead of} & L_+ = (M_4 - M_3) + (M_2 - M_1) \\
 \text{dm} = & -(\delta M_1 + \delta M_2) + (\delta M_3 + \delta M_4) & \text{the usual} & l_- = (M_3 - RM) - (M_1 - RM + BS) \\
 \text{cm} = & (\delta M_1 + \delta M_2) + (\delta M_3 + \delta M_4) & & l_+ = (M_1 - RM) + (M_3 - RM)
 \end{array}$$

where

$$\delta M_N = M_N + \delta x$$

and  $M_N$  defines the absolute position of the mirror. The usual length definitions are defined by Fig. 16 and Eq. 7. The SMAC definitions are defined by Fig. 15. While Fig. 5 shows  $l_{\pm}$  going to both the input and end test masses, the  $l_{\pm}$  connection to the input TMs is there only to control the common mode swinging of the arms. The SMAC definition can be reconciled with the usual definitions by realizing that to control the  $l_{\pm}$  modes, SMAC moves each F-P mirror pair  $M_{1,2}$  and  $M_{3,4}$  together by the same distance  $\delta x$ , thus maintaining the  $L_{\pm}$  distance.

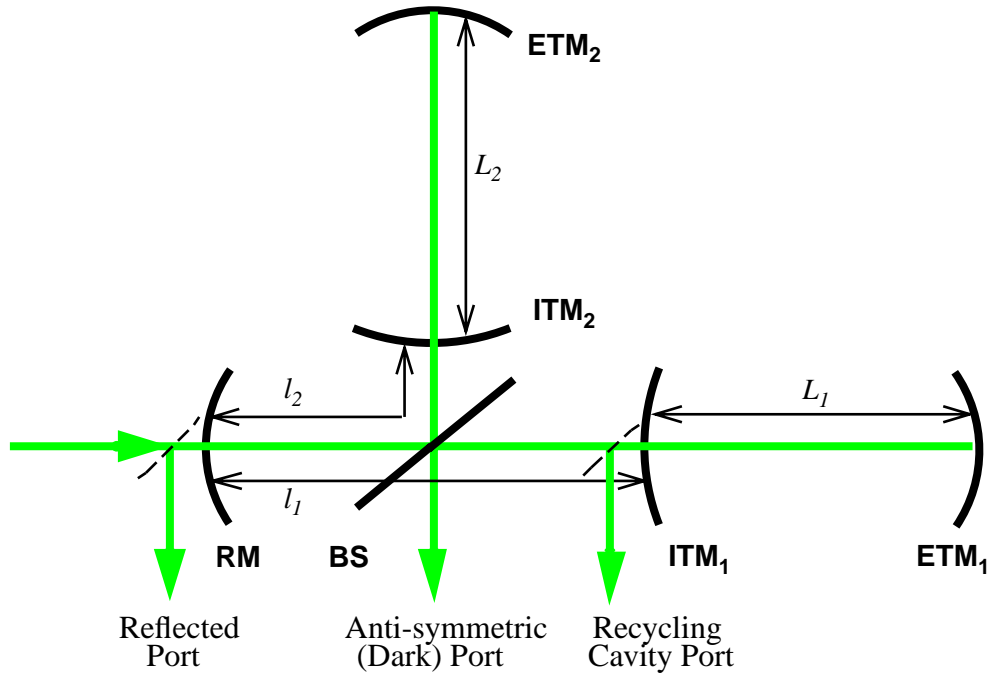


Figure 16: Definition of servo lengths in the system.

## 6 Equations

### 6.1 Basic definitions

Mnemonic	SMAC	Description
R	D1	<b>R</b> elected
A	D3	<b>A</b> ntisymmetric/dark port
P	D6	recycling <b>P</b> ickoff
I	cosine	<b>I</b> n-phase
Q	sine	<b>Q</b> uad-phase

Table 1: Mnemonic designations.

$$\begin{aligned}
 L_+ &= \frac{L_\perp + L_\parallel}{2} & l_+ &= \frac{l_\perp + l_\parallel}{2} \\
 L_- &= \frac{L_\perp - L_\parallel}{2} & l_- &= \frac{l_\perp - l_\parallel}{2}
 \end{aligned} \tag{7}$$

$$\begin{aligned}
 \delta\Phi_\parallel &= \frac{1}{2}(\Phi_+ + \Phi_-) & \delta\phi_\parallel &= \frac{1}{2}(\phi_+ + \phi_-) \\
 \delta\Phi_\perp &= \frac{1}{2}(\Phi_+ - \Phi_-) & \delta\phi_\perp &= \frac{1}{2}(\phi_+ - \phi_-)
 \end{aligned} \tag{8}$$

For a resonant cavity, (from [4] via [3]):

$$r_c = \frac{r_i - r_e}{1 - r_i r_e} \quad r_m = \cos \frac{2\omega_m l_{asym}}{c} \quad \text{carrier and sideband (modulated) reflectivity of F-P cavity} \tag{9}$$

$$r'_c = \frac{(1 - r_i^2)r_e}{(1 - r_i r_e)^2} \quad r'_m = \frac{(1 - r_i^2)r_e}{(1 + r_i r_e)^2} \quad \text{change in reflectivity with change in cavity length} \tag{10}$$

$$g_{cr} = \frac{t_r}{1 + r_r r_c} \quad g_{sb} = \frac{t_r}{1 - r_r r_m} \quad \text{root of recycling gain} \tag{11}$$

$$r_{cr} = \frac{r_r + r_c}{1 + r_r r_c} \quad r_{sb} = \frac{r_r - r_m}{1 - r_r r_m} \quad \text{amplitude of reflected fields} \tag{12}$$

$$t_{cr} = 0 \quad t_{sb} = \frac{t_r \sqrt{1 - r_m^2}}{1 - r_r r_m} \quad \text{amplitude of fields transmitted to asymmetric port} \tag{13}$$

## 6.2 Field equations [3]

In a Fabry-Perot cavity, the reflected electric field is related to the incident field by a combination of the directly reflected field and the phase-shifted field leaking out of the cavity:

$$\frac{E_{\text{refl}}}{E_{\text{inc}}} = r_i + \frac{t_i^2 r_e e^{-i\phi}}{1 + r_i r_e e^{-i\phi}} \equiv r_c(\phi) \quad (14)$$

where  $\phi = 2kl$ . Resonance occurs when  $e^{-i\phi} = -1 \implies \phi = (2n+1)\pi \implies l = (2n+1)\lambda/2$  (see Fig 17):

$$r_c(\pi) \equiv r_c^\pi = r_i - \frac{t_i^2 r_e}{1 - r_i r_e} \quad (15)$$

(which is equal to Eq. 9, assuming the losses of the input mirror are negligible). Anti-resonance occurs when  $e^{-i\phi} = 1 \implies \phi = 2n\pi \implies l = n\lambda/2$ :

$$r_c(0) \equiv r_c^0 = r_i + \frac{t_i^2 r_e}{1 + r_i r_e} \quad (16)$$

For the IFO values shown in Table 2, these are  $-0.98984$  and  $0.99996$ , respectively, and their combination  $[r_c^0 + r_c^\pi]/2 = 5.06 \times 10^{-3} \simeq 1/198$ .

The fields inside an F-P cavity relative to the incident field are

$$\frac{E_{\rightarrow}}{E_{\text{inc}}} = \frac{t_i}{1 + r_i r_e e^{-i\phi}} \quad \frac{E_{\leftarrow}}{E_{\text{inc}}} = \frac{t_i r_e e^{-i\phi}}{1 + r_i r_e e^{-i\phi}} \quad (17)$$

Writing Eq. 14 in terms of its real and imaginary parts,

$$r_c(\phi) = r_i + \frac{r_i r_e^2 t_i^2 + t_i^2 r_e e^{-i\phi}}{1 + r_i^2 r_e^2 + 2r_i r_e \cos \phi} \quad (18)$$

For small deviations away from resonance (ignoring losses)

$$r_c^{\pi'}(\delta\phi) = r_c^\pi + i r_e' \delta\phi \quad (19)$$

## 6.3 Carrier

From the basic equations of a F-P cavity, the fields of a recycled Michelson coupled F-P IFO can be found.

Assuming that  $t_{bs} = r_{bs} = 1/\sqrt{2}$ , the fields reflected from the F-P cavities at the recycling cavity pick-offs PO3 and PO4 are (see Fig. 14 for reference points – the pick-offs, in actuality, are reflections from the anti-reflection coatings on the back of the input test masses, so their transmission can be taken to be unity)

$$\frac{E_{\parallel\leftarrow}}{E_{2\rightarrow}} = \frac{1}{\sqrt{2}} r_c(\Phi_{\parallel}) e^{-i\phi_{\parallel}} \quad \frac{E_{\perp\leftarrow}}{E_{2\rightarrow}} = \frac{1}{\sqrt{2}} r_c(\Phi_{\perp}) e^{-i\phi_{\perp}} \quad (20)$$

for each arm (where  $\Phi_{\parallel(\perp)} \Rightarrow L_{1(2)}, \phi_{\parallel(\perp)} \Rightarrow l_{1(2)}$  in Fig. 16). The field at the anti-symmetric port D3 is

$$t_{cr}(\Phi, \phi) \equiv \frac{E_A}{E_{2\rightarrow}} = \frac{1}{2} \left[ r_c(\Phi_{\perp}) e^{-i\phi_{\perp}} - r_c(\Phi_{\parallel}) e^{-i\phi_{\parallel}} \right] \quad (21)$$



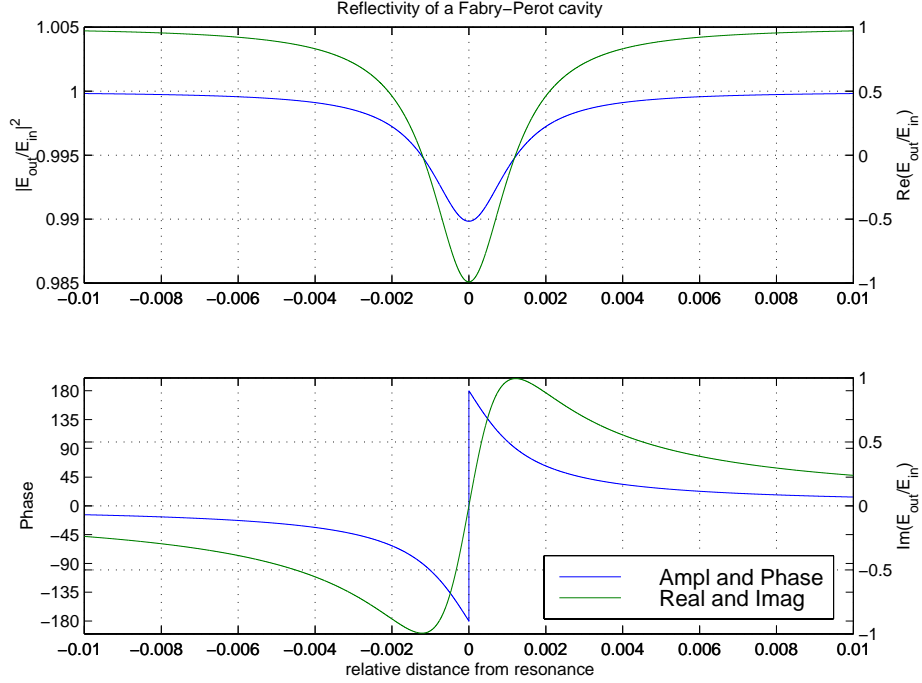


Figure 17: Reflectivity of a Fabry-Perot cavity.

At the pick-off position PO2, upstream of the beamsplitter, the field travelling towards the symmetric port is

$$r_T(\Phi, \phi) \equiv \frac{E_{2\leftarrow}}{E_{2\rightarrow}} = \frac{1}{2} \left[ r_c(\Phi_{\perp}) e^{-i\phi_{\perp}} + r_c(\Phi_{\parallel}) e^{-i\phi_{\parallel}} \right] \quad (22)$$

This can be viewed as the reflection of the beamsplitter and two F-P arms taken as a one-port reflecting cavity (Thevenin equivalent), so using the right-travelling part of Eq. 17 and plugging the above in for  $r_e e^{-i\phi}$ ,

$$g_{cr}(\Phi, \phi) \equiv \frac{E_{2\rightarrow}}{E_{inc}} = \frac{t_r}{1 + \frac{1}{2} r_r \left[ r_c(\Phi_{\perp}) e^{-i\phi_{\perp}} + r_c(\Phi_{\parallel}) e^{-i\phi_{\parallel}} \right]} \quad (23)$$

The field which is actually used to obtain  $S_P$  is the reflection off the anti-reflection coating on the upstream side of the input test mass<sup>1</sup>, so the field at that point is

$$r_P(\Phi, \phi) \equiv \frac{1}{\sqrt{2}} \frac{E_{2\rightarrow}}{E_{inc}} = \frac{1}{\sqrt{2}} \frac{t_r}{1 + \frac{1}{2} r_r \left[ r_c(\Phi_{\perp}) e^{-i\phi_{\perp}} + r_c(\Phi_{\parallel}) e^{-i\phi_{\parallel}} \right]} \quad (24)$$

The field reflected from the recycling mirror, the symmetric port, can be found from the F-P equation and the Thevenin equivalent

$$r_{cr}(\Phi, \phi) = r_r + \frac{t_r^2 r_T}{1 + r_r r_T} \simeq \frac{r_r + r_T}{1 + r_r r_T} \quad (25)$$

<sup>1</sup>The actual signal is of course attenuated by  $r_{AR}$ , the reflection fraction of the anti-reflective coating, just as the actual signals which would be gotten from the pick-offs would be attenuated by the reflection fraction there; these will be understood in the following equations.

The field at the down stream pick-off PO3,  $E_{||\leftarrow}$ , is the field returning from the input mirror

$$r_3 \equiv \frac{E_{||\leftarrow}}{E_{inc}} = \frac{E_{2\rightarrow} E_{||\leftarrow}}{E_{inc} E_{2\rightarrow}} = \frac{1}{\sqrt{2}} \frac{t_r r_c(\Phi_{||}) e^{-i\phi_{||}}}{1 + \frac{1}{2} r_r \left[ r_c(\Phi_{\perp}) e^{-i\phi_{\perp}} + r_c(\Phi_{||}) e^{-i\phi_{||}} \right]} \quad (26)$$

The field at PO2 is then taken from the left-travelling field of Eq. 17 and using Eq. 22 to replace  $r_e e^{-i\phi}$

$$r_2 \equiv \frac{E_{2\leftarrow}}{E_{inc}} = \frac{1}{2} \frac{t_r \left[ r_c(\Phi_{\perp}) e^{-i\phi_{\perp}} + r_c(\Phi_{||}) e^{-i\phi_{||}} \right]}{1 + \frac{1}{2} r_r \left[ r_c(\Phi_{\perp}) e^{-i\phi_{\perp}} + r_c(\Phi_{||}) e^{-i\phi_{||}} \right]} \quad (27)$$

## 6.4 Fields in each state

It is useful to restate Eqs. 21 and 22 in terms of small deviations from resonance in each state and the differential and common-mode degrees of freedom:

$$\begin{aligned} & \frac{1}{2} \left[ r_c^{\pi'}(\delta\Phi_{\perp}) e^{-i(\phi_+ - \phi_-)/2} \pm r_c^{\pi'}(\delta\Phi_{||}) e^{-i(\phi_+ + \phi_-)/2} \right] \\ &= \frac{1}{2} e^{-i\phi_+/2} \left[ \left( r_c^{\pi} + \frac{i}{2} r_c'(\Phi_+ - \Phi_-) \right) e^{i\phi_-/2} \pm \left( r_c^{\pi} + \frac{i}{2} r_c'(\Phi_+ + \Phi_-) \right) e^{-i\phi_-/2} \right] \\ &= \frac{1}{2} e^{-i\phi_+/2} \left[ r_c^{\pi} \left( e^{i\phi_-/2} \pm e^{-i\phi_-/2} \right) + \frac{i}{2} r_c' \Phi_+ \left( e^{i\phi_-/2} \pm e^{-i\phi_-/2} \right) - \frac{i}{2} r_c' \Phi_- \left( e^{i\phi_-/2} \mp e^{-i\phi_-/2} \right) \right] \end{aligned}$$

$$\begin{aligned}
r_T^4(\delta\Phi, \delta\phi) &= \frac{1}{2} e^{-i\phi_+/2} \left[ 2r_c^\pi \cos \frac{\phi_-}{2} + i\Phi_+ r_c' \cos \frac{\phi_-}{2} - \Phi_- r_c' \sin \frac{\phi_-}{2} \right] \\
&\simeq \frac{1}{2} e^{-i\phi_+/2} \left[ 2r_c^\pi + ir_c' \Phi_+ - \frac{r_c'}{2} \Phi_- \phi_- \right]
\end{aligned} \tag{28}$$

$$\begin{aligned}
t_{cr}^4(\delta\Phi, \delta\phi) &= \frac{1}{2} e^{-i\phi_+/2} \left[ 2r_c^\pi \cos \frac{\phi_-}{2} + i\Phi_+ r_c' \sin \frac{\phi_-}{2} - \Phi_- r_c' \sin \frac{\phi_-}{2} \right] \\
&\simeq \frac{i}{2} e^{-i\phi_+/2} \left[ r_c^\pi \phi_- - \frac{r_c'}{2} \Phi_+ \phi_- - r_c' \Phi_- \right]
\end{aligned} \tag{29}$$

$$\begin{aligned}
r_T^3(\delta\Phi, \delta\phi) &= \frac{1}{2} \left[ r_c^0 e^{-i(\phi_+ - \phi_-)/2} + r_c^{\pi'}(\delta\Phi_{\parallel}) e^{-i(\phi_+ + \phi_-)/2} \right] \\
&= \frac{1}{2} e^{-i\phi_+/2} \left[ r_c^0 e^{i\phi_-/2} + (r_c^\pi + ir_c' \delta\Phi_{\parallel}) e^{-i\phi_-/2} \right]
\end{aligned} \tag{30}$$

$$\begin{aligned}
t_{cr}^3(\delta\Phi, \delta\phi) &= \frac{1}{2} \left[ r_c^0 e^{-i(\phi_+ - \phi_-)/2} - r_c^{\pi'}(\delta\Phi_{\parallel}) e^{-i(\phi_+ + \phi_-)/2} \right] \\
&= \frac{1}{2} e^{-i\phi_+/2} \left[ r_c^0 e^{i\phi_-/2} - (r_c^\pi + ir_c' \delta\Phi_{\parallel}) e^{-i\phi_-/2} \right]
\end{aligned} \tag{31}$$

$$\begin{aligned}
r_T^2(\delta\phi) &= \frac{1}{2} \left[ r_c^0 e^{-i(\phi_+ - \phi_-)/2} + r_c^0 e^{-i(\phi_+ + \phi_-)/2} \right] \\
&= r_c^0 e^{-i\phi_+/2} \cos \frac{\phi_-}{2} \\
&\simeq r_c^0 e^{-i\phi_+/2}
\end{aligned} \tag{32}$$

$$\begin{aligned}
t_{cr}^2(\delta\phi) &= \frac{1}{2} \left[ r_c^0 e^{-i(\phi_+ - \phi_-)/2} - r_c^0 e^{-i(\phi_+ + \phi_-)/2} \right] \\
&= ir_c^0 e^{-i\phi_+/2} \sin \frac{\phi_-}{2} \\
&\simeq \frac{ir_c^0}{2} e^{-i\phi_+/2} \phi_-
\end{aligned} \tag{33}$$

The recycling gain in each state (Eq. 23) proves to be a useful quantity in the following derivation:

$$g_{cr} \Big|_4 = \frac{t_r}{1 + r_r r_c^\pi} \quad g_{cr} \Big|_3 = \frac{t_r}{1 + \frac{1}{2} r_r [r_c^0 + r_c^\pi]} \quad g_{cr} \Big|_2 = \frac{t_r}{1 + r_r r_c^0} \tag{34}$$

Now what happens at each of these pick-offs in each of the states? The simplest state to deal with is State 4. In State 4, the arm cavities are resonant, so  $\Phi_{\parallel\perp} = \pi$ . To obtain maximum power buildup in the recycling cavity, the recycling gain (Eq. 23) is maximized by having the carrier be anti-resonant in the recycling cavity, thus  $\phi_{\parallel\perp} = 0$ . Eqs. 26-24 become

$$r_3 \Big|_4 = \frac{1}{\sqrt{2}} \frac{t_r r_c^\pi}{1 + r_r r_c^\pi} = \frac{1}{\sqrt{2}} r_c^\pi g_{cr} \Big|_4 \quad r_2 \Big|_4 = \frac{t_r r_c^\pi}{1 + r_r r_c^\pi} = r_c^\pi g_{cr} \Big|_4 \quad r_P \Big|_4 = \frac{1}{\sqrt{2}} \frac{t_r}{1 + r_r r_c^\pi} = \frac{1}{\sqrt{2}} g_{cr} \Big|_4 \tag{35}$$

In State 3, only the recycling cavity and the in-line arm are locked, so Eqs. 26-24 become

$$\begin{aligned}
r_3 \Big|_3 &= \frac{1}{\sqrt{2}} \frac{t_r r_c^\pi}{1 + \frac{1}{2} r_r [r_c(\Phi_\perp) + r_c^\pi]} \\
r_2 \Big|_3 &= \frac{1}{2} \frac{t_r [r_c(\Phi_\perp) + r_c^\pi]}{1 + \frac{1}{2} r_r [r_c(\Phi_\perp) + r_c^\pi]} \\
r_P \Big|_3 &= \frac{1}{\sqrt{2}} \frac{t_r}{1 + \frac{1}{2} r_r [r_c(\Phi_\perp) + r_c^\pi]} \quad (36)
\end{aligned}$$

Since  $r_c(\phi)$  changes only near resonance,  $r_c(\phi) \simeq r_c^0$  for all values of  $\phi$  away from  $(2n + 1)\pi$  (see Fig. 17):

$$\begin{aligned}
r_3 \Big|_3 &= \frac{1}{\sqrt{2}} \frac{t_r r_c^\pi}{1 + \frac{1}{2} r_r [r_c^0 + r_c^\pi]} = \frac{1}{\sqrt{2}} r_c^\pi g_{cr} \Big|_3 \\
r_2 \Big|_3 &= \frac{1}{2} \frac{t_r [r_c^0 + r_c^\pi]}{1 + \frac{1}{2} r_r [r_c^0 + r_c^\pi]} = (r_c^0 + r_c^\pi) g_{cr} \Big|_3 \\
r_P \Big|_3 &= \frac{1}{\sqrt{2}} \frac{t_r}{1 + \frac{1}{2} r_r [r_c^0 + r_c^\pi]} = \frac{1}{\sqrt{2}} g_{cr} \Big|_3 \quad (37)
\end{aligned}$$

In State 2, only the recycling cavity is locked, so the equations of state become

$$\begin{aligned}
r_3 \Big|_2 &= \frac{1}{\sqrt{2}} \frac{t_r r_c^0}{1 + r_r r_c^0} = \frac{1}{\sqrt{2}} r_c^0 g_{cr} \Big|_2 \\
r_2 \Big|_2 &= \frac{t_r r_c^0}{1 + r_r r_c^0} = r_c^0 g_{cr} \Big|_2 \\
r_P \Big|_2 &= \frac{1}{\sqrt{2}} \frac{t_r}{1 + r_r r_c^0} = \frac{1}{\sqrt{2}} g_{cr} \Big|_2 \quad (38)
\end{aligned}$$

For the  $l_+$  degree of freedom,  $r_{cr}$  is the variable of interest.

$$r_{cr}(\Phi, \phi) = r_r + \frac{1}{2} \frac{t_r^2 [r_c(\Phi_\perp) e^{-i\phi_\perp} + r_c(\Phi_\parallel) e^{-i\phi_\parallel}]}{1 + \frac{1}{2} r_r [r_c(\Phi_\perp) e^{-i\phi_\perp} + r_c(\Phi_\parallel) e^{-i\phi_\parallel}]} \quad (39)$$

#### 6.4.1 Sign changes

### 6.5 Sidebands

A similar, simpler derivation can be undertaken for the sidebands. Simpler because for the sidebands<sup>2</sup>, the arm lengths are forced to be almost exactly anti-resonant,  $\Phi \simeq 0$ . Then Eq. 14 is very nearly unity for  $\Phi = 2k_\pm L$ , where  $k_\pm = (2\pi\nu \pm \omega_m)/c$ . The sideband field reflected from each of the arms is similar to Eqs. 20

$$\frac{E_{\parallel\leftarrow}^\pm}{E_{2\rightarrow}^\pm} = \frac{1}{\sqrt{2}} e^{-i\phi_\parallel^\pm} \qquad \frac{E_{\perp\leftarrow}^\pm}{E_{2\rightarrow}^\pm} = \frac{1}{\sqrt{2}} e^{-i\phi_\perp^\pm} \quad (40)$$

---

<sup>2</sup>Parameters with no superscript are taken to be carrier properties; parameters with a  $\pm$  superscript are the upper and lower sidebands.

The sideband field at the anti-symmetric port D3 is

$$\frac{E_A^\pm}{E_{2\rightarrow\pm}} = \frac{1}{2} \left[ e^{-i\phi_\perp^\pm} - e^{-i\phi_\parallel^\pm} \right] \quad (41)$$

At the old pick-off position PO2, upstream of the beamsplitter, the field travelling towards the symmetric port is

$$r_T(\phi^\pm) \equiv \frac{E_{2\leftarrow}^\pm}{E_{2\rightarrow}^\pm} = \frac{1}{2} \left[ e^{-i\phi_\perp^\pm} + e^{-i\phi_\parallel^\pm} \right] \quad (42)$$

The distance between the beamsplitter and input test masses is  $(\lambda_m/2 \pm l_{asym})/2$ . Then

$$\begin{aligned} \phi_{\parallel\perp}^+ &= 2 \frac{2\pi\nu + \omega_m}{c} \left( \frac{\lambda_m}{4} \pm \frac{l_{asym}}{2} \right) \\ &= \phi_{\parallel\perp} + \frac{2\omega_m}{c} \left( \frac{\lambda_m}{4} \pm \frac{l_{asym}}{2} \right) \\ &= \pi \pm \theta \end{aligned} \quad (43)$$

since  $\phi_{\parallel\perp}$  is chosen to be 0 for maximum power buildup in the recycling cavity. The Schnupp asymmetry is incorporated into  $\theta \equiv \omega_m l_{asym}/c$  (see Eq. 9 – where does this factor of two come from?). If there is a small change in length of the cavity,  $\phi_{\parallel\perp}^+ = \pi \pm \theta$  becomes  $\pi \pm \theta + \delta\theta = \pi \pm \theta'$ , where  $\delta\theta = 2\omega_m \delta l/c$ , and  $\theta$  in all the equations below can be replaced with  $\theta'$ .

Then, using this simplification of the length variable  $\phi$  into a constant and the relationship  $e^{-i(\pi\pm\theta)} = -e^{\mp i\theta}$ , the anti-symmetric and symmetric (Thevenin equivalent) fields become

$$\frac{E_A^\pm}{E_{2\rightarrow\pm}} = \mp i \sin \theta \quad (44)$$

$$r_{Tsb} \equiv \frac{E_{2\leftarrow}^\pm}{E_{2\rightarrow}^\pm} = -\cos \theta \quad (45)$$

In other words, as long as the sidebands are anti-resonant in the arms, and we are in a state that we care about (i.e., State 2 or higher), the sidebands are independent of  $l_\pm$  and  $L_\pm$ , and the various states of locked and unlocked cavities.

The sideband recycling gain is defined in same way as the carrier gain (compare to Eq. 13):

$$g_{sb} \equiv \frac{E_{2\rightarrow}^\pm}{E_{inc}^\pm} = \frac{t_r}{1 + r_r r_{Tsb}} = \frac{t_r}{1 - r_r \cos \theta} \quad (46)$$

The pick-off field, from the anti-reflection coating on the ITM, is

$$r_{Psb} \equiv \frac{1}{\sqrt{2}} \frac{E_{2\rightarrow}^\pm}{E_{inc}^\pm} = \frac{1}{\sqrt{2}} g_{sb} \quad (47)$$

The sideband field reflected from the recycling mirror, the symmetric port, can again be found from the F-P equation and the Thevenin equivalent

$$r_{sb} \equiv \frac{E_{r\leftarrow}^\pm}{E_{inc}^\pm} = r_r + \frac{t_r^2 r_{Tsb}}{1 + r_r r_{Tsb}} \simeq \frac{r_r - \cos \theta}{1 - r_r \cos \theta} \quad (48)$$

The field transmitted to the anti-symmetric port is

$$t_{sb}^{\pm} \equiv \frac{E_A^{\pm}}{E_{inc}^{\pm}} = \frac{E_A^{\pm}}{E_{2 \rightarrow \pm}} \frac{E_{2 \rightarrow}^{\pm}}{E_{inc}^{\pm}} = \mp \frac{it_r \sin \theta}{1 - r_r \cos \theta} = \mp ig_{sb} \sin \theta \quad (49)$$

The field returning from the input mirror,  $E_{||\leftarrow}$ , related to the incident sideband field, is

$$r_3^{\pm} \equiv \frac{E_{||\leftarrow}^{\pm}}{E_{inc}^{\pm}} = \frac{E_{2 \rightarrow}^{\pm}}{E_{inc}^{\pm}} \frac{E_{||\leftarrow}^{\pm}}{E_{2 \rightarrow}^{\pm}} = \frac{1}{\sqrt{2}} \frac{-t_r e^{\mp i\theta}}{1 - r_r \cos \theta} \equiv r_3^{\mp*} \quad (50)$$

At the PO2 position,

$$r_2^{\pm} \equiv \frac{E_{2\leftarrow}^{\pm}}{E_{inc}^{\pm}} = \frac{t_r r_{Tsb}}{1 + r_r r_{Tsb}} = \frac{-t_r \cos \theta}{1 - r_r \cos \theta} = -g_{sb} \quad (51)$$

Note the sign change from  $r_P^{\pm}$ .

## 6.6 Signals – this section not finished!

To determine the signal seen at the output of the mixers, the following relationships are used [3]:

$$S_I = Re\{E^{-*}E + E^*E^+\} \quad S_Q = -Im\{E^{-*}E + E^*E^+\} \quad (52)$$

Since all the fields at any signal point are described in terms of the incident field, let us define the incident field. The incident field is described in terms of the sidebands as

$$\begin{aligned} E_{inc} &= E_l e^{i\Gamma \cos \omega_m t} \\ &\simeq J_0(\cdot) E_l + iJ_1(\cdot) E_l e^{i\omega_m t} + iJ_1(\cdot) E_l e^{-i\omega_m t} \\ &\equiv E_{inc} + E_{inc}^+ e^{i\omega_m t} + E_{inc}^- e^{-i\omega_m t} \end{aligned} \quad (53)$$

Note that  $E_{inc}^+ = E_{inc}^- = iJ_1(\cdot) E_l$ , and that  $E_{inc}^{-*} E_{inc} + E_{inc}^* E_{inc}^+ = 2J_0(\cdot) J_1(\cdot) |E_l|^2 \sin \omega_m t$ , and  $|E_l|^2 = P_{in}$ .

At the recycling cavity pickoff, the quad-phase (differential-mode) signal is given by

$$\begin{aligned} S_{PQ} &= -Im\{(r_{Psb} E_{inc}^-)^* r_P E_{inc} + (r_P E_{inc})^* r_{Psb} E_{inc}^+\} \\ &= -\frac{1}{\sqrt{2}} g_{sb} Im\{r_P^s E_{inc}^{-*} E_{inc} + r_P^{s*} E_{inc}^* E_{inc}^+\} \end{aligned} \quad (54)$$

At PO2,

$$S_{2Q} = -Im\{(r_2^- E_{inc}^-)^* r_2 E_{inc} + (r_2 E_{inc})^* r_2^+ E_{inc}^+\} \quad (55)$$

At the symmetric port, the in-phase (common-mode) signal is

$$S_{PI} = Re\{(r_{sb} E_{inc}^-)^* r_{cr} E_{inc} + (r_{cr} E_{inc})^* r_{sb} E_{inc}^+\} \quad (56)$$

quantity	State		Description		
<i>Recycling Mirror</i>					
$r_r$	$\sqrt{0.97} = 0.985$		reflectivity		
$l_r$	$\sqrt{30 \times 10^{-6}}$		absorption loss		
$t_r$	$\sqrt{1 - r^2 - l^2} = \sqrt{0.02997} = 0.173$		transmission		
<i>Input Test Mass</i>					
$l_i$	$\sqrt{75 \times 10^{-6}} = 0.008660$		absorption loss		
$r_{AR}$	$\sqrt{300 \times 10^{-6}}$		AR loss		
$t_i$	$\sqrt{0.03} = 0.173$		transmission		
$r_i$	$\sqrt{1 - t^2 - l^2} = 0.970 = 0.985$		reflectivity		
<i>End Test Mass</i>					
$t_e$	$\sqrt{10 \times 10^{-6}} = 0.003162$		transmission		
$l_e$	$\sqrt{70 \times 10^{-6}} = 0.008367$		loss		
$r_e$	0.99996		reflectivity		
<i>Beam Splitter</i>					
$l_{bs}$	$\sqrt{30 \times 10^{-6}}$		absorption loss		
$r_{AR}$	$\sqrt{300 \times 10^{-6}}$		AR loss		
$r_{bs}$	$\sqrt{1/2}$		reflectivity		
$t_{bs}$	$\sqrt{1 - r^2 - l^2} = 0.4997 = 0.707$		transmission		
<i>Misc.</i>					
$l_{asym}$	0.23 m		Schnupp asymmetry		
$l_{\pm}$	9.38 m		recycling cavity average length		
$\omega_m$	$2\pi$ (23.97) MHz		modulation frequency		
$\lambda$	1.064 $\mu\text{m}$		laser wavelength		
<i>Fabry-Perot derived quantities</i>					
	<b>antiresonant</b>	<b>resonant</b>			
$r_c$	0.99996	-0.98984	carrier reflectivity of FP cavity ( $r_e^0, r_e^\pi$ )		
$r_m$		0.97342	sideband reflectivity of FP cavity		
$r_c'$		130.31	$dr_c/dL$ (resonant)		
$r_m'$		0.007634	$dr_m/dL$		
$f_c$	91 Hz		Fabry-Perot cavity pole		
<i>IFO derived quantities</i>					
	<b>1</b>	<b>2</b>	<b>3</b>	<b>4</b>	
$g_{cr}$		0.0872	0.173	$\sqrt{46} = 6.74$	recycling carrier gain
$g_{sb}$		$\sqrt{17} = 4.135$			recycling sideband gain
$r_T$		0.99996	0.005	-0.98984	reflected Thevenin equivalent
$r_2$		0.002	-0.0017	-6.74	carrier field at PO2
$r_3$		0.001	-0.061	-4.77	carrier field at PO3
$r_P$		0.12	0.122	4.76	carrier field reflected from ITM
$r_{cr}$		1.000	0.958	-0.1971	reflected carrier field
$r_{sb}$		0.30128			reflected sideband field
$t_{cr}$				0	fields transmitted to asymmetric port
$t_{sb}$		0.94452			fields transmitted to asymmetric port
$f_{cc}$		$f_c$	$f_c/2$	1.16 Hz	double cavity pole (recycling + FP)
$f_r$		$f_c$	$f_c/2$	6.0 Hz	reflection zero
$f_p$		$f_c$	$f_c/2$	-0.74 Hz	recycling cavity zero

Table 2: Interferometer parameters.

## 6.7 Derived frequency response of the plant [4]

$$S_A = 4Sk g_{cr} t_{sb} \frac{1}{1+s_c} \left[ r_c \delta \mathbf{l}_- - r'_c \delta \mathbf{L}_- \right] \sin \omega_m t \quad (57)$$

$$S_R = -4Sk g_{sb} t_{sb} r_{cr} \left[ r'_m \delta \mathbf{L}_- + \delta \mathbf{l}_- \right] \sin \omega_m t \\ + 4Sk \frac{1}{1+s_{cc}} \left[ g_{cr}^2 r_{sb} r'_c \delta \mathbf{L}_+ - (g_{cr}^2 r_{sb} r_c + g_{sb}^2 r_{cr} r_m)(1+s_r) \delta \mathbf{l}_+ \right] \cos \omega_m t \quad (58)$$

$$S_P = 4Sk \frac{g_{cr} g_{sb} t_{sb}}{t_r} \left[ r'_m \delta \mathbf{L}_- - \delta \mathbf{l}_- \right] \sin \omega_m t \\ + 4Sk \frac{g_{cr} g_{sb} r_m}{t_r} \frac{1}{1+s_{cc}} \left[ r_c (g_{cr} - g_{sb})(1+s_p) \delta \mathbf{l}_+ - g_{cr} r'_c \delta \mathbf{L}_+ \right] \cos \omega_m t \quad (59)$$

$$S_P^\nu = S g_{cr} g_{sb} r_m \frac{1-r_c}{1+r_r} \frac{is_{cc}}{1+s_{cc}} \boldsymbol{\nu} \cos \omega_m t \quad (60)$$

$$S_R^\nu = -S r_{sb} (1-r_{cr}) \frac{is_{cc}}{1+s_{cc}} \boldsymbol{\nu} \cos \omega_m t \quad (61)$$

These equations do not include the resonances at the free spectral range and its harmonics.

$$S = 2J_0(\cdot) J_1(\cdot) P_{in} \quad \text{unit signal strength} \quad (62)$$

$$k = \frac{2\pi}{\lambda} \quad \text{wave number of laser frequency} \quad (63)$$

Pickoff equations were derived for D2 configuration – different for D6 by a factor of  $1/\sqrt{2}$  ?

$$s_c = \frac{i\omega_a}{\omega_c} \quad \omega_c = \frac{c}{2L} \left( \frac{1-r_i r_e}{\sqrt{r_i r_e}} \right) \quad f_c = 91 \text{ Hz} \quad \text{cavity pole, all states} \quad (64)$$

$$s_{cc} = \frac{i\omega_a}{\omega_{cc}} \quad \omega_{cc} = \left( \frac{1+r_r r_c}{1+r_r} \right) \omega_c \quad f_{cc} = 91, 46, 1.16 \text{ Hz} \quad \text{double cavity pole} \quad (65)$$

$$s_r = \frac{i\omega_a}{\omega_r} \quad \omega_r = \left( 1 + \frac{g_{cr}^2 r_{sb} r_c}{g_{sb}^2 r_{cr} r_m} \right) \omega_{cc} \quad f_r = 91, 46, 6.0 \text{ Hz} \quad \text{reflection zero} \quad (66)$$

$$s_p = \frac{i\omega_a}{\omega_p} \quad \omega_p = \left( 1 - \frac{g_{cr}}{g_{sb}} \right) \omega_{cc} \quad f_p = 91, 46, -0.74 \text{ Hz} \quad \text{negative recycling cavity zero} \quad (67)$$

If the condition  $S_{RI} (S_{PI}) = 0$  is enforced by adjusting  $\delta L_+$  with feedback, then the frequency independent terms

$$S_{PI} \Big|_{S_{RI}=0} \propto -4Sk \frac{g_{sb}^2 r_m}{t_r r_{sb}} (r_m + r_c) \delta \mathbf{l}_+ \cos \omega_m t \quad (68)$$

$$S_{RI} \Big|_{S_{PI}=0} \propto -4Sk g_{sb} (r_m + r_c) \delta \mathbf{l}_+ \cos \omega_m t \quad (69)$$

are obtained, where  $(g_{cr} r_{sb} r_c + g_{sb} r_{cr} r_m) \propto (r_m + r_c)$ .



From the PDR [5]:

$$\begin{aligned}
S_{PI} &\propto L_+ + \frac{l_+}{300} & S_{PQ} &\propto l_- \\
S_{RI} &\propto -\left(\frac{l_+}{100} + L_+\right) & S_{RQ} &\propto l_- \approx \frac{S_{PQ}}{250} \\
&\text{acq} \quad \text{det} & S_{AQ} &\propto L_- + \frac{l_-}{100}
\end{aligned} \tag{70}$$

Plugging in numbers, and rounding to reasonable values ( $\epsilon = \pi/2\mathcal{F} \simeq 1/132$ ), In State 2,

$$S_{AQ} \simeq -6.06 \times 10^4 S \frac{1}{s + 2\pi 91} [\delta L_- - \epsilon \delta l_-] \tag{71}$$

$$S_{RQ} \simeq -3.9 S [\epsilon \delta L_- + \delta l_-] \tag{72}$$

$$S_{PQ} \simeq -1.96 S [\epsilon \delta L_- - \delta l_-] \tag{73}$$

$$S_{RI} \simeq -166 S \frac{1}{s + 2\pi 91} \left[ \frac{1}{10} (s + 2\pi 91) \delta l_+ - \delta L_+ \right] \tag{74}$$

$$S_{PI} \simeq -1.3 \times 10^4 S \frac{1}{s + 2\pi 91} \left[ \frac{1}{1556} (s - 2\pi 91) \delta l_+ + \delta L_+ \right] \tag{75}$$

In State 3,

$$S_{AQ} \simeq -1.2 \times 10^4 S \frac{1}{s + 2\pi 91} \left[ \delta L_- - \frac{\epsilon}{200} \delta l_- \right] \tag{76}$$

$$S_{RQ} \simeq -3.8 S [\epsilon \delta L_- + \delta l_-] \tag{77}$$

$$S_{PQ} \simeq -3.9 S [\epsilon \delta L_- - \delta l_-] \tag{78}$$

$$S_{RI} \simeq -327 S \frac{1}{s + 2\pi 46} \left[ \frac{1}{20} (s + 2\pi 46) \delta l_+ - \delta L_+ \right] \tag{79}$$

$$S_{PI} \simeq -2.6 \times 10^4 S \frac{1}{s + 2\pi 46} \left[ \frac{1}{3 \times 10^5} (s - 2\pi 46) \delta l_+ + \delta L_+ \right] \tag{80}$$

In State 4,

$$S_{AQ} \simeq -4.8 \times 10^5 S \frac{1}{s + 2\pi 91} [\delta L_- + \epsilon \delta l_-] \tag{81}$$

$$S_{RQ} \simeq 0.77 S [\epsilon \delta L_- + \delta l_-] \tag{82}$$

$$S_{PQ} \simeq 155 S [\epsilon \delta L_- - \delta l_-] \tag{83}$$

$$S_{RI} \simeq 1.33 \times 10^4 S \frac{1}{s + 2\pi 1.16} \left[ \frac{1}{4000} (s + 2\pi 6) \delta l_+ + \delta L_+ \right] \tag{84}$$

$$S_{PI} \simeq -1.025 \times 10^6 S \frac{1}{s + 2\pi 1.16} \left[ \frac{1}{1570} (s - 2\pi 0.74) \delta l_+ + \delta L_+ \right] \tag{85}$$

Signal State	$\delta L_-$	$\delta l_-$	$\delta L_+$	$\delta l_+$	$\nu$
$S_{AQ}$	2	$-6.1 \times 10^3 \frac{1}{s+2\pi 91}$	+46.5		
	3	$-1.2 \times 10^4 \frac{1}{s+2\pi 91}$	+0.465		
	4	$-4.8 \times 10^5 \frac{1}{s+2\pi 91}$	$-3.6 \times 10^3$		
$S_{RQ}$	2	-0.0297	-3.85		
	3	-0.0295	-3.84		
	4	+0.006	+0.77		
$S_{PQ}$	2	+0.015	-1.96		
	3	-0.0295	-3.85		
	4	+1.2	-155		
$S_{RI}$	2		$+166 \frac{1}{s+2\pi 91}$	$-16.55 \frac{s-2\pi 91}{s+2\pi 91}$	$1.4 \times 10^{-3} \frac{s}{s+2\pi 91}$
	3		$+327 \frac{1}{s+2\pi 46}$	$-16.31 \frac{s-2\pi 46}{s+2\pi 46}$	$37 \frac{s}{s+2\pi 46}$
	4		$+1.3 \times 10^4 \frac{1}{s+2\pi 1.16}$	$+3.26 \frac{s-2\pi 6}{s+2\pi 1.16}$	$75 \frac{s}{s+2\pi 1.16}$
$S_{PI}$	2		$-1.3 \times 10^4 \frac{1}{s+2\pi 91}$	$-8.34 \frac{s-2\pi 89}{s+2\pi 91}$	$-5.4 \times 10^{-4} \frac{s}{s+2\pi 91}$
	3		$-2.5 \times 10^6 \frac{1}{s+2\pi 46}$	$-0.083 \frac{s-2\pi 44}{s+2\pi 46}$	$-1.4 \times 10^{-3} \frac{s}{s+2\pi 46}$
	4		$-1.0 \times 10^6 \frac{1}{s+2\pi 1.16}$	$+652 \frac{s-2\pi 0.74}{s+2\pi 1.16}$	$-2832 \frac{s}{s+2\pi 1.16}$

Table 3: Signal responses in each of the states

## 7 Design

### 7.1 Acquisition mode system

$$\begin{bmatrix} S_{PI} \\ S_{RI} \\ S_{AQ} \\ S_{PQ} \end{bmatrix} = \begin{bmatrix} p_{21} & p_{22} & p_{23} & p_{24} & p_{26} \\ p_{11} & p_{12} & p_{13} & p_{14} & p_{16} \\ p_{31} & p_{32} & p_{33} & p_{34} & p_{36} \\ p_{41} & p_{42} & p_{43} & p_{44} & p_{46} \end{bmatrix} \begin{bmatrix} \phi \\ l_+ \\ L_- \\ l_- \\ L_+ \end{bmatrix} \quad (86)$$

$$\begin{bmatrix} \phi \\ l_+ \\ L_- \\ l_- \\ L_+ \end{bmatrix} = \begin{bmatrix} c_{11} & 0 & 0 & 0 \\ 0 & c_{22} & 0 & 0 \\ 0 & 0 & c_{33} & 0 \\ 0 & 0 & 0 & c_{44} \\ c_{66} & 0 & 0 & 0 \end{bmatrix} \begin{bmatrix} S_{PI} \\ S_{RI} \\ S_{AQ} \\ S_{PQ} \end{bmatrix} \quad (87)$$

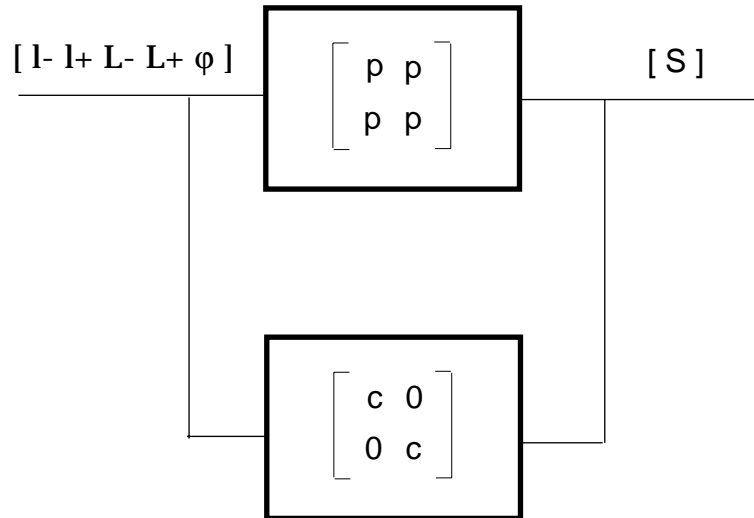


Figure 18: Block diagram of closed loop system

## 7.2 Controller and Plant transfer functions

The SMAC IFO plant takes displacement as its inputs, and has demodulated voltage as its output. The gain factor for the demodulator is almost certainly wrong, and should be checked. The SMAC controllers have a dimensionless transfer function of V/V. Subsumed into the controller are all the other systems between the IFO and the electronic controllers: the pendulum, the OSEMs, the whitening and dewhitening and anti-aliasing filters. For example, SMAC converts voltage to force with a simple 1 N/V conversion; from Section 7.4.1 below, we know this gain factor is wrong, so this gain factor must be accounted for when deconvolving the actual physical controller. The sensor sensitivity used by SMAC is  $0.8 e/\gamma$  and 1 V/A (1  $\Omega$  impedance). For the moment, all these are subsumed into the total controller transfer function. For the LIGO design, these will have to be deconvolved into each function (make a figure for this !).

### 7.2.1 Pendulum

The differential equation describing a damped, driven pendulum, or indeed, any damped simple harmonic oscillator, is:

$$m\ddot{x} + b\dot{x} + kx = F \quad (88)$$

$$b = \frac{\omega_0 m}{Q} \quad k = \frac{mg}{l} = m\omega_0^2 \quad (89)$$

The characteristic equation of this differential equation has the solutions

$$-\frac{\omega_0}{2Q} \pm i\frac{\omega_0}{2} \sqrt{4 - \frac{1}{Q^2}} \simeq -\frac{1}{\tau_0} \pm i\omega_0 \quad (90)$$

The last approximation is true for  $Q \gg 1/2$  ( $Q = 1/2$  is the critically damped case). The solution of the driven D.E. with a large  $Q$  (if  $1/Q^2$  isn't negligible, replace  $\omega_0$  with the appropriate term from the imaginary part of the C.E.) is:

$$x = e^{-t/\tau_0} \left[ \cos \omega_0 t \left( c_1 - \frac{1}{m\omega_0} \int e^{t/\tau_0} F(t) \sin \omega_0 t dt \right) + \sin \omega_0 t \left( c_2 + \frac{1}{m\omega_0} \int e^{t/\tau_0} F(t) \cos \omega_0 t dt \right) \right] \quad (91)$$

For the special case that the oscillator is driven by a sinusoid  $F \sin \omega t$  (of interest because the ground motion is very like a sinusoid over short periods, and because the  $Q$  of the internal modes of the mass is large enough that it's reasonable to assume that the only frequency contributing to the internal mode resonance is at that frequency), the solution becomes

$$x = e^{-t/\tau_0} [c_1 \cos \omega_0 t + c_2 \sin \omega_0 t] + \frac{F (\omega_0^2 - \omega^2) \sin \omega t - \frac{\omega_0 \omega}{Q} \cos \omega t}{m (\omega_0^2 - \omega^2)^2 + (\frac{\omega_0 \omega}{Q})^2} \quad (92)$$

Since I am interested in how long it takes to drive up an oscillation, take the initial conditions of the SHO to be that  $x|_{t=0} = 0$  and that  $\dot{x}|_{t=0} = 0$ ; then  $c_1 = c_2 \omega_0 \tau_0 = c_2 2Q$ .  $c_2$  ?.

For the even yet more special case of an oscillation driving the SHO at its resonant frequency ( $\omega = \omega_0$ ), this becomes

$$x = c_2 e^{-t/\tau_0} [2Q \cos \omega_0 t + \sin \omega_0 t] - \frac{FQ}{m\omega_0^2} \cos \omega_0 t \quad (93)$$

I suspect that I've done some math incorrectly (for shame! – it's been too long), because I think this ought to be something like

$$x = [1 - e^{-t/\tau_0}] \frac{F}{m\omega_0^2} Q \cos \omega_0 t \quad (94)$$

$F/m\omega_0^2$  is just  $x_{in}$ , so  $x/x_{in} \equiv A_r$ , the attenuation of the open-loop system at that frequency. The effective mass of the internal mode resonance is either  $3.43 \times 10^3$  kg at 9.206 kHz [10] or approximately 0.5 kg at 9.421 kHz [11] ?.

The pendulum transfer function is a special case in SMAC; the controller transfer functions in the pole-zero model must include the pendulum transfer function, since the pendulum is external to the SMAC IFO plant from which the model plant was derived (Fig. 2). The voltage output by the controller is converted to directly to force (1 N/V), which then is converted to units of displacement by the pendulum transfer function of m/N:

$$\left. \frac{x_{out}}{x_{in}} \right|_{\text{pendulum}} = \frac{\omega_0^2}{s^2 + \frac{\omega_0}{Q}s + \omega_0^2} \quad (95)$$

which is the much simpler steady state Laplace solution of the above differential equations, and where

$$Q = \frac{\omega_0 \tau_0}{2} \quad \omega_0^2 = \frac{g}{l} \quad (96)$$

Then the transfer function of the pendulum as used by SMAC is

$$\frac{x_{out}}{F_{in}} = \frac{1}{m} \frac{1}{s^2 + \frac{\omega_0}{Q}s + \omega_0^2} \frac{\text{m}}{\text{N}} \quad (97)$$

Neglecting the damping term, this reduces to the familiar

$$F = mgx/l = m\omega_0^2 x \quad (98)$$

For LIGO  $m\omega_0^2 = 233$ , so the gain of any loop which has a pendulum in it is reduced by 47 dB in the Design Tool.

At resonance,  $F_{in}$  is increased (or reduced) by the  $Q$  of the system:

$$x_{out} = Q F_{in} / m \quad (99)$$

For a critically damped system,  $Q = 1/2$ .

## 7.3 Driving resonant modes

### 7.3.1 Internal test mass modes

The physical deformation due to a particular internal resonance mode of the test mass is given by  $\delta = \mathbf{T}F$  [10]. The deformation of the test mass at its first internal resonance is

$$x_n[\text{m}/\sqrt{\text{Hz}}] = e_n[\text{V}/\sqrt{\text{Hz}}] f [\text{N}/\text{V}] T_{\delta,r,0} [\text{m}/\text{N}] A_r \quad (100)$$

where  $T_{\delta,n}$  is the deformation of the mass due to a particular resonance, and  $A_r$  is the attenuation of the loop at the resonance frequency.

The inherent noise of the ADCs is the largest noise source in the system, with a flat noise spectrum of  $e_N = 10 \mu\text{V}/\sqrt{\text{Hz}}$ , so the maximum deformation at the 9.421 kHz internal resonance is

$$x_n = (10 \times 10^{-6})(60 \times 10^{-6})(2.2 \times 10^{-4})(10^{-2}) = 1.3 \times 10^{-15} \text{ m}/\sqrt{\text{Hz}} \quad (101)$$

for the current lock acquisition design. For comparison, the amplitude of the resonance due to thermal excitation will be

$$x_{rms} = \frac{\sqrt{kT/m}}{\omega_0} = 3 \times 10^{-16} \text{ m}/\sqrt{\text{Hz}} \quad (102)$$

This is a few times larger than the motion at the wire resonance, but the demodulation signal produced by it is 1/10 smaller than the wire resonance signal because of the cavity pole [13].

### 7.3.2 Excitation time

The amount of time it takes to excite an internal mode is determined by the time constant due to the  $Q$  of the mode ( $Q = 1.3 \times 10^6$  at 9.4764 kHz [12]). For the crucial first internal drumhead mode, assuming it behaves as an SHO,

$$\tau_0 = \frac{2Q}{\omega_0} = \frac{1.3 \times 10^6}{\pi 9.4764 \text{ kHz}} = 54 \text{ s} \quad (103)$$

From Eq. 94,

$$t|_{0 \text{ dB}} = -\tau_0 \ln \left[ 1 - \frac{1}{A_r Q} \right] \quad (104)$$

the result being that if the acquisition mode controller is down 40 dB at the first internal mode resonance,

$$t|_{0 \text{ dB}} = -54 \ln \left[ 1 - \frac{100}{1.3 \times 10^6} \right] \simeq 54 \frac{1}{A_r Q} \Big|_{1/A_r \ll Q} \simeq 4 \text{ ms}$$

So it doesn't take very long to ring up this internal mode to the point where it ruins the stability of the controller. Even if it's down 100 dB, it only takes a few seconds to ring up above unity gain, and thus, make the loop unstable. It's only when the attenuation is greater than or equal to the  $Q$  gain that the loop is safe from instability, at  $-122$  dB.

### 7.3.3 Wire violin modes

## 7.4 Actuator ranges

### 7.4.1 OSEMs

In detection mode, the OSEMs have a force capability of 20 mN/A/coil (four coils), and the maximum current is  $400 \text{ V}_{pp}/7.83 \text{ k}\Omega = 51.1 \text{ mA}$  [9]. So  $(4)(20 \times 10^{-3})(51.1 \times 10^{-3}) = 4.1 \text{ mN}$  per test mass, and  $x_{max} = F_{max}/(m\omega_0^2) = 17.5 \mu\text{m}$  per test mass. This gives a gain of  $10 \mu\text{m}/400 \text{ V} = 44 \text{ nm/V}$ . The OSEM coil drivers have a zero at 40 Hz and a pole at 1 Hz [6].

In acquisition mode, the maximum current is 300 mA. So  $(4)(20 \times 10^{-3})(300 \times 10^{-3}) = 24 \text{ mN}$  per test mass ( $60 \times 10^{-6} \text{ N/V}$ ), and  $x_{max} = F_{max}/(m\omega_0^2) = 100 \mu\text{m}$  per test mass. This gives a gain of  $K = 100 \mu\text{m}/400 \text{ V} = 250 \text{ nm/V}$ .

### 7.4.2 PSL frequency

The frequency of the PSL can be varied by  $\pm 5$  MHz [8], so

$$\frac{c/2L}{\delta\nu} = \frac{\lambda/2}{\delta L},$$

where  $c/2L = \text{FSR}$  is 37.4 kHz, giving a laser frequency control of  $\delta L|_{\delta\nu_{\max}} = 133.7\lambda$ , or  $n = 2\delta L/\lambda = 267$  fringes.

In SMAC, the control parameter is not the PSL frequency, but the phase (position of the source [7]). Due to this, the limitations on the PSL frequency change are a bit harder to calculate. The laser phase is

$$e^{-i(\omega t - kx)} = e^{-i(2\pi\nu t - \frac{2\pi}{\lambda}x)} \quad (105)$$

SMAC varies  $x$  and holds  $\nu$  constant, while LIGO varies  $\nu$  (and thus  $\lambda$ ;  $\implies \delta\lambda \sim 10^{-13}$  m). Rewriting the source wave equation as

$$e^{-i2\pi(\nu t - \frac{x}{\lambda})} = e^{-i2\pi(\nu_0 + \delta\nu - [\frac{x_0}{\lambda t} + \frac{\delta x}{\lambda t}])t} \quad (106)$$

gives  $\delta\nu = \delta x/\lambda t$  ( $= c/\delta\lambda$ ), or  $\delta\nu = \delta x/t$  in units of  $\lambda$ , which looks like a velocity. So  $v_{\max} = \delta\nu_{\max} \lambda = 10^7 \lambda/\text{s}$ .

Thus a linear change in displacement results in a constant velocity, which corresponds to a source frequency change. *Voilà* – Doppler shift! This can be verified by calculating the velocity necessary to obtain the equivalent Doppler shift from the Lorentz transformation

$$\nu' = \nu \frac{1 - \beta}{\gamma} \quad \implies \quad \beta = \frac{1 - (\nu'/\nu)^2}{1 + (\nu'/\nu)^2} \quad (107)$$

and using a program like Mathematica to calculate  $\beta$  to the required degree of accuracy ( $\nu'/\nu = (10^{14} + 10^7)/10^{14}$ ). The limits on the real-world laser frequency variation then translate into a SMAC limitation on the rate of change of the source phase displacement.

### 7.4.3 Laser frequency variations and common mode lock

The common modes are locked when  $\phi = m\pi$ , where  $m$  is either  $2n+1$  or  $2n$ , depending on whether the cavity is resonant or anti-resonant. This condition is true even if the laser frequency varies, changing the resonant frequency (think about history in cavities ?).

$$\begin{aligned} \phi = m\pi = 2kl &= \frac{4\pi\nu}{c}l & \implies & m = \frac{4}{c}(\nu_0 + \delta\nu)(l_0 + \delta l) \\ \frac{m}{4} &= \frac{\nu_0 l_0 + \nu_0 \delta l + l_0 \delta\nu + \delta\nu \delta l}{c} & \frac{m}{4} &= \frac{l_0}{\lambda_0} + \frac{\delta l}{\lambda_0} + \frac{\delta\nu}{c}(l_0 + \delta l) \end{aligned} \quad (108)$$

But if the cavity was resonant before the changes of frequency and length, then  $m/4 = l_0/\lambda_0$ , and the change in frequency and length must negate each other

$$\frac{\delta l}{\lambda_0} + \frac{\delta\nu}{c}(l_0 + \delta l) = 0 \quad (109)$$

## 7.5 Sensor limitations

The photodiodes have a pole at 4 MHz, and a gain of 0.7 A/W. The tuned circuit has a transimpedance of 300  $\Omega$  at resonance, and its preamp a gain of 10, for a total of 3000 V/A, with a maximum output voltage of 4 V. Nergis uses a gain of  $9.6 \times 10^{12}$  V/m [6].

## 7.6 Transfer function gain

How much gain do we need in the loop? The worst-case  $L_-$  ground motion seen has a peak-to-peak amplitude of 20  $\mu\text{m}$  (Fig. 13) at the microseismic frequency after filtering through stack and pendulum. The width of an arm fringe is  $\lambda/2\mathcal{F} = 1.064 \times 10^{-6}/2(208) = 2.6$  nm. So the open loop gain needed to reduce the ground motion to the width of a fringe is  $x_{L\text{gnd}}/x_{\text{fringe}} = 2 \times 10^{-5}/2.6 \times 10^{-9} \sim 8 \times 10^3$ , or 80 dB. For stable operation, the motion needs to be reduced to some small fraction of the fringe width. 10% ? was chosen arbitrarily, corresponding to a required gain of 100 dB at the microseismic peak.

The corresponding value for the Michelson DOFs can be calculated by calculating the finesse of the cavity

$$\mathcal{F} = \frac{\pi\sqrt{r_i r_e}}{1 - r_i r_e} \quad (110)$$

where  $r_e$  in this case is the Thevenin equivalent reflectance,  $r_T$ , of the beamsplitter/arms Thevenin equivalent cavity from Eq. 22. In State 2,  $r_T$  is very close to one, and the reflectance of the recycling mirror is the same as the input test mass, so the finesse is the same as a single arm,  $\mathcal{F}_M^2 = 207$ , and the corresponding width of the fringe is 2.6 nm. In State 3,  $r_T$  is small, and  $\mathcal{F}_M^3 = 0.002$ ; the width of a fringe  $2.4 \times 10^{-6}$  m, or 2.25 times bigger than the laser wavelength! In State 4, the situation returns to normal and  $\mathcal{F}_M^4 = \mathcal{F} = 207$  (despite the sign change of the Thevenin cavity). The loop gain required then is  $x_{l\text{gnd}}/x_{\text{fringe}} = 200 \times 10^{-9}/2.6 \times 10^{-9} \sim 77$ , or 38 dB. The 10% requirement thus requires 48 dB at the microseismic peak.

The FSR of the Michelson cavity is  $c/2l_{\pm} = 16$  MHz.

## 7.7 Delays

The FDR quotes a 127  $\mu\text{s}$  time delay for the  $L_-$  loop, and 101  $\mu\text{s}$  for the  $l_{\pm}$ . The frequency loop is analog and local, so not subject to as much delay (how much ?). How does changing control of  $L_-$  loop to input test masses change this ?



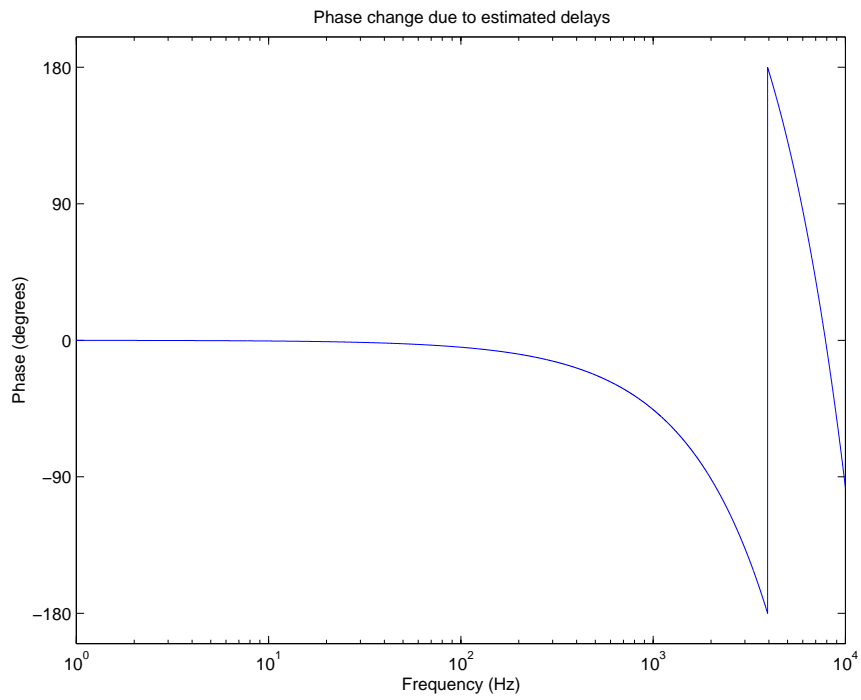


Figure 19: Phase change in the  $L_-$  loop due to delays in the system, assuming a  $127 \mu\text{s}$  total delay.

This page intentionally left unblank.

## 7.8 Current detection mode SMAC controller transfer functions

$$c_{11} \Big|_{\text{MC offset}} (S_{PI} \rightarrow \phi) = + K \frac{(s + 2\pi \cdot 1)^3}{(s + 2\pi \cdot 50)^3} \quad (111)$$

$$c_{11} \Big|_{\text{MC length}} (S_{PI} \rightarrow \phi) = + K (s + 2\pi \cdot 1) \quad (112)$$

$$\begin{aligned} c_{22}(S_{RI} \rightarrow l_+) &= + K \frac{(s + 2\pi \cdot 10)^3}{(s + 2\pi \cdot 0.1)(s + 2\pi \cdot 40)} \frac{(s + 2\pi \cdot 40)}{(s + 2\pi \cdot 1)} \\ &\times (\text{resonant gain at 13 Hz}) \\ &\times (8 \text{ pole } 80 \text{ dB elliptic notch } 9.1 \text{ kHz-} 10.1 \text{ kHz}) \end{aligned} \quad (113)$$

$$\begin{aligned} c_{33}(S_{AQ} \rightarrow L_-) &= + K \frac{(s + 2\pi \cdot 10)(s + 2\pi \cdot 40)^3}{(s + 2\pi \cdot 0.1)^2} \frac{(s + 2\pi \cdot 40)}{(s + 2\pi \cdot 1)} \\ &\times (\text{resonant gain at 13 Hz}) \\ &\times (6 \text{ pole, } 0.1\% \text{ ripple, } 60 \text{ dB stopband, } 7.5 \text{ kHz elliptic}) \\ &\times (8 \text{ pole } 80 \text{ dB elliptic notch } 9.1 \text{ kHz-} 10.1 \text{ kHz}) \end{aligned} \quad (114)$$

$$\begin{aligned} c_{44}(S_{PQ} \rightarrow l_-) &= + K \frac{(s + 2\pi \cdot 1)^2 (s + 2\pi \cdot 10)^2}{(s + 2\pi \cdot 0.1)^2 (s + 2\pi \cdot 1)(s + 2\pi \cdot 40)} \frac{(s + 2\pi \cdot 40)}{(s + 2\pi \cdot 1)} \\ &\times (\text{resonant gain at 13 Hz}) \\ &\times (6 \text{ pole, } 0.1\% \text{ ripple, } 60 \text{ dB stopband, } 7.5 \text{ kHz elliptic}) \\ &\times (6 \text{ pole, } 0.1\% \text{ ripple, } 60 \text{ dB stopband, } 5.5 \text{ kHz elliptic}) \\ &\times (2 \text{ kHz } 5 \text{ pole Butterworth}) \end{aligned} \quad (115)$$

$$\begin{aligned} c_{66}(S_{PI} \rightarrow L_+) &= + K \frac{(s + 2\pi \cdot 1)^2}{(s + 2\pi \cdot 0.1)} \frac{(s + 2\pi \cdot 40)}{(s + 2\pi \cdot 1)} \\ &\times (4\text{th order } 30 \text{ Hz Chebyshev}) \\ &\times (4\text{th order } 30 \text{ Hz, } 150 \text{ Hz } 40 \text{ dB stopband}) \end{aligned} \quad (116)$$

## 7.9 Current best design acquisition mode SMAC controller transfer functions

$$c_{11} \Big|_{2,3,4} (S_{PI} \rightarrow \phi) = - \frac{1}{10} \frac{(s + 2\pi 500)(s + 2\pi 50 \text{ kHz})}{s(s + 2\pi 1)(s + 2\pi 10 \text{ kHz})} \quad (117)$$

$$c_{22} \Big|_{2,3} (S_{RI} \rightarrow l_+) = - \frac{1}{400} \frac{(s + 2\pi 10)}{(s + 2\pi 8.0 \text{ kHz})} \quad (118)$$

$$c_{22} \Big|_4 (S_{RI} \rightarrow l_+) = + \frac{1}{250} \frac{(s + 2\pi 0.74)^2}{(s - 2\pi 0.354)(s + 2\pi 500)(s + 2\pi 8.0 \text{ kHz})} \quad (119)$$

$$\begin{aligned} c_{33} \Big|_{3,4} (S_{AQ} \rightarrow L_-) &= + \frac{1}{250} (s + 2\pi 90)(s + 2\pi 130) \quad (120) \\ &\times (6 \text{ pole, } 0.1\% \text{ ripple, } 60 \text{ dB stopband, } 7.5 \text{ kHz elliptic}) \\ &\times (8 \text{ pole } 80 \text{ dB elliptic notch } 9.1 \text{ kHz-} 10.1 \text{ kHz}) \end{aligned}$$

$$\begin{aligned} c_{44} \Big|_2 (S_{PQ} \rightarrow l_-) &= - \frac{1}{316} \frac{(s + 2\pi 10)}{(s + 2\pi 8.0 \text{ kHz})} \quad (121) \\ &\times (2 \text{ kHz } 5 \text{ pole Butterworth}) \end{aligned}$$

$$\begin{aligned} c_{44} \Big|_{3,4} (S_{PQ} \rightarrow l_-) &= + \frac{1}{30} \frac{1}{316} \frac{(s + 2\pi 10)}{(s + 2\pi 8.0 \text{ kHz})} \quad (122) \\ &\times (2 \text{ kHz } 5 \text{ pole Butterworth}) \end{aligned}$$

$$c_{66} \Big|_{2,3} (S_{PI} \rightarrow L_+) = + \frac{1}{5000} \frac{(s + 2\pi 1)^2}{(s + 2\pi 0.1)} \quad (123)$$

$$c_{66} \Big|_4 (S_{PI} \rightarrow L_+) = + \frac{1}{30} \frac{1}{5000} \frac{(s + 2\pi 1)^2}{(s + 2\pi 0.1)} \quad (124)$$

Loop	$\phi$	$L_+$	$l_-$	$L_-$	$l_+$
$v_{thr}$			0.5	> 5.0	0.5

Table 4: Threshold velocities,  $\lambda/s$

CONTROLLER	STATE 2		STATE 3		STATE 4	
	Gain (dB)	Phase (deg.)	Gain (dB)	Phase (deg.)	Gain (dB)	Phase (deg.)
$S_{PQ} \rightarrow l_-$	64 @ 883 Hz	48 @ 2 Hz	83 @ 883 Hz	141 @ 0 Hz	49 @ 883 Hz	44 @ 6 Hz
$S_{RI} \rightarrow l_+$	28 @ 1.12 kHz	80 @ 135 Hz	24 @ 1.12 kHz	64 @ 210 Hz	17 @ 804 kHz	60 @ 204 Hz
$S_{PI} \rightarrow L_+$			65 @ 679 Hz	79 @ 6 Hz	30 @ 86 Hz	3 @ 15 Hz
$S_{AQ} \rightarrow L_-$			55 @ 2.7 kHz	14 @ 24 Hz	24 @ 2.67 kHz	53 @ 212 Hz
$S_{PI} \rightarrow \nu$			$\infty$ @ -	40 @ 300 Hz	$\infty$ @ -	45 @ 2 kHz

Table 5: Gain and phase margins of system in each state

	SMAC identifier	State				
Signal	Matlab/Fortran	1	2	3	4	Description
$S_P^{sb}$	Id6_1sb/ID_6_sb1		> 0.001 W			unique
$S_R^{sb}$	ID1sb/ID_1_sb1		< 0.04 W			unique
$S_A^{sb}$	Id2sb/ID2_sb1		> 0.066 W			
$S_A^{sb}$	Id2sb/ID2_sb1		> 0.114 W			equilibrium
$P_M^{sb}$	IABsb		> 0.5 W			
$S_P^c$	ID6/ID6			> 0.1 $\mu$ W		
$S_A^c$	ID2/ID2			> 0.1 W		
$S_R^c$	ID1/ID1			> 5.25 W		
$P_M^{sb}$	IABsb			> 0.5 W		
$P_M^c$	IAB			> 0.1 W		
$P_{\parallel}^c$	IBC			> 1.0 W		
$S_P^c$	ID6/ID6			> 0.04 mW < 0.05 mW		
$S_P^{sb}$	Id6_1sb/ID6_sb1			> 3 mW		
$S_A^c$	ID2/ID2			> 0.15 mW		
$S_{\parallel}^c$	IDC1/ID4			> 0.1 mW < 0.2 mW		
$S_{\parallel}^{sb}$	IC1sb/ID4_sb1			> 0.5 $\mu$ W		
$S_P^c$	ID6/ID6				> 0.2 $\mu$ W	unique
$S_R^c$	ID1/ID1				< 5.25 W	unique
$P_M^{sb}$	IABsb				> 0.5 W	
$P_M^c$	IAB				> 0.1 W	
$P_{\perp}^c$	IEF				> 1.0 W	
$P_{\parallel}^c$	IBC				> 1.0 W	
$S_{\parallel}^c$	IDC1/ID4				> 0.15 W	
$S_{\parallel}^c$	IDC1/ID4				> 0. W	
$S_A^c$	ID2/ID2				< 0.15 W	not unique
$S_P^c$	ID6/ID6				> 0.04 mW	
$S_{\perp}^c$	IDF1/ID5				> 0.04 mW	
$S_{\parallel}^c$	IDC1/ID4				> 0.04 mW	
$P_{\perp}^c$	IEF				> 1.0 W	
$P_{\parallel}^c$	IBC				> 1.0 W	
$S_{\perp}^c$	IDF1/ID5				> 0.305 mW	equilibrium
$S_{\parallel}^c$	IDC1/ID4				> 0.305 mW	

Table 6: Threshold values for state transitions, 6 W input power. Groups within a single box denotes a logical *and* of the conditions. S is the power incident on a sensor, P is the power within a cavity. c – carrier, sb – sideband. A – asymmetric port, R – reflected (symmetric) port, P – pickoff. M – Michelson cavity,  $\parallel$  – in-line cavity,  $\perp$  – perpendicular cavity.

Controller	Path	State 1	State 2	State 3	State 4 (acq)	State 4 (det)
$c_{11}$	$S_{PI} \rightarrow \phi$	ConPhia	ConPhia	ConPhia	ConPhia	ConPhid
$c_{22}$	$S_{RI} \rightarrow \text{RM}$	ConRMa23	ConRMa23	ConRMa23	ConRMa23/ConRMa4	ConRMd
	$S_{RI} \rightarrow l_+$	Concma	Concma	Concma	Concma	Concmd
$c_{33}$	$S_{AQ} \rightarrow L_-$	na	na	ConDMaT	ConDMaT	ConDMd
$c_{44}$	$S_{PQ} \rightarrow l_-$	Condma	Condma	Condma	Condma	Condm
$c_{66}$	$S_{PI} \rightarrow L_+$	ConCMa	ConCMA	ConCMA	ConCMA	ConCMD

Table 7: Linear controller code corresponding to  $c_{nn}$  for each state.

State Transition	Loop	Trigger	Effect	Code
1 $\rightarrow$ 2	$l_+$ $l_-$ $\phi$ $L_+$	$P_r^{sb} < 0.04 \text{ W}$	State 2 acquired	nIRMa23 nldma nlPhia nlCMA
2 $\rightarrow$ 3	$l_-$ $L_-$	$P_a^c > 0.1 \text{ \& } P_r^c > 5.25 \text{ W}$	-30 dB $l_- \pm l_-$ actuator sign enable $L_-$	nldma nlDMaitm
3 $\rightarrow$ 4 (acq)	$l_+$ $L_+$	$P_r^c < 5.25 \text{ W}$	switch to state 4 $l_+$ mode -30 dB $L_+$	nIRMa4 nlCMA
4 (acq) $\rightarrow$ 4 (det)	all	$P_{tr  }^c \text{ \& } P_{tr\perp}^c > 0.305 \text{ W}$	switch to detection mode	
2 $\rightarrow$ $2_{sb}$		?		
3 $\rightarrow$ $3_{sb}$		?		

Table 8: Transition through the acquisition states, showing triggers and controller enabling. c – carrier, sb – sideband, tr – transmitted, a – asymmetric port, r – reflected port.

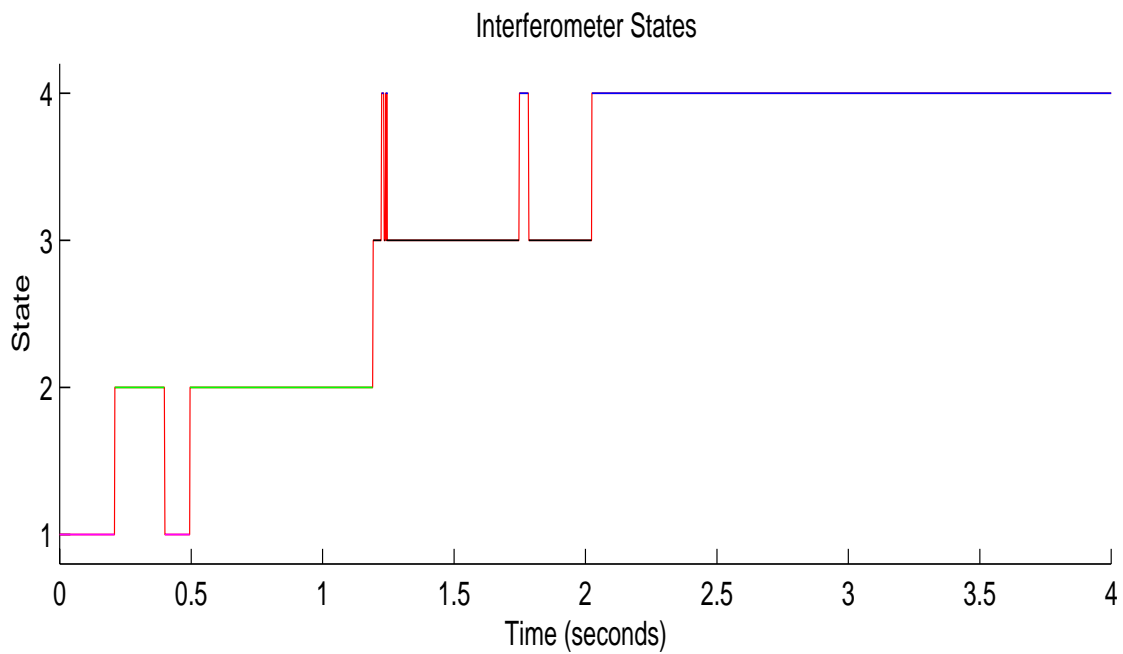
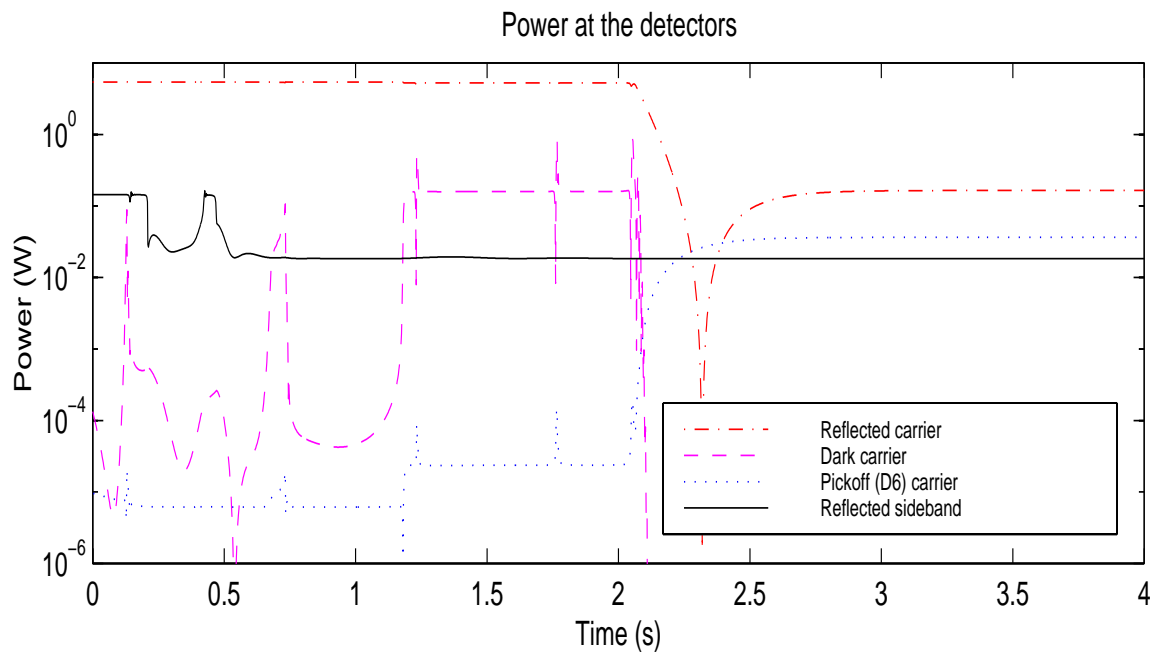


Figure 20: Power at standard detectors in each state.



## 8 Questions

- 1 Is the system unconditionally stable and have maximum bandwidth ( $> 1$  kHz)?
- 2 What are the acquisition threshold velocities in each state?
- 2 Probability distribution of test mass velocity based on site characteristics (GG/PF); probability that all test masses have velocity below acquisition threshold at near-resonant displacement? Is this velocity with local damping?
- 2 How long does it take the simulation to acquire with a reasonable distribution of initial displacements and velocities?
- 3 Is guided lock acquisition needed? What hooks need to be made into the design to ensure that it can be added if needed?
- 4 Are the controllers within the dynamic range, power capacity, sensitivity of the available PDs, ADCs, and coil drivers?
- 4 Are the triggers for the state transitions reasonable given the sensors and signals available?
- 5 How to discriminate between State 2(3) and State 2(3)sb? Will the IFO lock into these states? Will it lock in State 3? (yes)
- 6 How can the acquisition mode controllers be integrated with detection mode? Does there need to be a separate path?
- 7 Develop GLA for faster acquisition?

Check with Dennis for driving functions of longitudinal modes. Can steeper filters be used to avoid driving them? With  $Q$  so high, is this an issue anyway? How long does it take to drive up the 10 kHz internal resonance (85 seconds); conversely, how far down do the filters need to be at that frequency?

## 9 TTD as of January 27, 1999

Is it possible that in State 3, the  $L_+$  loop is driving up the out-of-lock arm? This is seen in the 40m (B. Kells).

Use  $\perp$  arm pickoff to control  $\parallel$  arm, then switch when State 3 lock has been achieved to avoid sign change.

- ✓ Drive ITMs to control  $L_{\pm}$  to decrease phase delay.

Modify controllers' gain to be proportional to modulation index.

- ✓ Am I using the correct pickoff?
- ✓ How do mixer phases in SMAC affect signals?
- ✓ Lock  $L_-$  before  $L_+$  lower  $L_+$  bandwidth to OSEM bw; lower  $L_-$  bw, figure out appropriate sequencing given probable lack of control over MC and laser loop.

Figure of merit for SMAC  $L_{\pm}$   $l_{\pm}$  which takes out source frequency variations.

- ✓ Why the sensitive dependence to initial conditions?
- ✓ Common mode controllers.

Crossovers to MC, PSL, IFO.

- ✓ Stable controller with notch to reduce gain at first internal mode.
- ✓ DT State 2.
- ✓ Input latest optical parameters.
- ✓ Realistic triggers.

Implement phases in dynamic mode for  $l_{\pm}$  loops.

Derive relationship between gain, bandwidth, and  $v_{thr}$ .

Photodiode limitations.

Think about non-minimum phases, etc.

Is there a smarter way to design this MIMO system?

What's going on with the sine sweep in the TF mode?

- ✓ Reconcile dm, ifo, DT, SMAC, twiddle phases, phase margins, gain margins.
- ✓ SMAC/Twiddle comparison.

Take into account horizontal/vertical transfer functions due to magnets on rear wedge causing bounce mode, and bounce mode changing  $L_{\pm}$  due to front wedge.

## 10 From the FDR

New seismic model.

✓ Understand sign switches, 30 dB decrease, and switch timing.

✓ Are violin modes relevant for LA? (no)

✓ Sensor ranges

PSL inputs – bandwidth, limits.

✓ Delays

✓ Phase margins and stability

✓ Lock to detection transition

✓ Alignment effects on LA

✓ Triggers

Crossovers

✓ New IFO params

This page intentionally not left completely blank

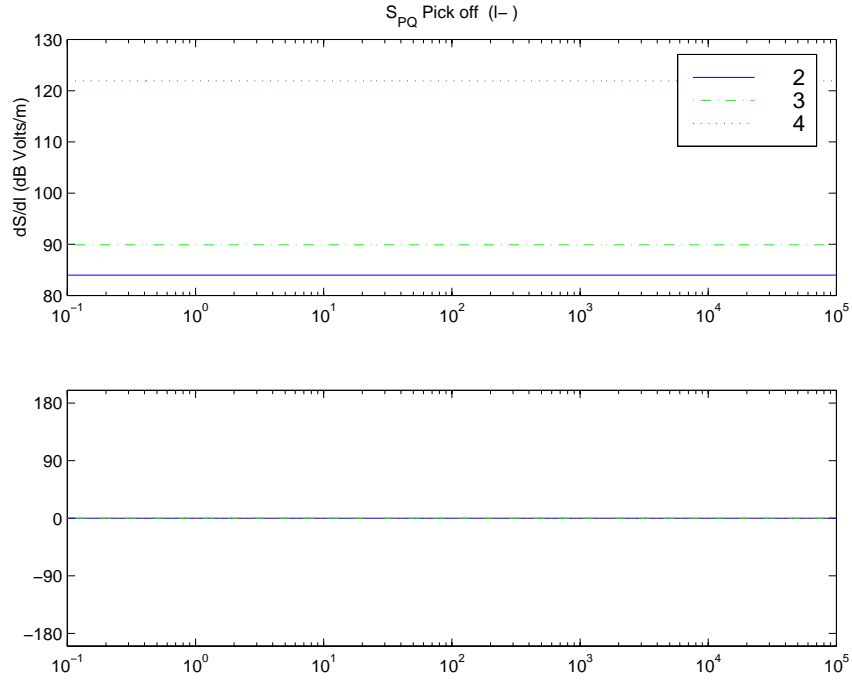


Figure 21: Michelson differential mode transfer function ( $l_-$ ), from Eq. 61 and Table 3, all states.

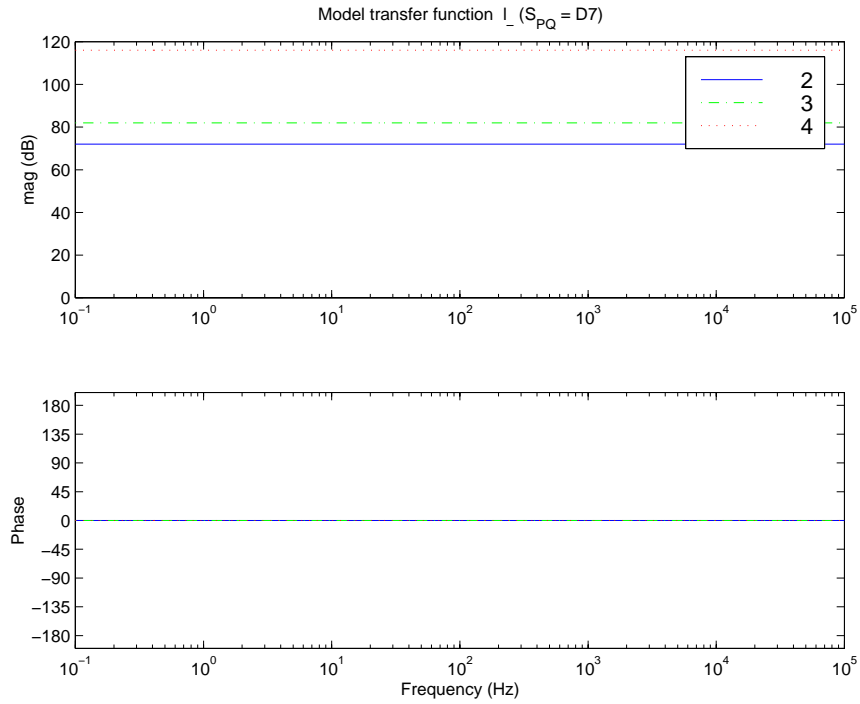


Figure 22: Michelson differential mode transfer function ( $l_-$ ), tweaked model, all states.

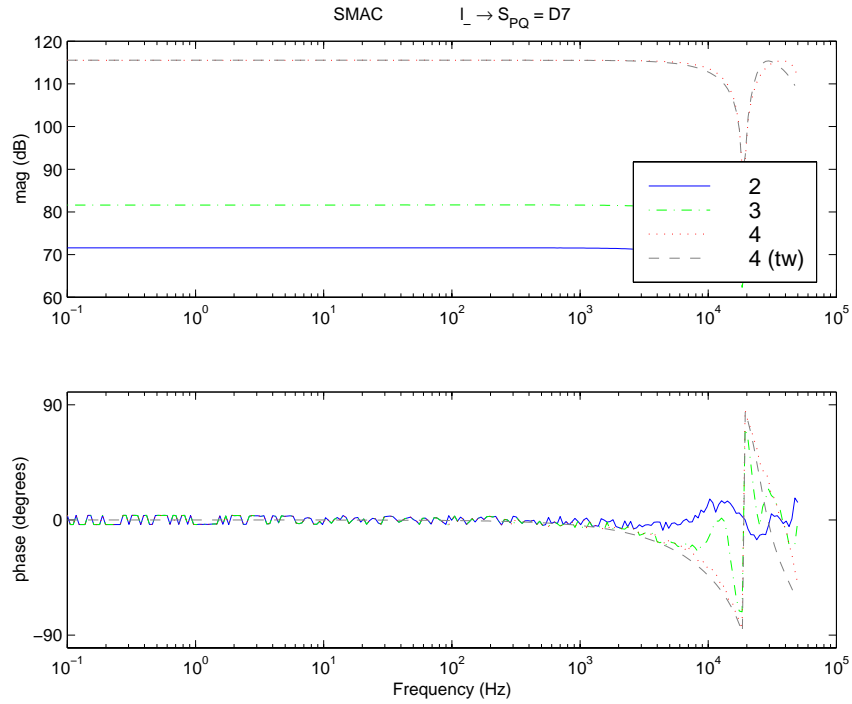


Figure 23: Michelson differential mode transfer function  $(-M_1 - M_2) + (M_3 + M_4)$  at D7, SMAC and Twiddle, all states.

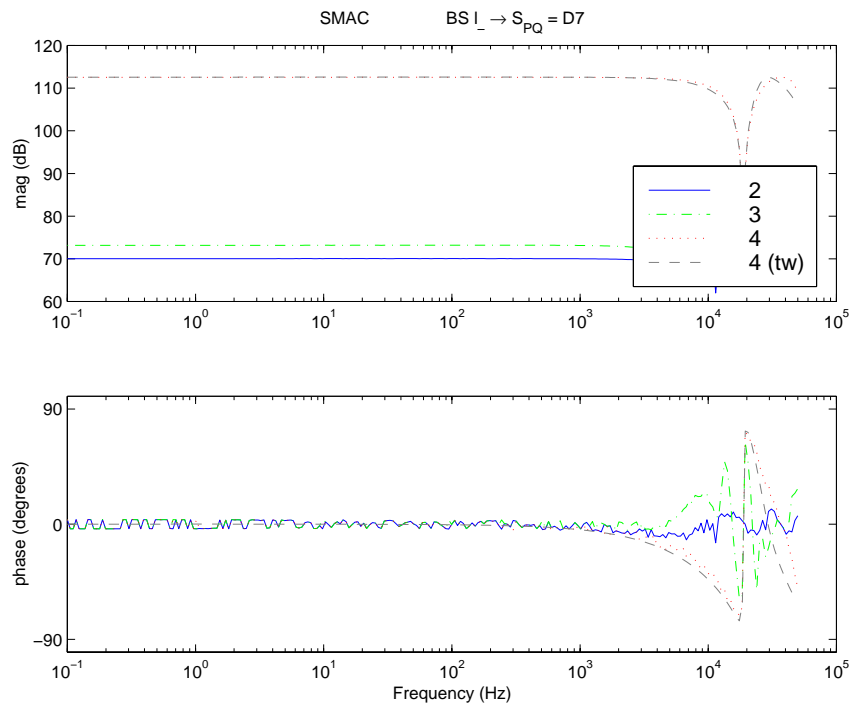


Figure 24: Michelson differential mode transfer function (beamsplitter-driven  $l_-$ ) at D7, SMAC and Twiddle, all states.

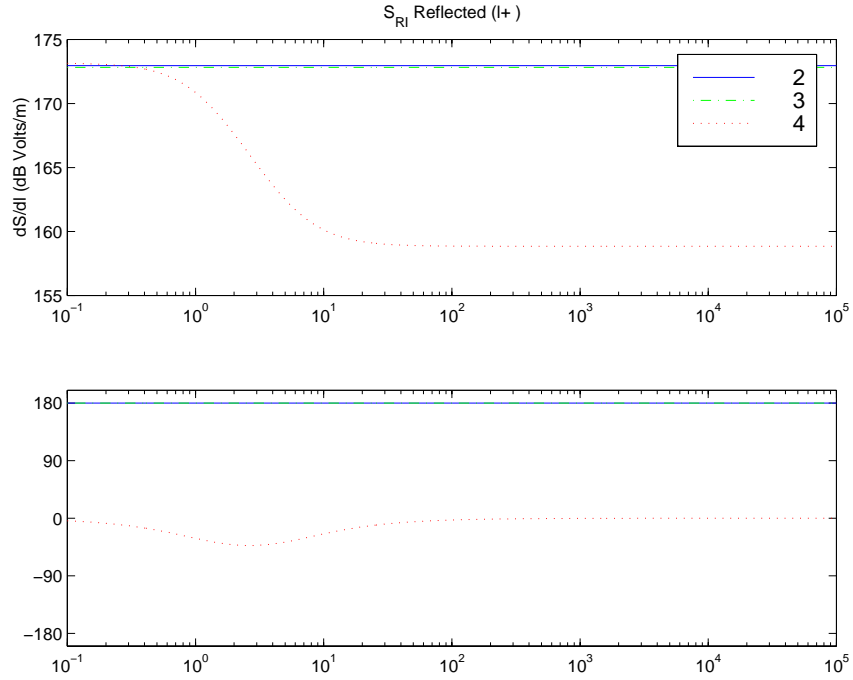


Figure 25: Michelson common mode transfer function ( $l_+$ ), from Eq. 61 and Table 3, all states.

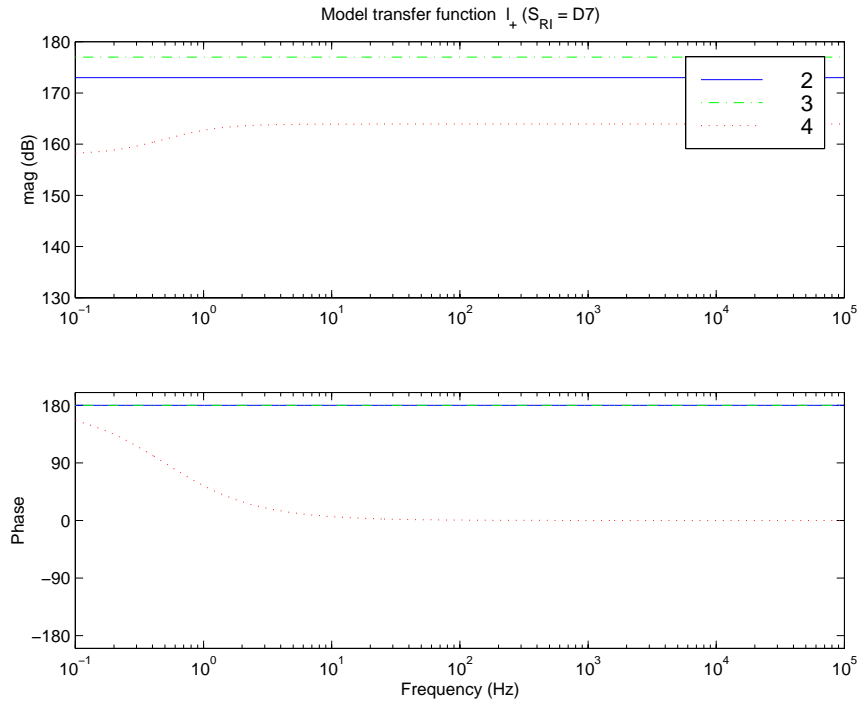


Figure 26: Michelson common mode transfer function ( $l_+$ ), tweaked model, all states.

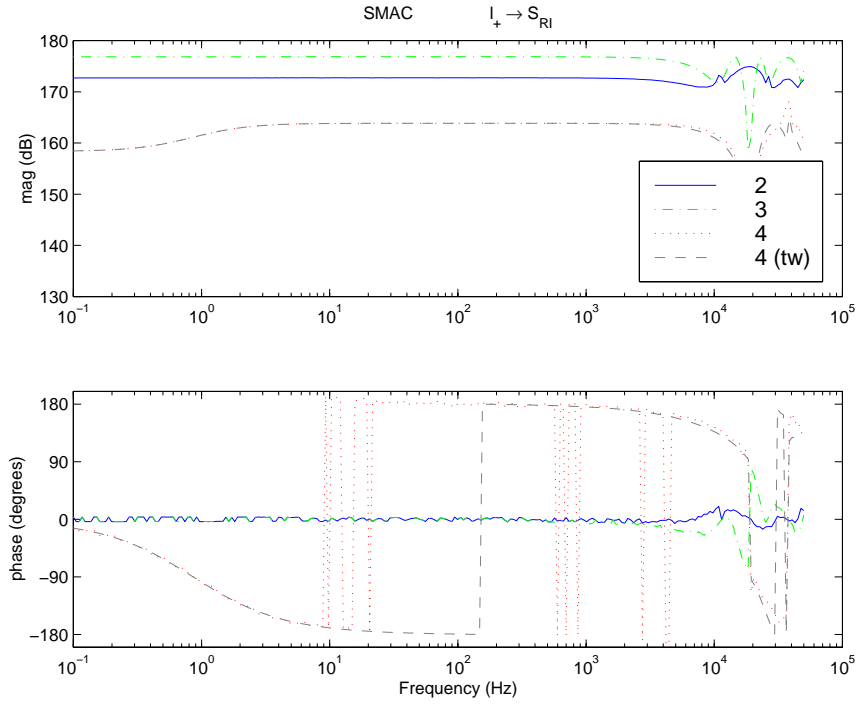


Figure 27: Michelson common mode transfer function ( $+(M_1 + M_2) + (M_3 + M_4)$ ), SMAC and Twiddle (+120 dB), all states.

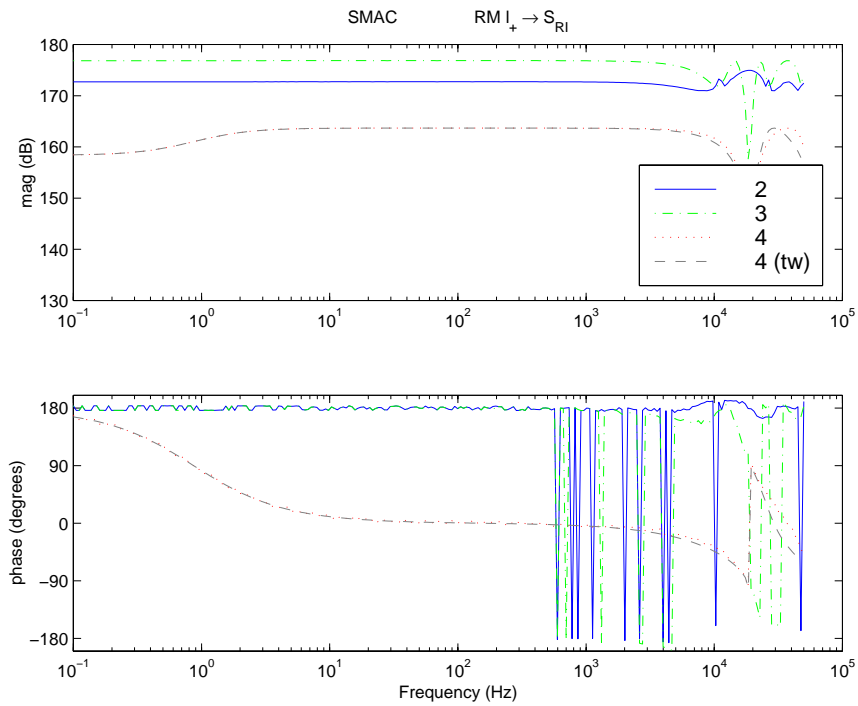


Figure 28: Michelson common mode transfer function (recycling mirror-driven  $l_+$ ), SMAC and Twiddle (+120 dB), all states.



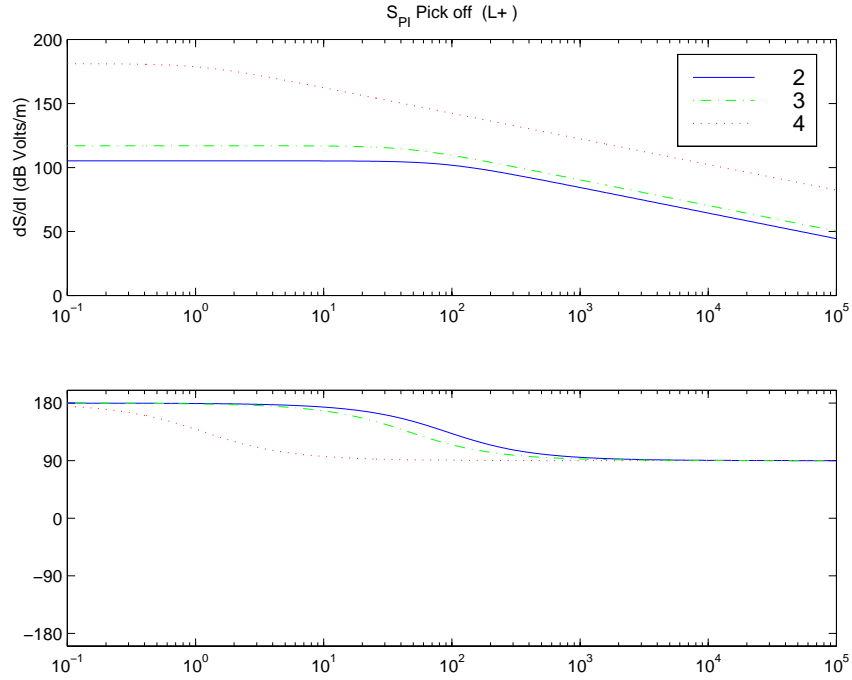


Figure 29: Common mode transfer function ( $L_+$ ), from Eq. 61 and Table 3, all states.

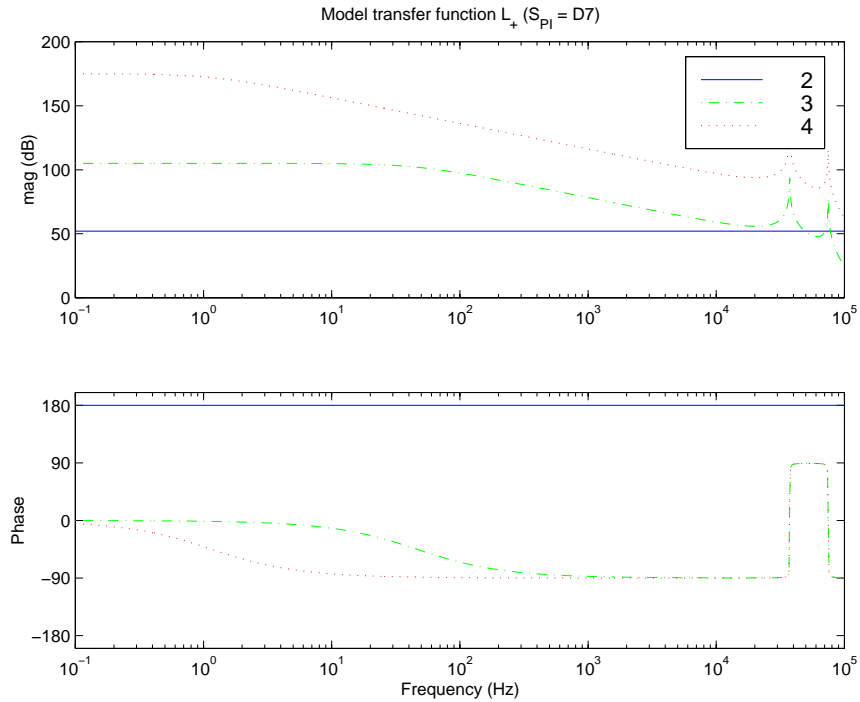


Figure 30: Common mode transfer function ( $L_+$ ), tweaked model, all states.

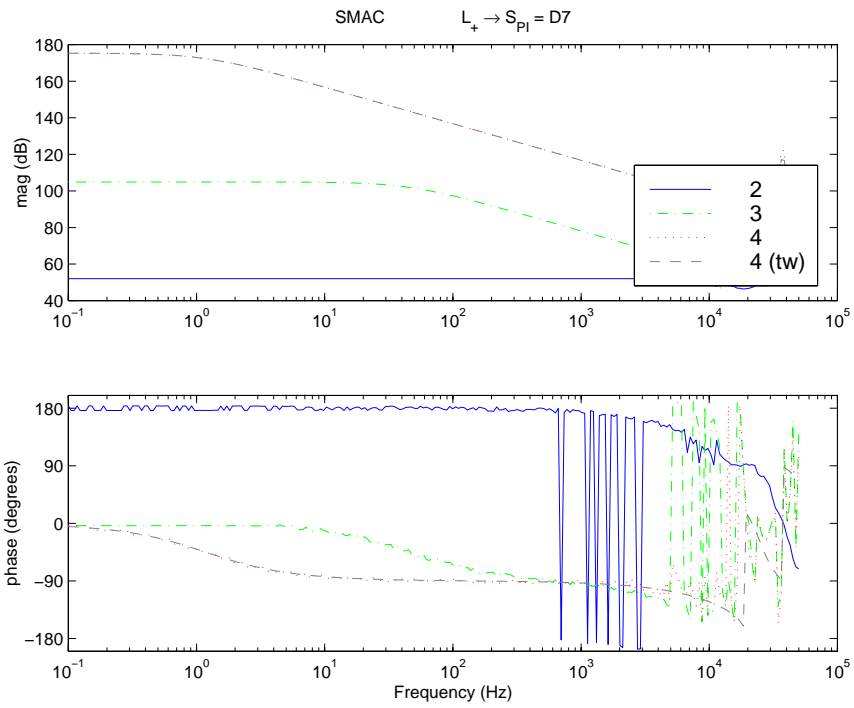


Figure 31: Common mode transfer function ( $L_+$ ) at D7, SMAC and Twiddle, all states.

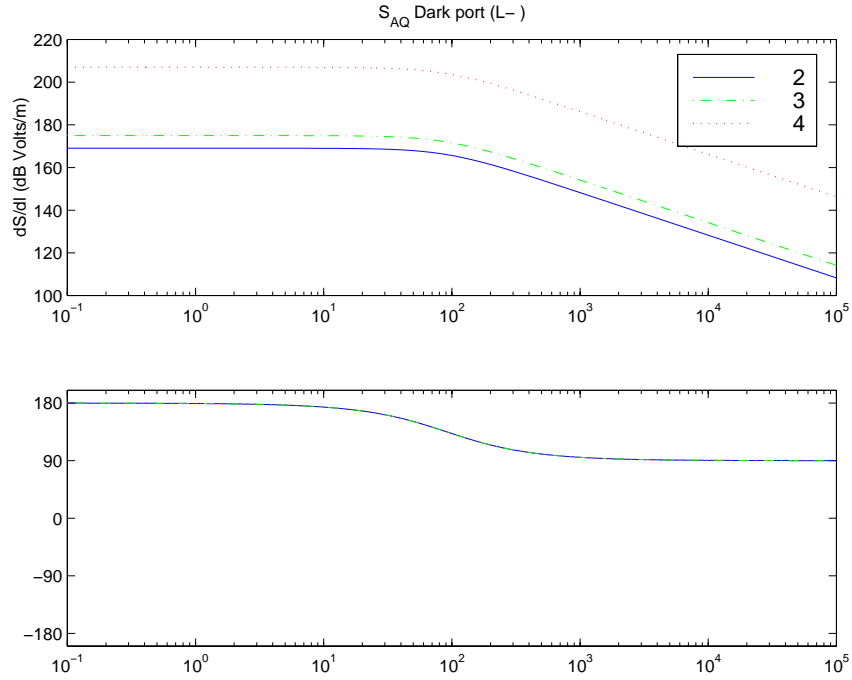


Figure 32: Differential mode transfer function ( $L_-$ ), from Eq. 61 and Table 3, all states.

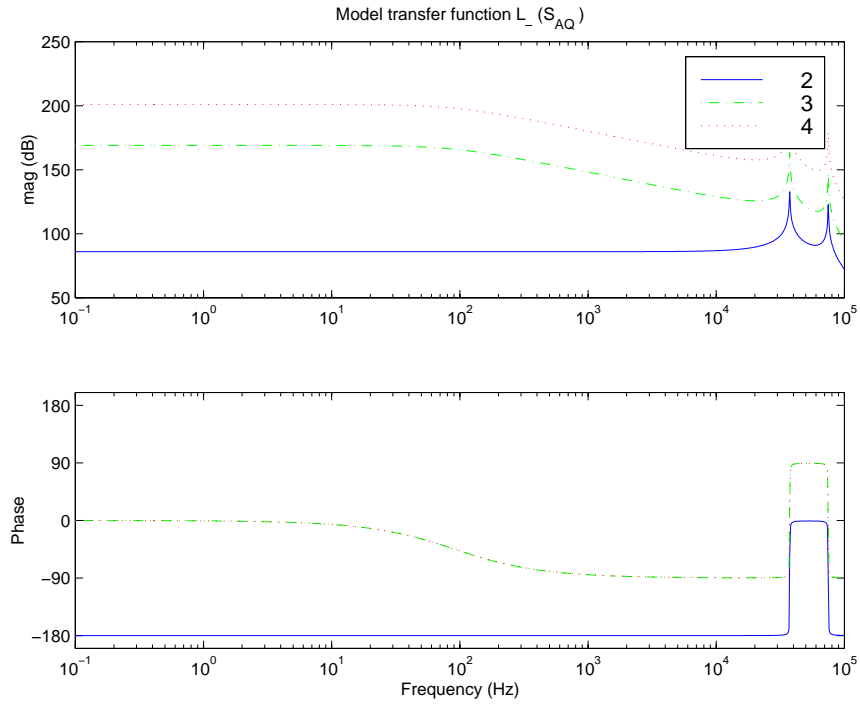


Figure 33: Differential mode transfer function ( $L_-$ ), tweaked model, all states.

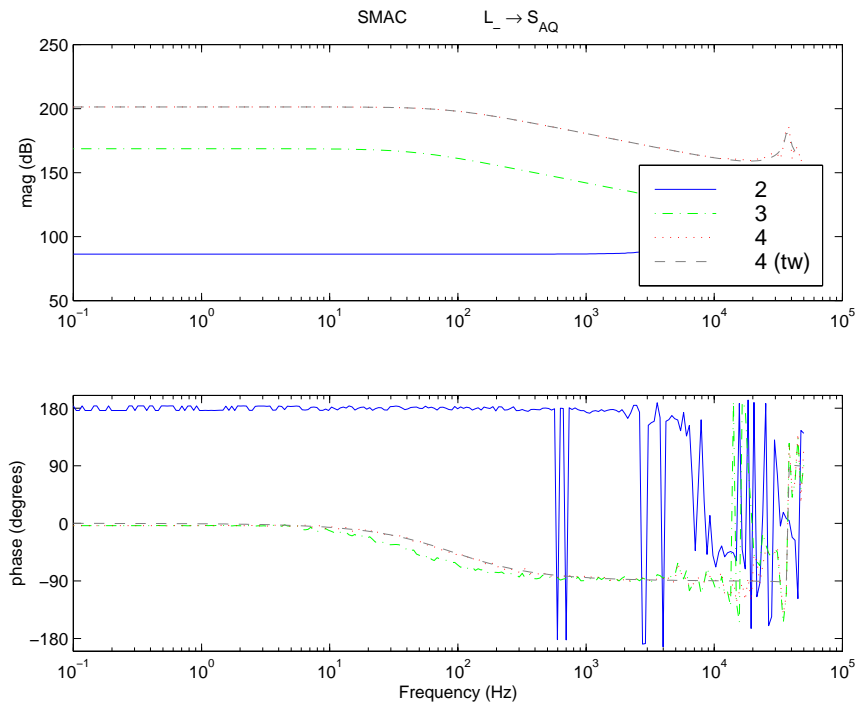


Figure 34: Michelson differential mode transfer function ( $L_-$ ), SMAC and Twiddle, all states.

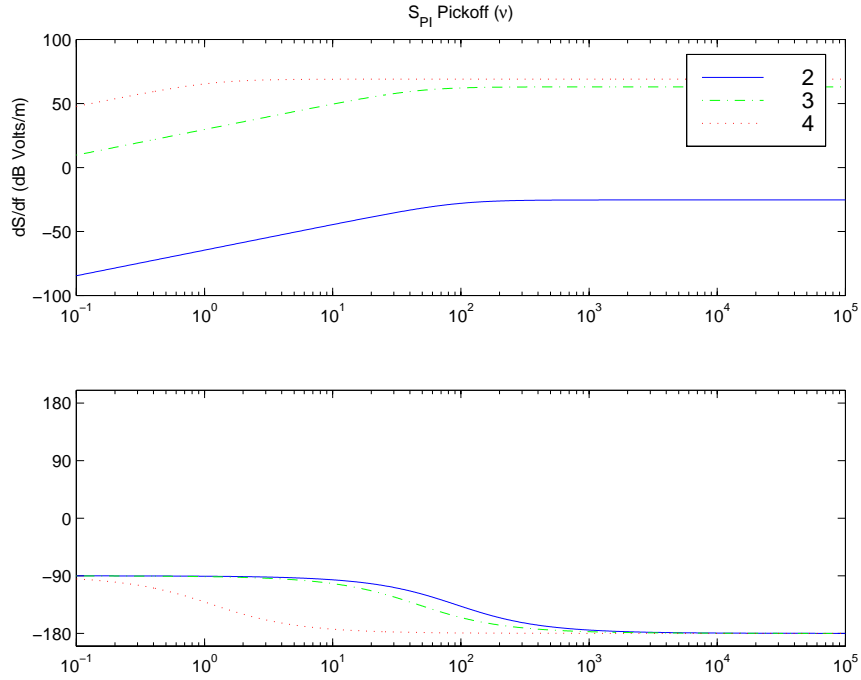


Figure 35: Source transfer function ( $\nu$ ), from Eq. 61 and Table 3 (reflectivity = 1), all states.

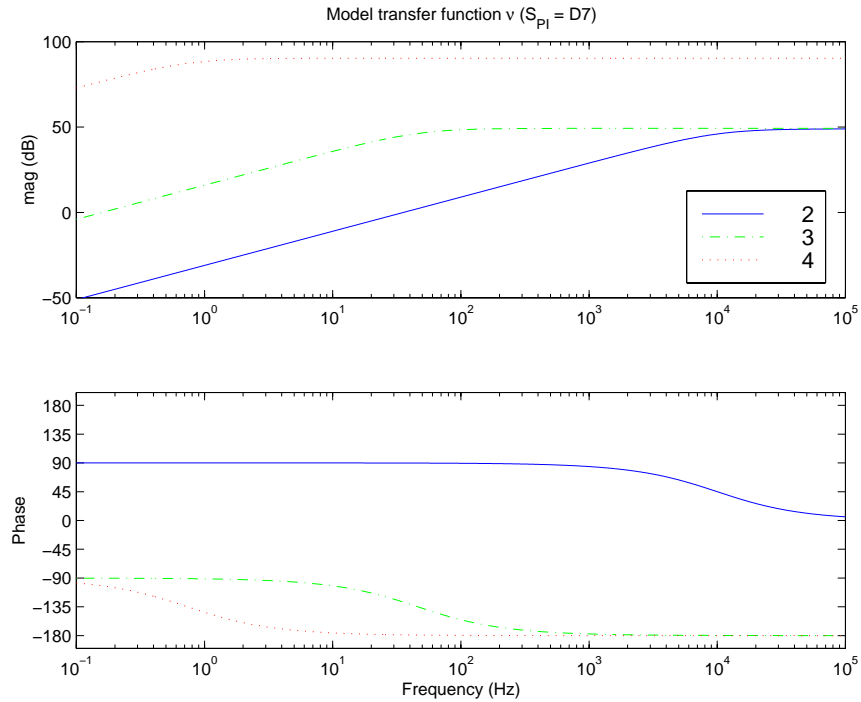


Figure 36: Source transfer function ( $\nu$ ), tweaked model, all states.

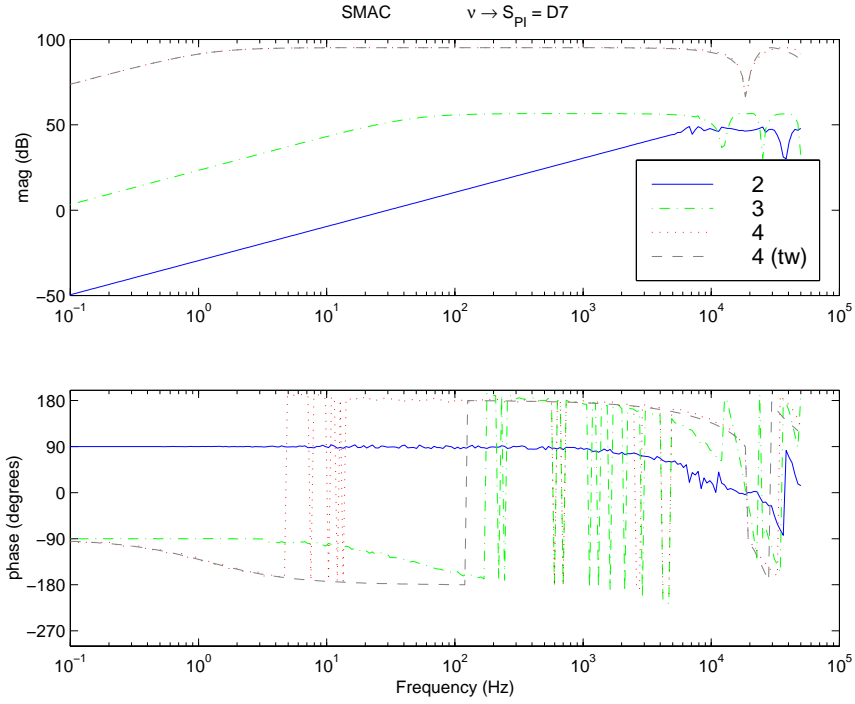


Figure 37: Source transfer function ( $\nu$ ) at D7, SMAC and Twiddle, all states.

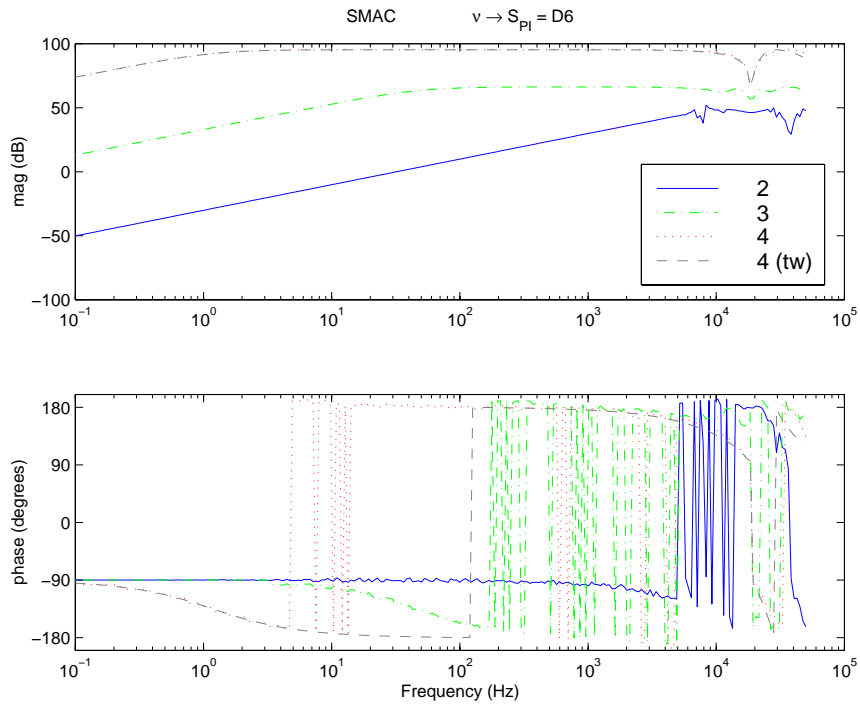


Figure 38: Source transfer function ( $\nu$ ) at D6, SMAC and Twiddle, all states.

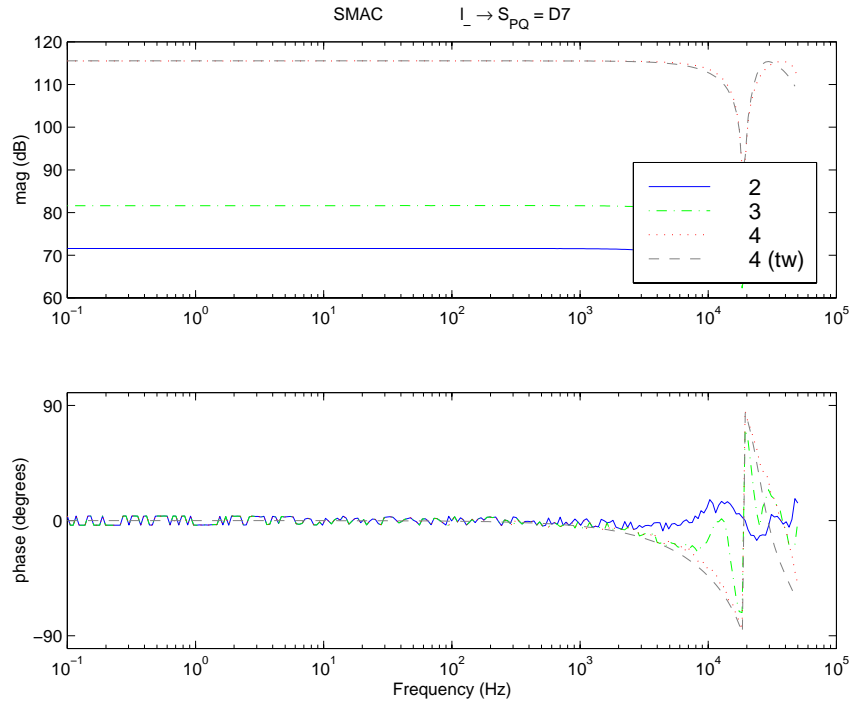


Figure 39: Michelson differential mode transfer function  $-(M_1 + M_2) + (M_3 + M_4)$  at D7, SMAC and Twiddle, all states.

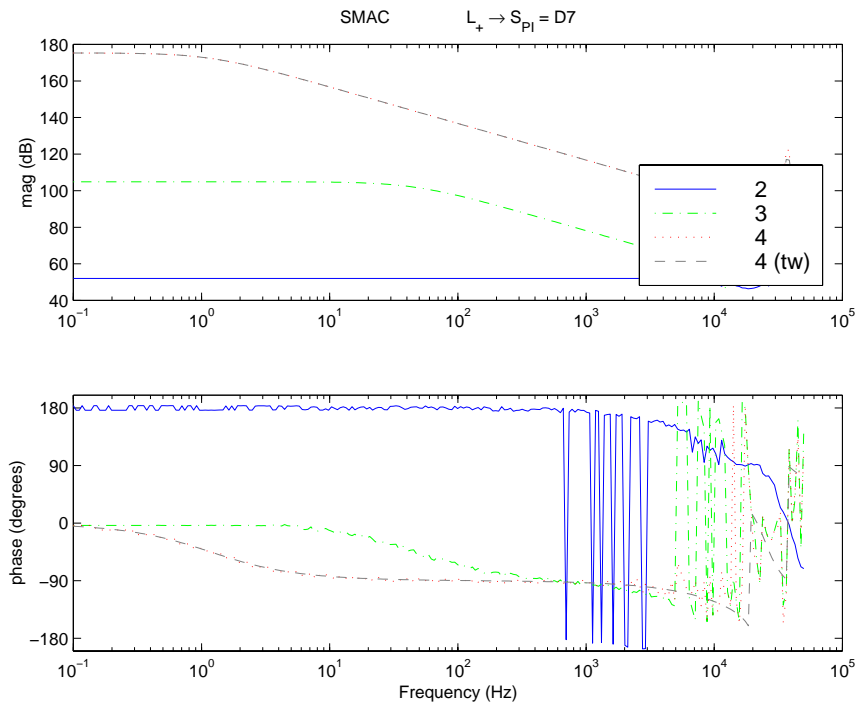


Figure 40: Common mode transfer function  $(L_+)$  at D7, SMAC and Twiddle, all states.

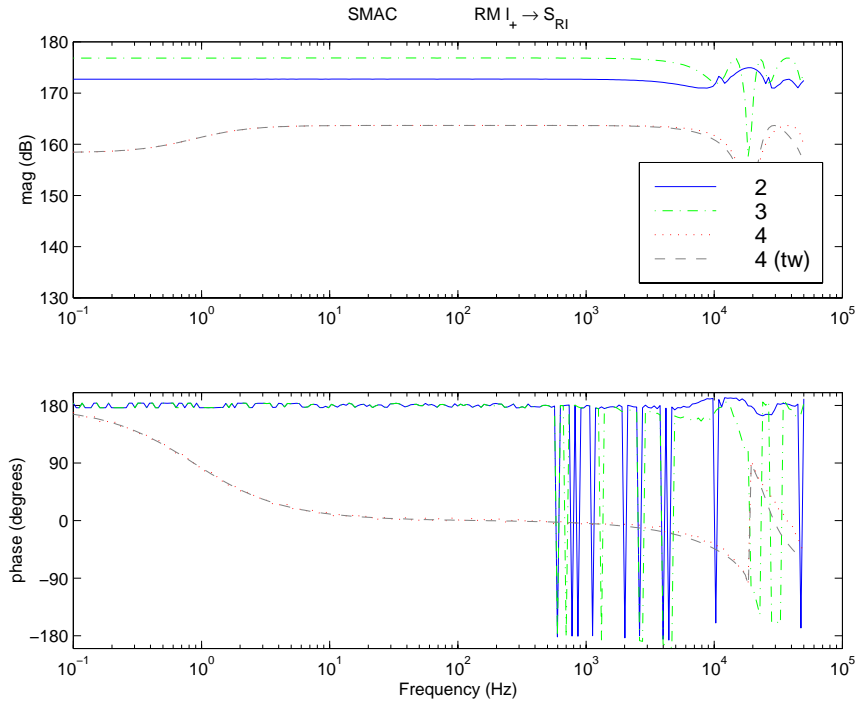


Figure 41: Michelson common mode transfer function (recycling mirror-driven  $l_+$ ), SMAC and Twiddle, all states.

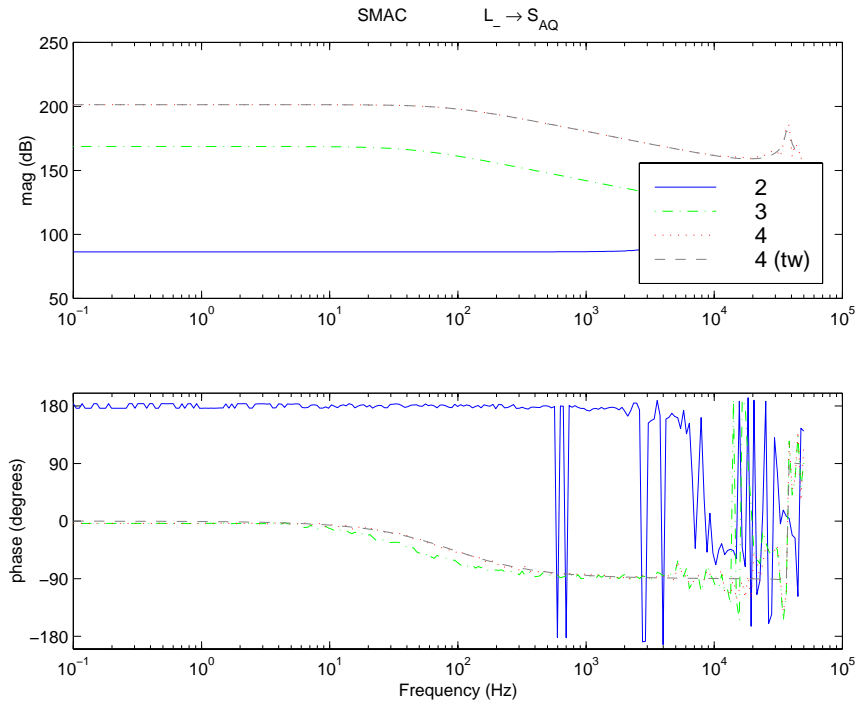


Figure 42: Michelson differential mode transfer function ( $L_-$ ), SMAC and Twiddle, all states.



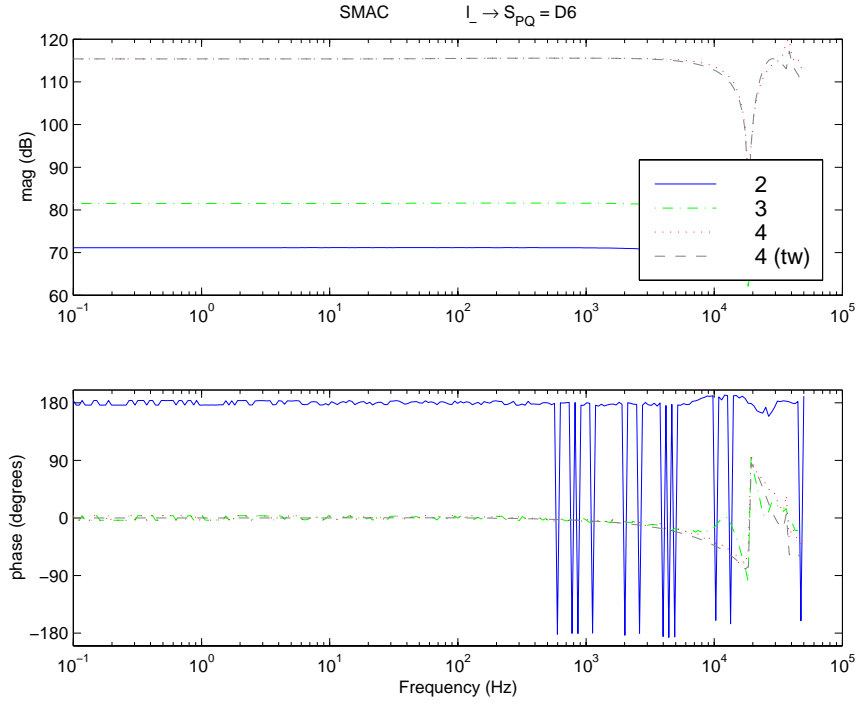


Figure 43: Michelson differential mode transfer function  $(-(M_1 + M_2) + (M_3 + M_4))$  at D6, SMAC and Twiddle, all states.

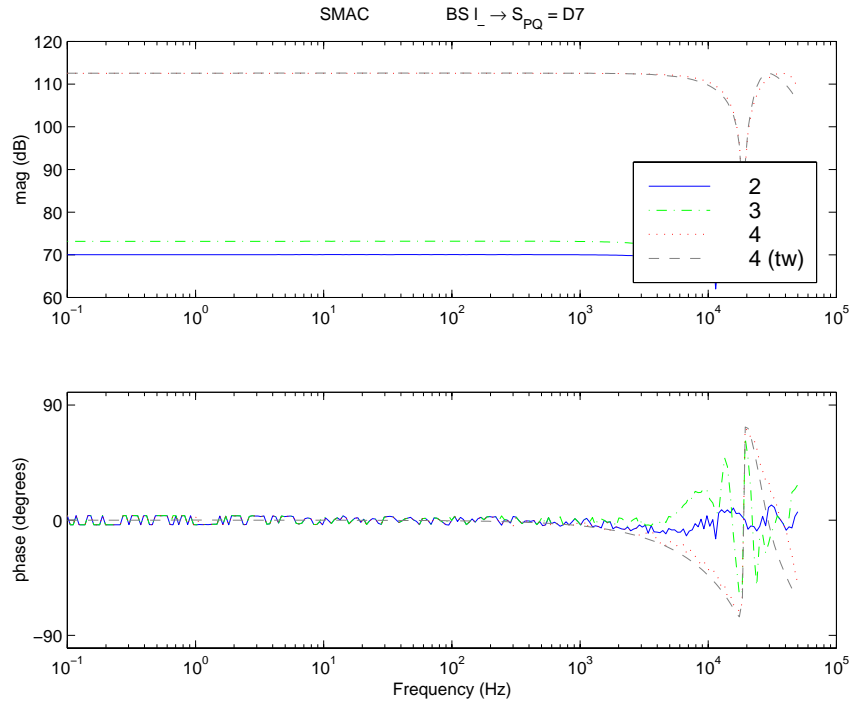


Figure 44: Michelson differential mode transfer function (beamsplitter-driven  $l_-$ ) at D7, SMAC and Twiddle, all states.

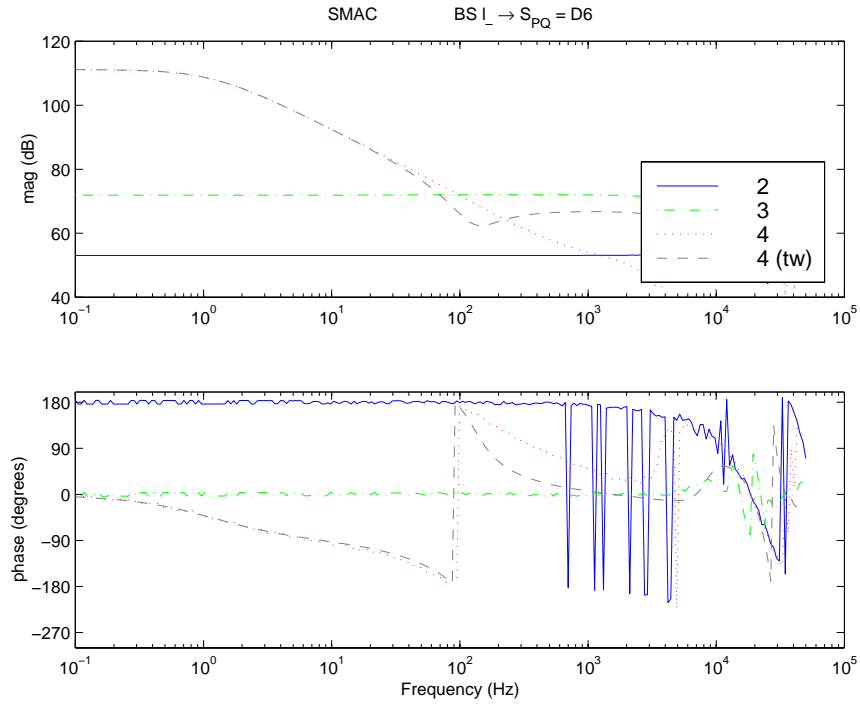


Figure 45: Michelson differential mode transfer function (beamsplitter-driven  $l_-$ ) at D6, SMAC and Twiddle, all states.

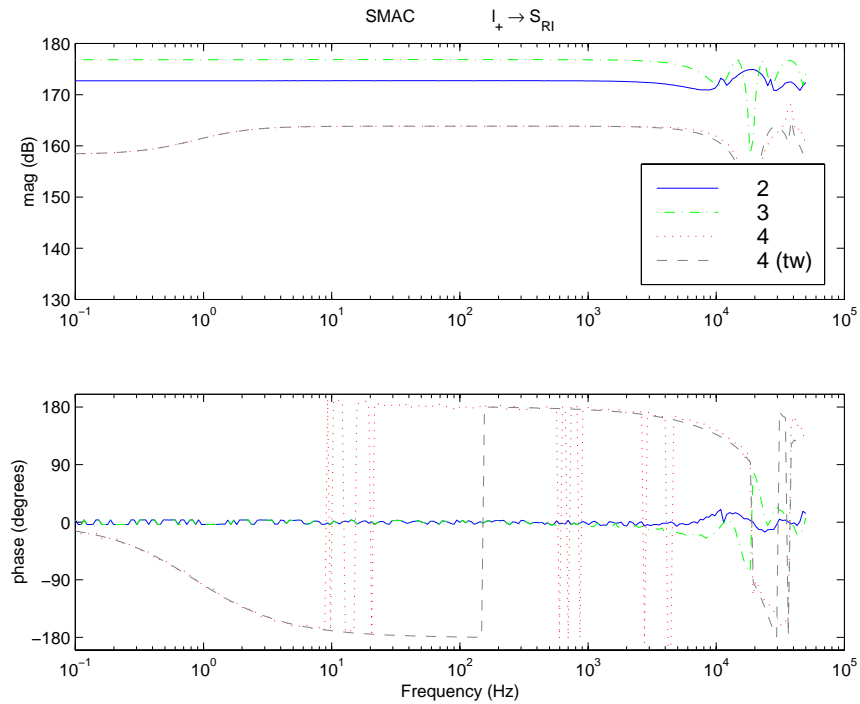


Figure 46: Michelson common mode transfer function  $(+(M_1 + M_2) + (M_3 + M_4))$ , SMAC and Twiddle, all states.

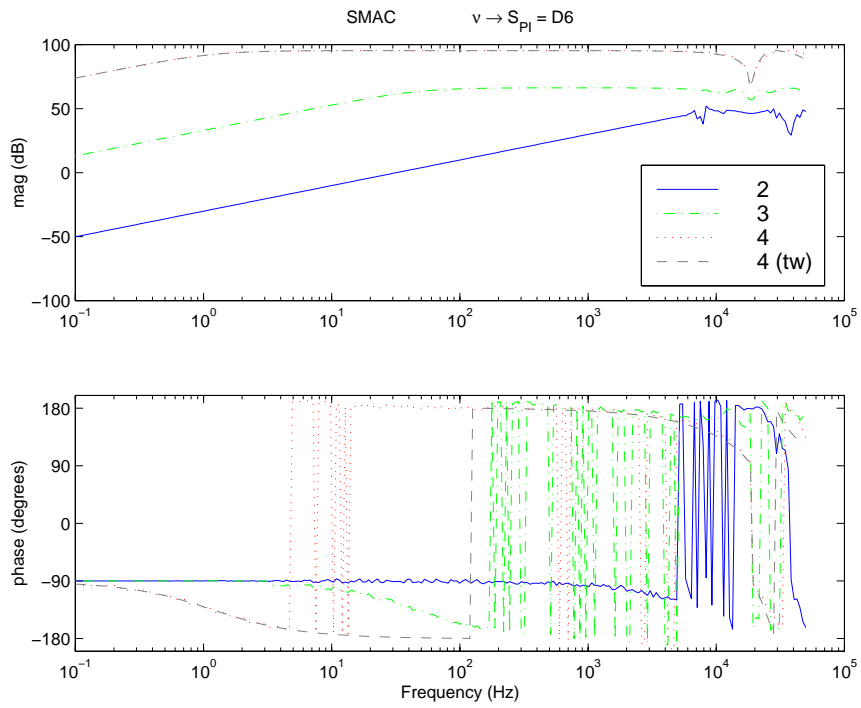


Figure 47: Source transfer function ( $\nu$ ) at D6, SMAC and Twiddle, all states.

This page not intentionally left blank

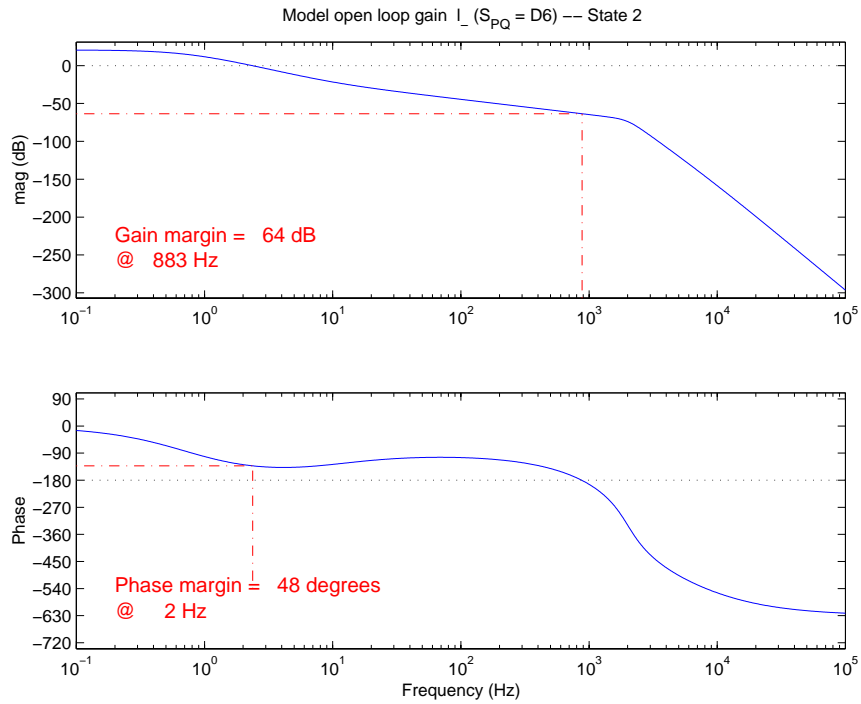


Figure 48: Michelson differential mode open loop gain ( $l_-$ ), from SMAC model times controller, State 2.

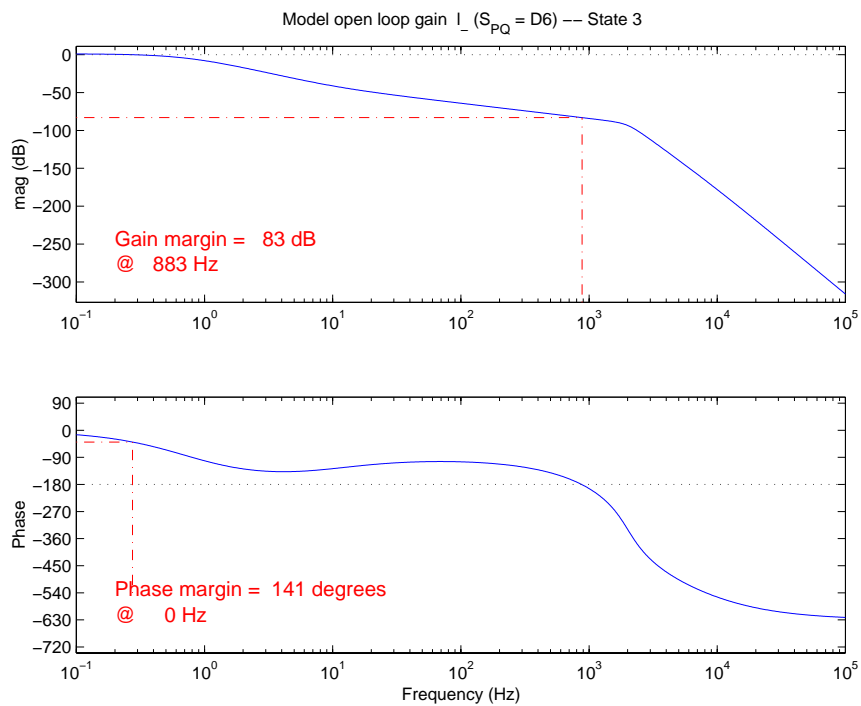


Figure 49: Michelson differential mode open loop gain ( $l_-$ ), from SMAC model times controller, State 3.

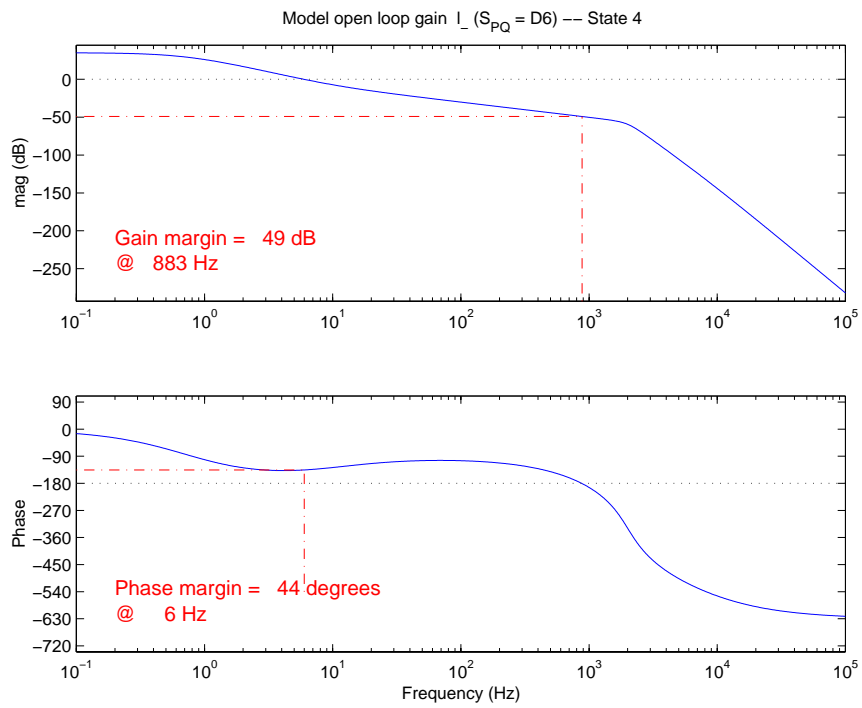


Figure 50: Michelson differential mode open loop gain ( $l_-$ ), from SMAC model times controller, State 4.

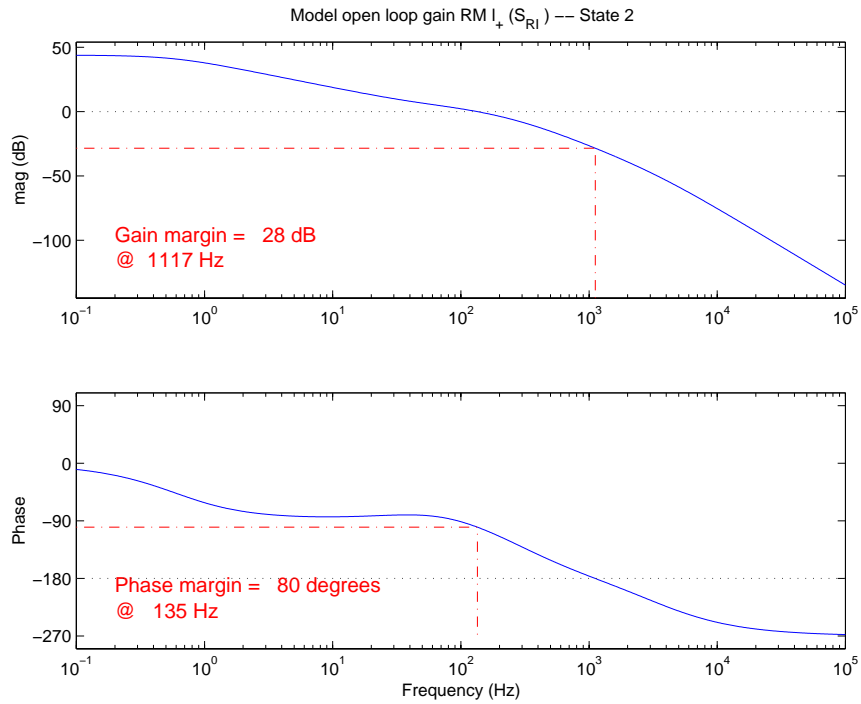


Figure 51: Michelson common mode open loop gain ( $l_+$ ), State 2, from SMAC model times controller, State 2.

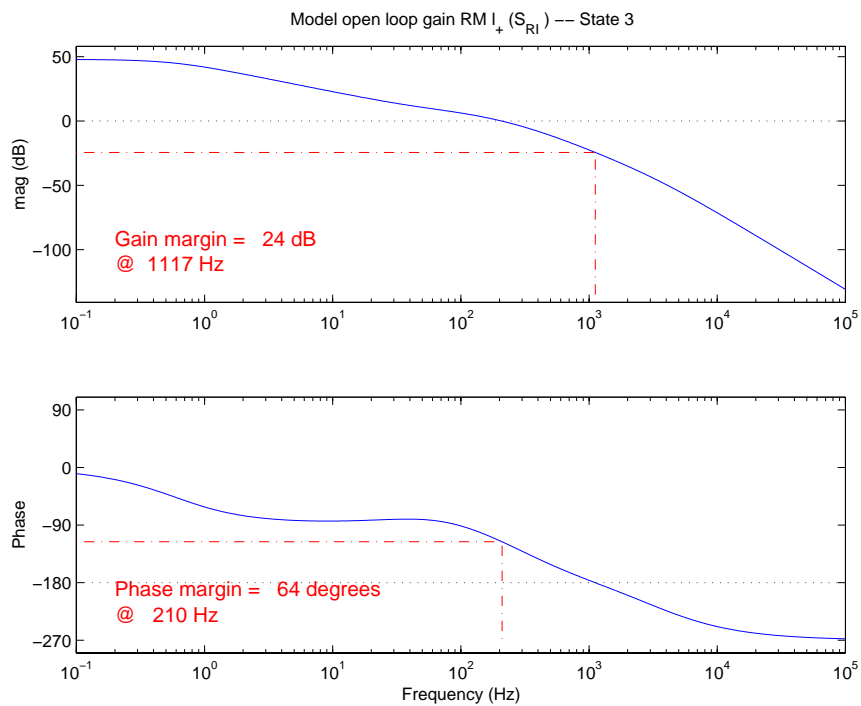


Figure 52: Michelson common mode open loop gain ( $l_+$ ), State 3, from SMAC model times controller, State 3.

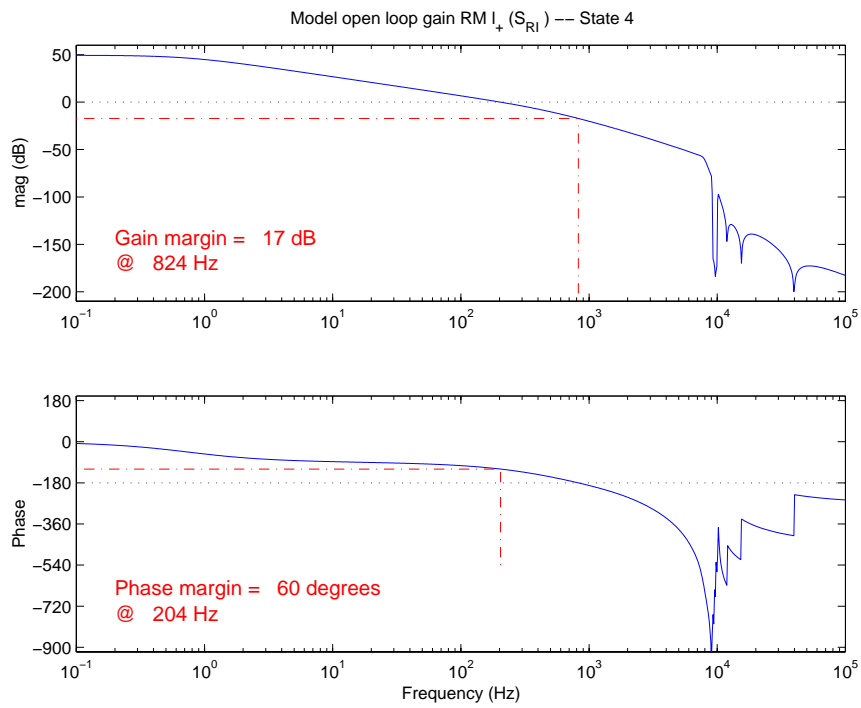


Figure 53: Michelson common mode open loop gain ( $l_+$ ), State 4, from SMAC model times controller, State 4.



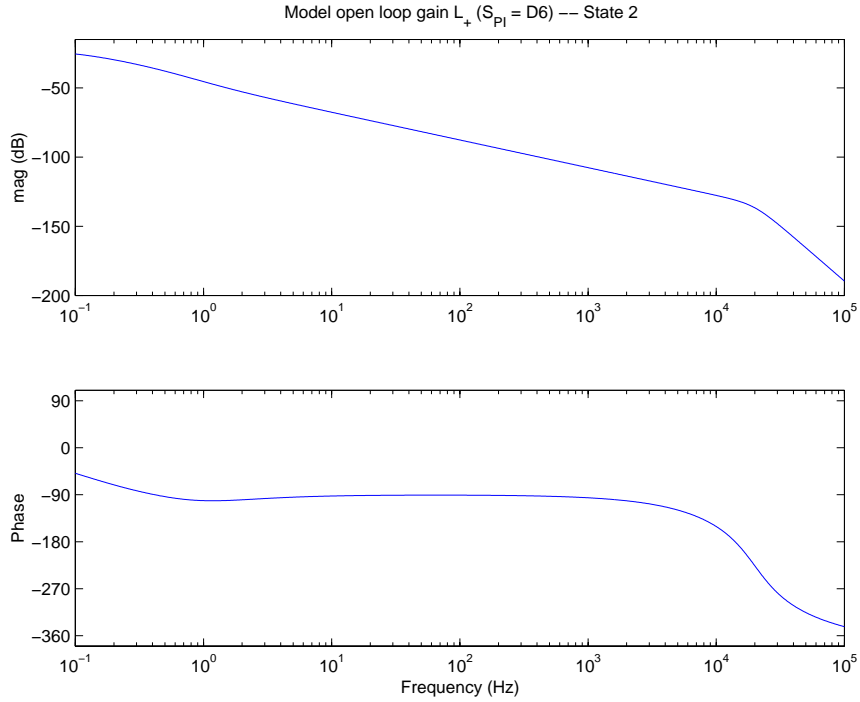


Figure 54: Common mode open loop gain ( $L_+$ ), from SMAC model times controller, State 2.

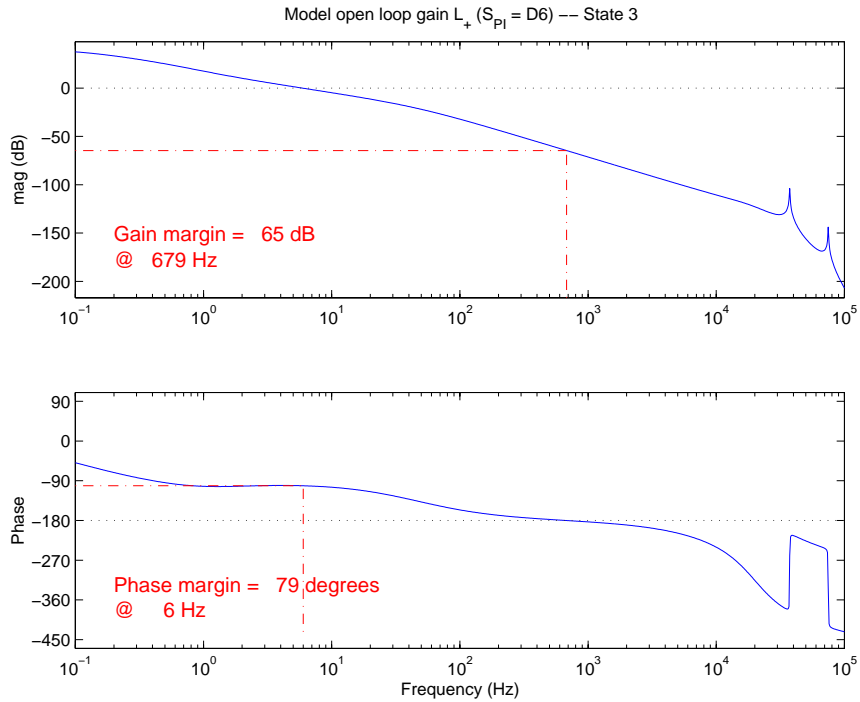


Figure 55: Common mode open loop gain ( $L_+$ ), from SMAC model times controller, State 3.

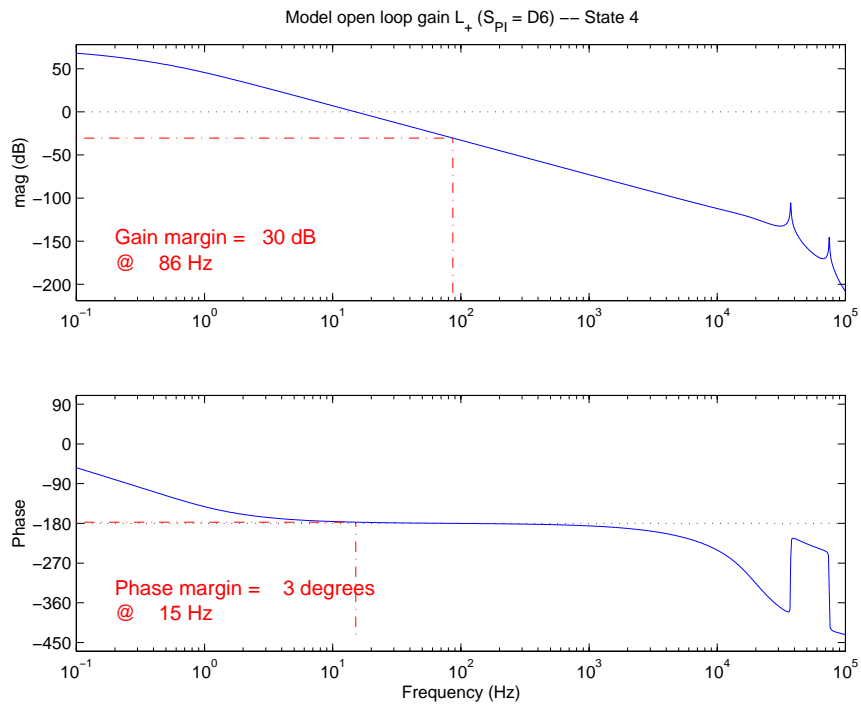


Figure 56: Common mode open loop gain ( $L_+$ ), from SMAC model times controller, State 4.

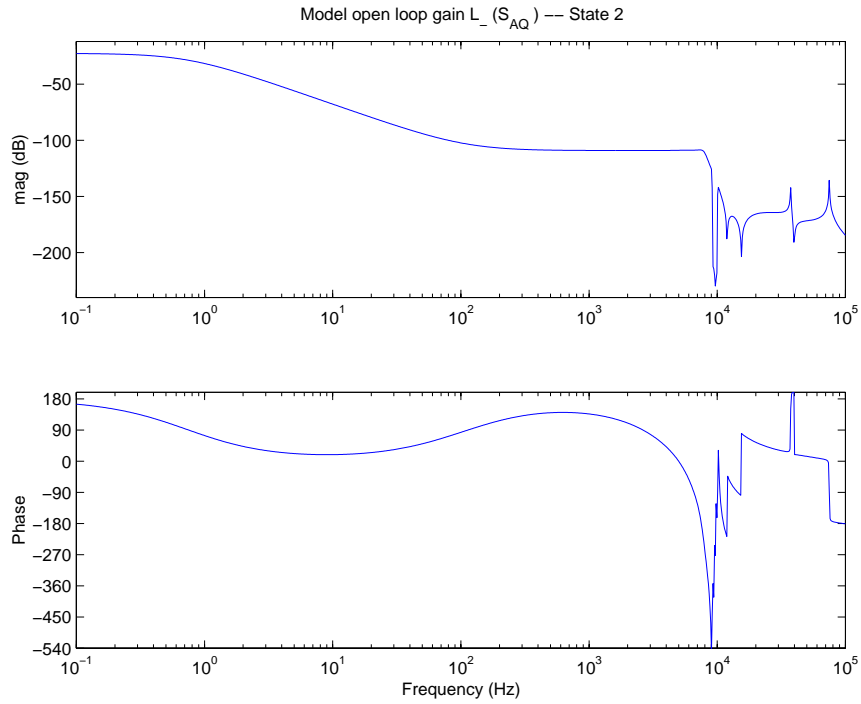


Figure 57: Differential mode open loop gain ( $L_-$ ), from SMAC model times controller, State 2.

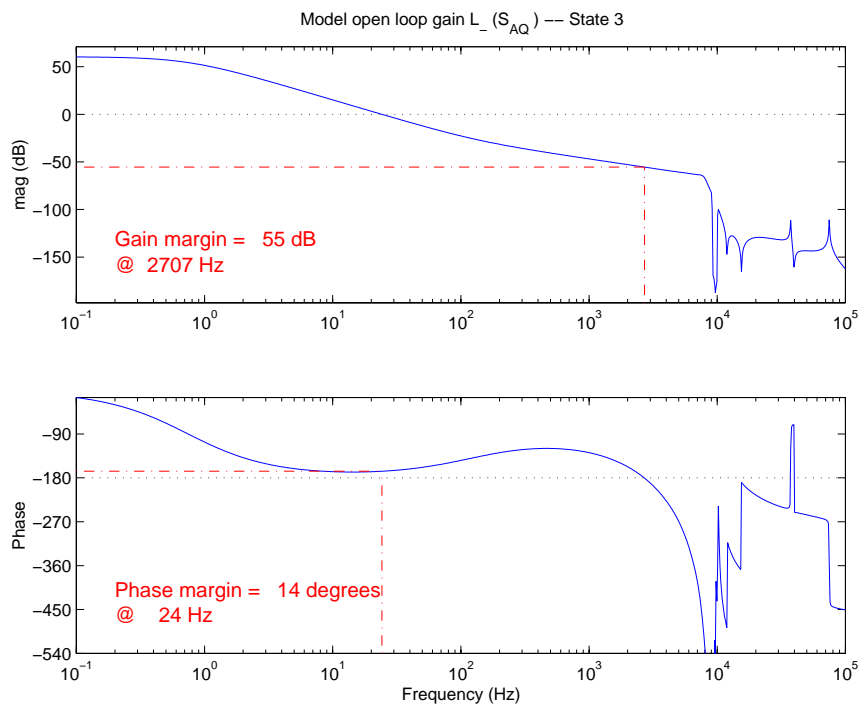


Figure 58: Differential mode open loop gain ( $L_-$ ), from SMAC model times controller, State 3.

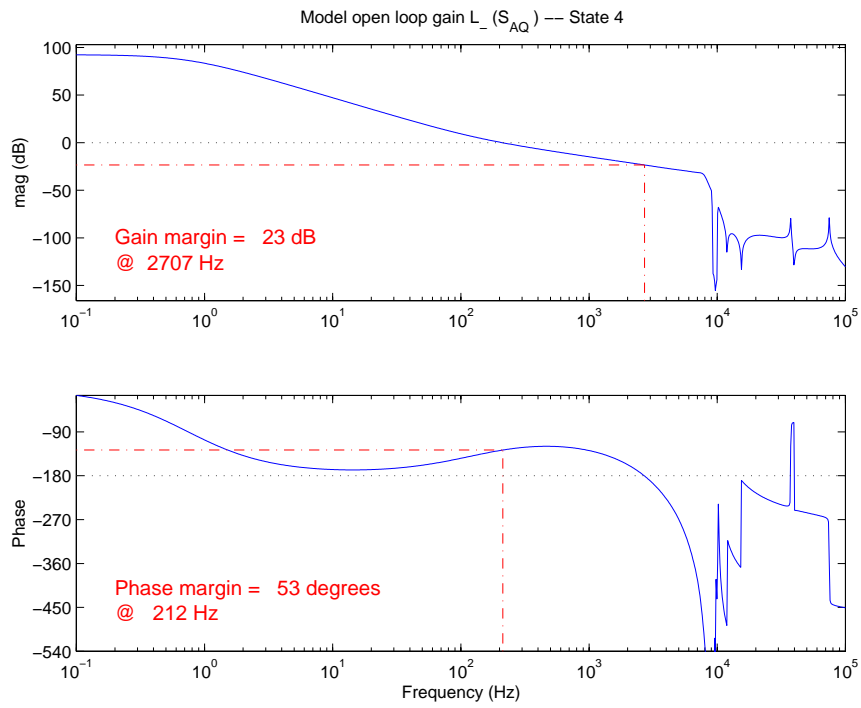


Figure 59: Differential mode open loop gain ( $L_-$ ), from SMAC model times controller, State 4.

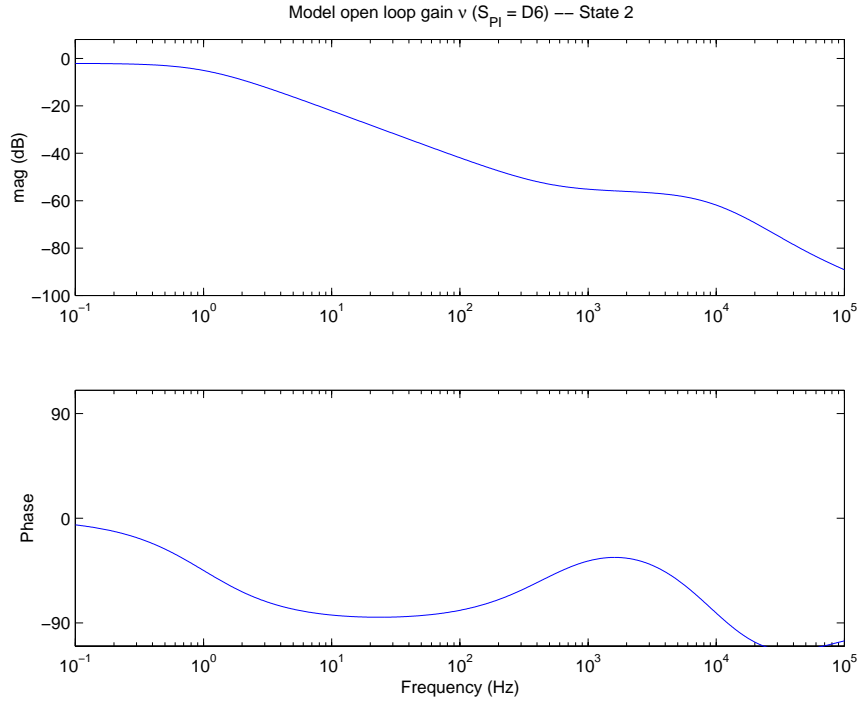


Figure 60: Common mode frequency open loop gain ( $\nu$ ), from SMAC model times controller, State 2.

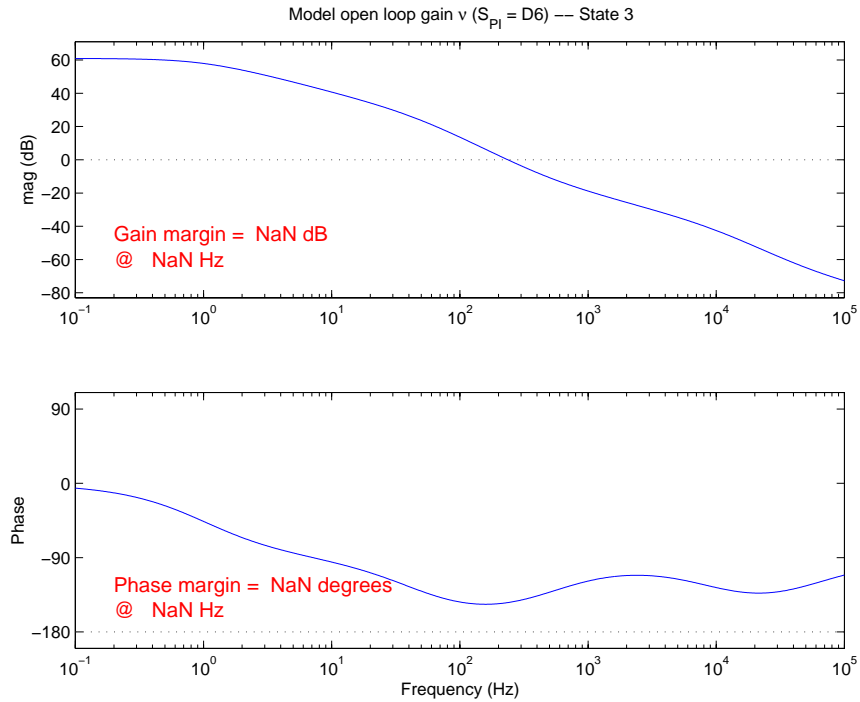


Figure 61: Common mode frequency open loop gain ( $\nu$ ), from SMAC model times controller, State 3.

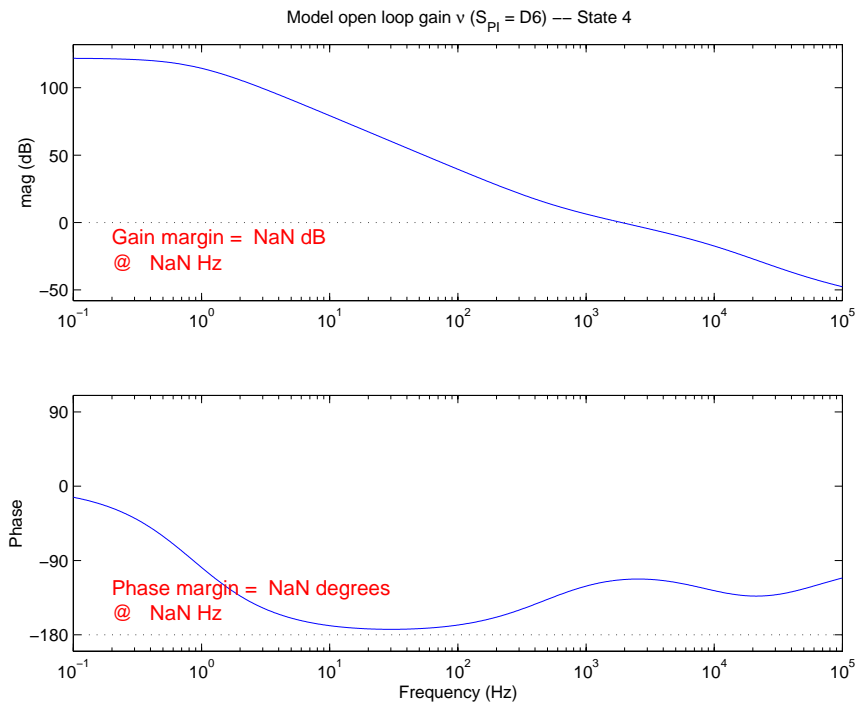


Figure 62: Common mode frequency open loop gain ( $\nu$ ), from SMAC model times controller, State 4.

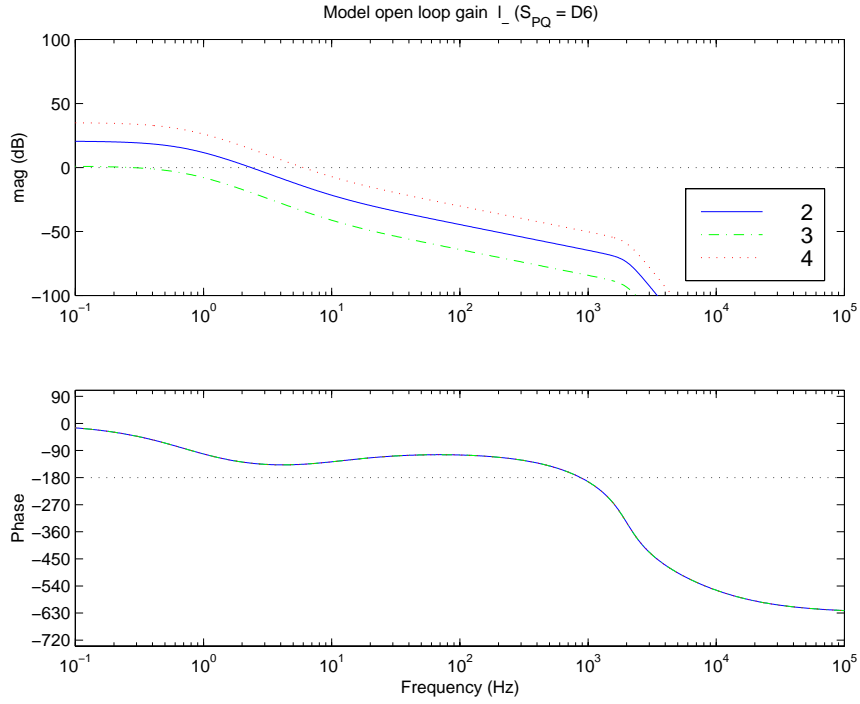


Figure 63: Michelson differential mode open loop gain ( $l_-$ ), all states.

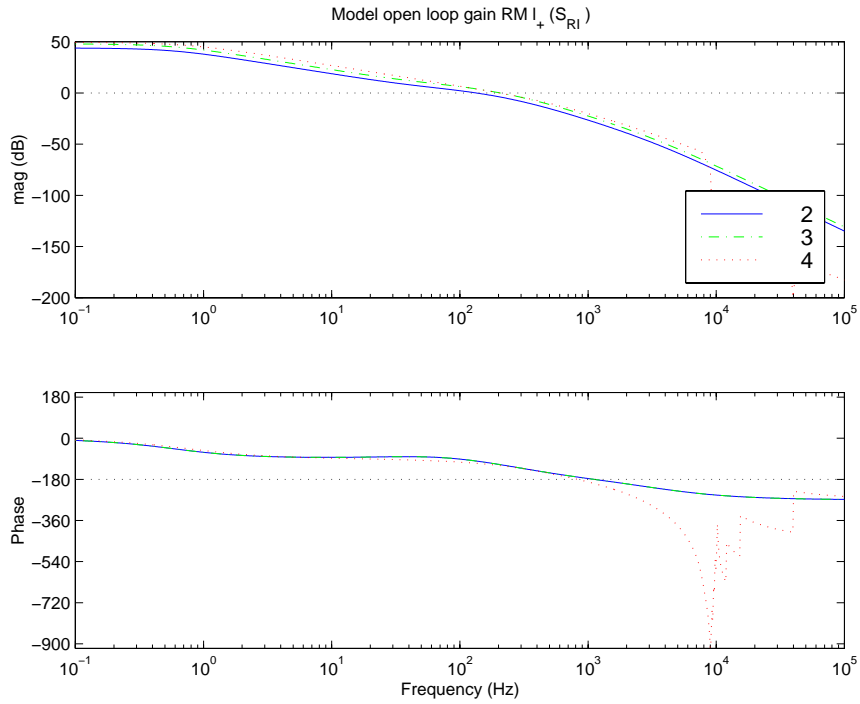


Figure 64: Michelson differential mode open loop gain ( $l_+$ ), all states.

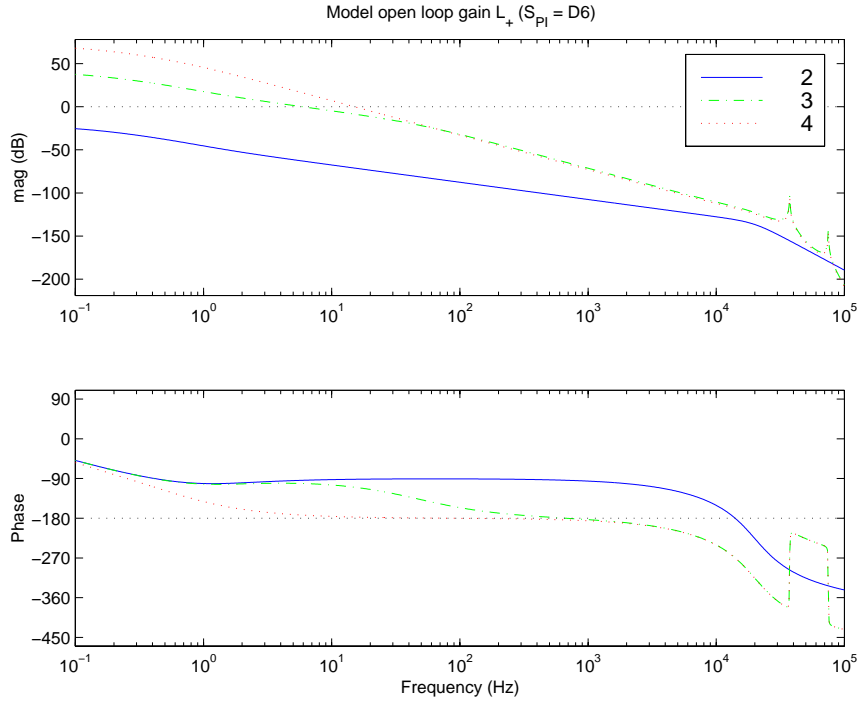


Figure 65: Common mode open loop gain ( $L_+$ ), all states.

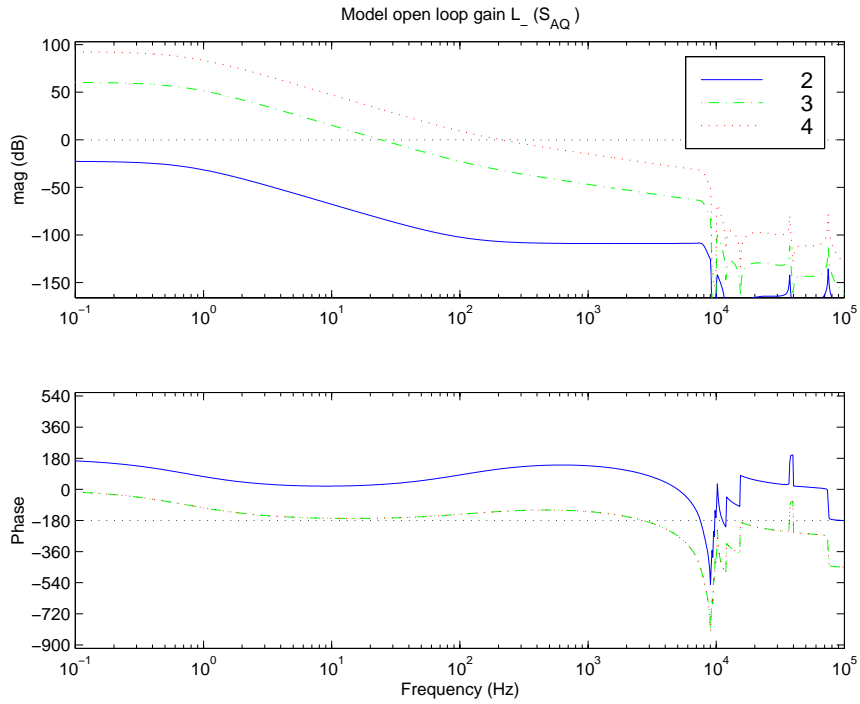


Figure 66: Differential mode open loop gain ( $L_-$ ), all states.



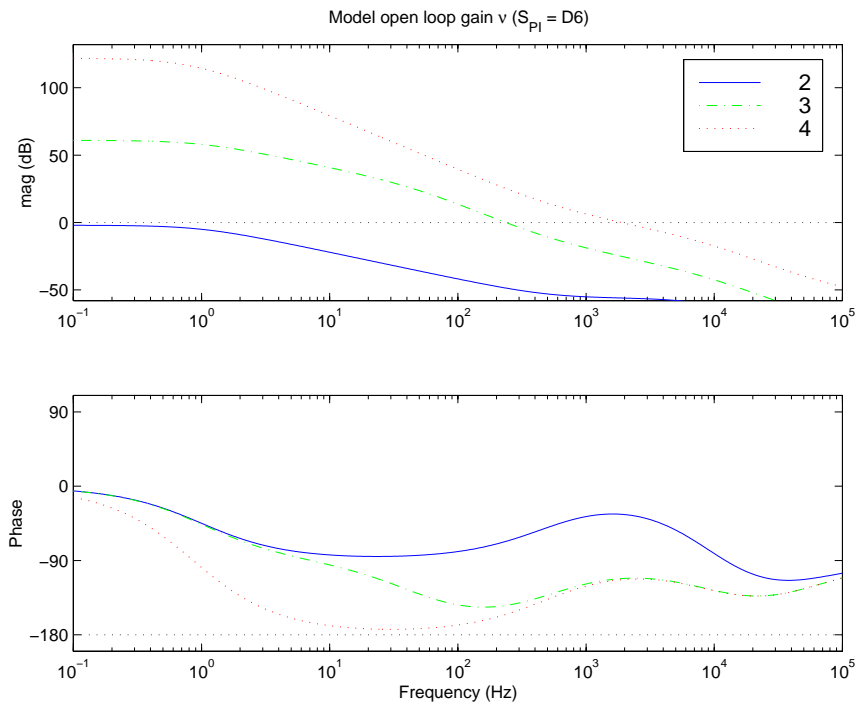


Figure 67: Common mode open loop gain ( $f$ ), all states.

This page not intentionally left blank

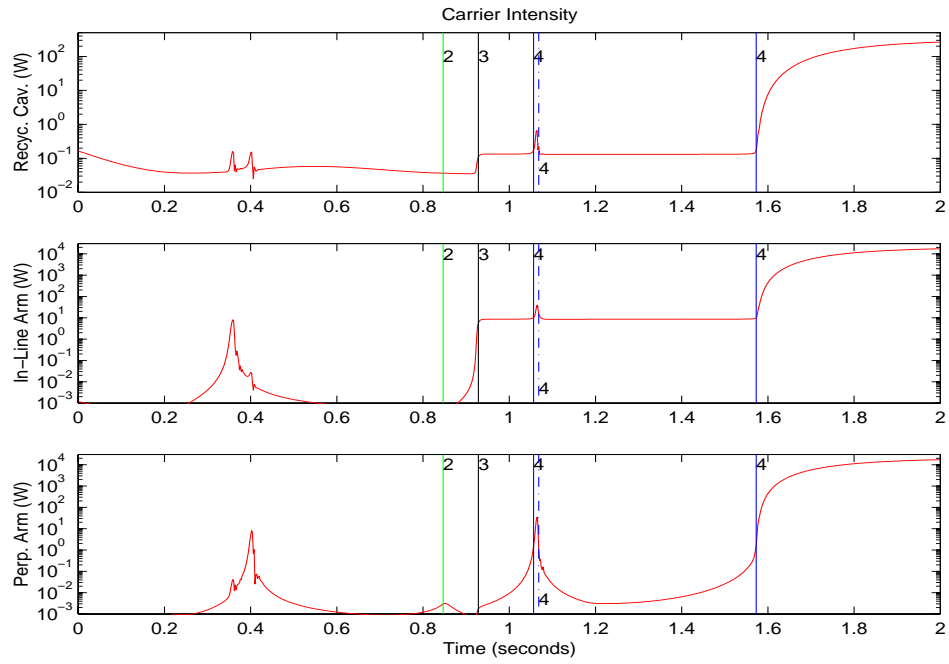


Figure 68: Lock acquisition sequence showing the carrier power in each cavity as it transitions through the acquisition states. The initial conditions for this simulation were chosen to accentuate the transitions between states.

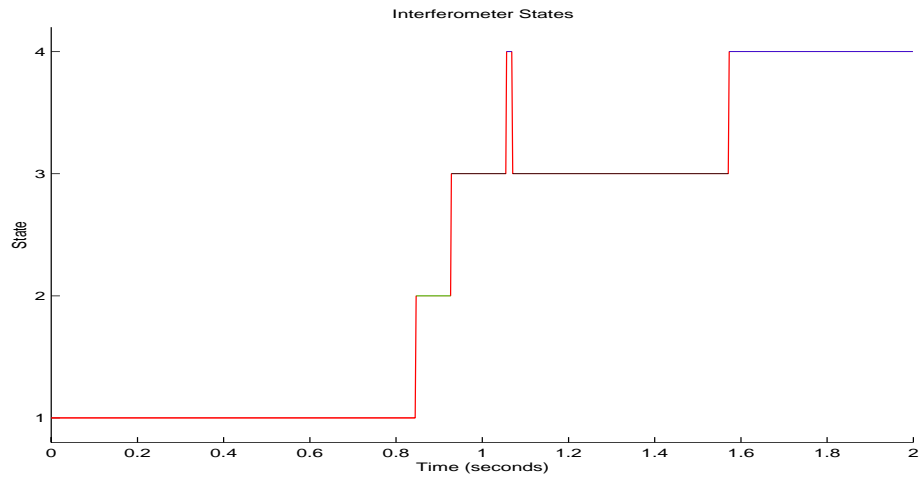


Figure 69: State indicator.

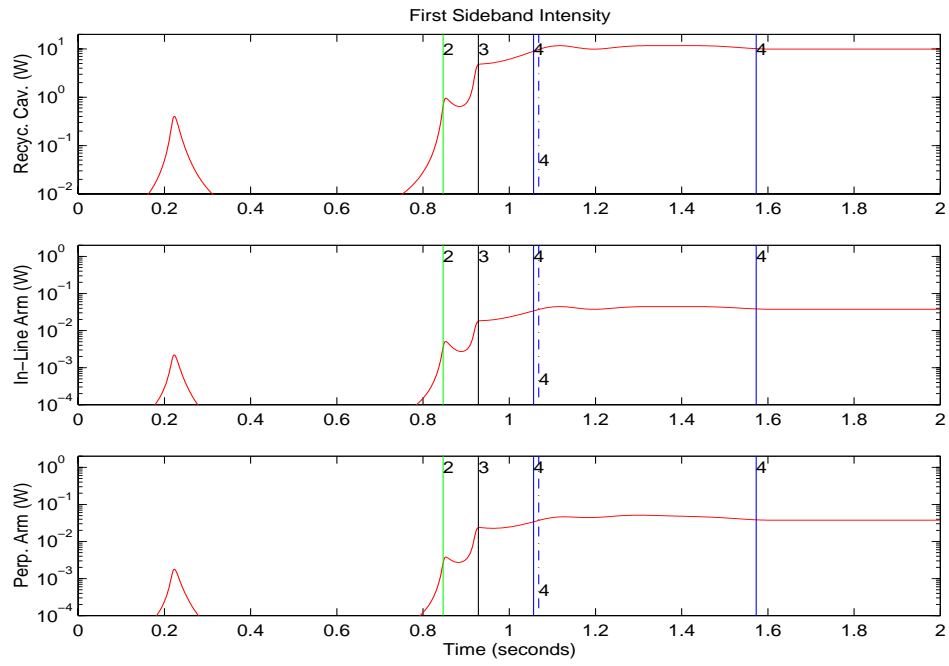


Figure 70: Lock acquisition sequence showing the sideband power in each cavity.

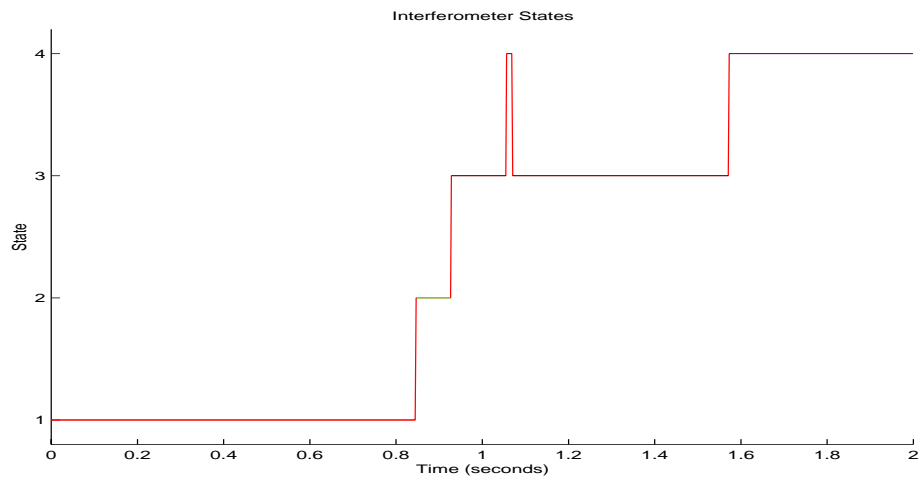


Figure 71: State indicator.

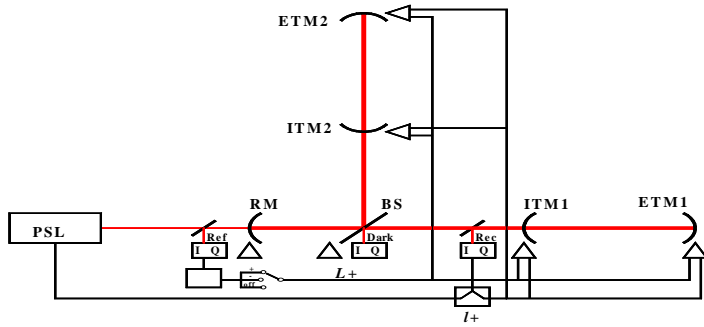


Figure 5: L1+L2 and I1+I2 servos in Acquisition Mode

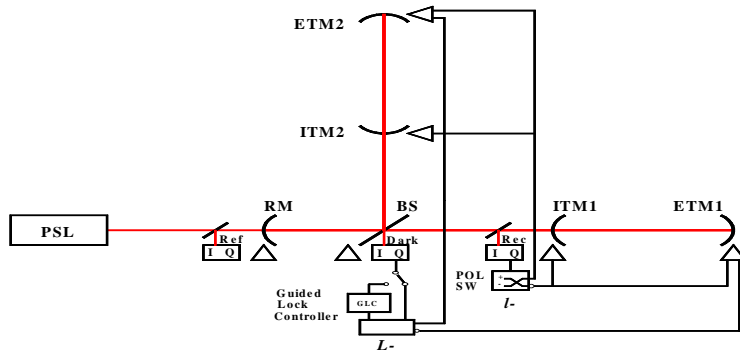


Figure 3: L1-L2 and I1-I2 servos in Acquisition Mode



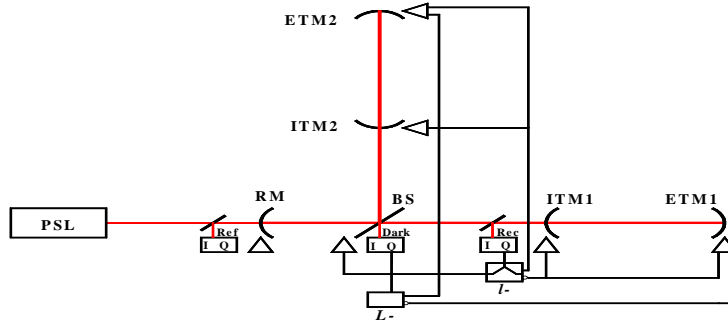


Figure 2:  $L1-L2$  and  $I1-I2$  servos in Detection Mode.  $L$ - crossover frequency ~ 1 to 2 Hz

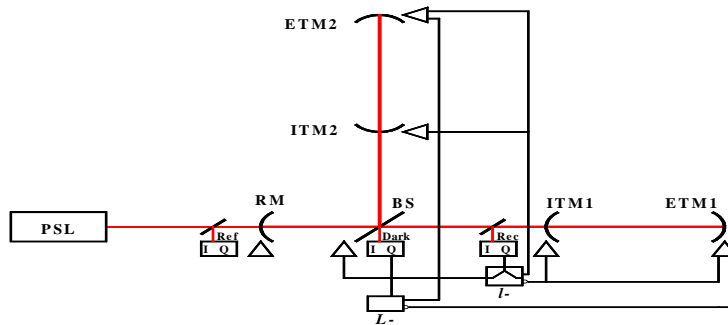


Figure 2:  $L1-L2$  and  $I1-I2$  servos in Detection Mode.  $L$ - crossover frequency ~ 1 to 2 Hz



## A How to Design Controllers

### A.1 SMAC manual

Read it. While it is often hard to find, there is useful information scattered like nuggets throughout. The original PDF files exist in `/home/ware/smac/man`, so, lacking an index, one can search these for keywords.

### A.2 LIGO parameters

The parameters I used are those given in Table 2, which I got from Nergis. The trick of course is dividing losses, transmissions, and reflectivities among the (real) mirrors representing LIGO interferometer elements, and the (fictive) pickoffs which are necessary to derive signals from SMAC, but which don't exist in the real interferometer. I've mostly done this correctly, as witness the correspondence between the idealized transfer functions and the SMAC transfer functions, but there is a difference in the State 2  $l_+$  poles and zeroes, for instance. Since it takes about a week of Ultra-30 CPU time to run a single DOF transfer function at the frequencies of interest, I never thought it was worthwhile to try to figure out how I misallocated the losses, etc.; rather, design another controller for the ideal model and use that in LIGO; use the tweaked controller so that SMAC works.

### A.3 Pickoffs

The SMAC D7 pickoff agrees with the derived equations, and is the pickoff that will be used in LIGO; Lisa started out using D6, and that's what I've continued using. As you can see from the transfer functions, there isn't much difference.

### A.4 Transfer functions

The transfer functions from the long simulations are found in `/home/ware/smac/tf`. Each state has a corresponding `TFstateN.mat` which contains all the variables of interest from the relevant DOFs to all relevant sensors. `TFtw4.mat` contains the results from the Twiddle comparison. By loading any `TFstateN` into Matlab and typing `rerun_menu`, one can review the results of the simulation as if it were just run. Using `TFstate4` and `TFtw4`, one can compare State 4 to the Twiddle simulation using `TFcheck`. `Tfallstates.mat` contains all the above, with each DOF/sensor combination appended with an `_N` corresponding to State N, suitable for comparison.

The Matlab program `tfstates.m` uses `Tfallstates.mat` and `TFtw4.mat` to do a comparison of states and sensor for various DOFs. By looking at the code, one can figure out what the Matlab variables are that correspond to the sensor/DOF combination; this is somewhat documented in the SMAC manual, but the variables are inconsistently named and guaranteed to cause error. One can also look at `/home/ware/smac/acqmodel/ryPlotSimL.m` and `ryPlotTFL.m` to see how these programs plot their results.

Not every possible transfer function has been included in this document, but they are all in these files, and so can be generated if you wish.

### A.5 Design tools

I have developed a set of largely undocumented design tools which take the poles, zeros, and gains derived from the SMAC transfer function simulations and multiply them by the current set of SMAC

controllers to obtain a system open loop gain and plot the resulting Bode plot so the designer can observe the results. These are located in the `/home/ware/matlab/` directory, along with other useful programs I've written or stolen. I recommend using my `startup.m` program, as it initializes several global variables, and places figures in logical places on your screen.

The model of the plant, derived from Nergis' work and tweaked to match the SMAC transfer function simulations is in `ideal_plant_common.m`. The model derived from the transfer function equations 61 is found in `perfect_plant_common.m`. `ideal_plant_common.m` is called by `ideal_plant.m` to plot the plant transfer functions, and by `ideal_olg.m` to plot the open loop gain of the system using the controller transfer functions. To compare the transfer functions in each state, `ideal_states.m` plots the plant transfer functions, and `olg_states.m` plots the open loop gain transfer functions in each state. A few comments: the `stats` global variable turns gain and phase margins on and off in the plots. When plotting multiple states, the programs turn `stats` off. `wrap` turns phase wrapping (between  $\pm 180$  degrees) on and off. `BS`, `RM`, `D6` determine what the configuration of the interferometer model will be. `dof` selects an individual degree of freedom – 0 turns all of them on.

Unfortunately, these tools are a bit persnickety, so to use them, you will have to be comfortable with the models and changing various things by hand. I've tried to make them easier for me to use, but never intended them for public access. They are fairly well commented, and I think fairly obvious about what they do.

## A.6 SMAC problems

I implemented a **Restart Computation** button in several of the menus in order to make it easier to change a controller, initial condition, or timing and restart without going through all the menus. Unfortunately, this button doesn't work from the final CONTINUE ANALYSIS (`rerun_menu.m`) menu; somehow the initial conditions get altered, and the simulation will not give the same results twice in a row. So you must go back to the INITIAL CONDITIONS (`run_sim.m`) menu (selectable from the CONTINUE ANALYSIS menu). I don't know why this is; I've spent quite a bit of time trying to fix it, but this is one of the more arcane parts of the SMAC code, and I lost patience with the stringy undocumented code. You don't have to change the initial conditions, and the **Restart Computation** button in the IC menu works, so just go back and restart from there after you've modified the controllers, or whatever.

For now, I've forced this button to take you back to the IC menu.

Should SMAC crash while displaying plots, or should you jump out of the SMAC menus, you can try to restart by typing `close all; rerun_menu` and redisplaying the plots. This is quite a useful trick.

## A.7 Pitfalls



## A.8 Typical analysis

My current working model resides in `/home/ware/smac/detlike/`. Begin a Matlab session in this directory (or a copy thereof). For a typical session, do the following at the Matlab prompts (SMALL CAPS is the name of the menu; **Boldface** is the button to press on that menu):

```
>> smac
```

SMAC MAIN MENU: **Recycled Configuration**

SIMULATION OPTIONS: **Choose Cavity Parameters** (default is a time simulation of a closed loop plant)

RECYCLED CAVITY PARAMETER: **Set Initial Conditions** (if the file `LIGO_params.mat` exists in this directory, it will be loaded by default – this is the current set of LIGO parameters)

INITIAL CONDITIONS: **Load Parameter Set**, select `IC_allstates.mat`, **Timing Menu**

TIMING PARAMETERS: set **Plotting Points** to 2000, set **Total Simulation Time** to 4.0, **Define Controllers**

CONTROLLER DEFINITION: **Load Controller Parameters**, load `ConWorkingSet.mat`, the current working controllers, **Pick Plotting Variables**

PLOTTING OPTIONS: **Start Computation**

After the simulation runs, you can choose different plot variables, turn state indicators on and off. I find the state indicators useful, unless the IFO is oscillating between states quickly, in which case the state indicators slow the plotting down considerably. The cavity overview plots give a quick indication of whether you've achieved lock or not, and if not, why not, and show a state overview indicator (a speedometer, if you like) which gives the same information as the state indicators in each plot. You can look at the displacements and combinations thereof to figure out what locked or didn't, and when. Unfortunately, the common-mode degrees of freedom are difficult to study, as the laser frequency variations are not incorporated, and you never get a flat-line lock as you do with the differential modes.

If you determine that you want to change a controller, you can do so, and run `ideal_olg` for that degree of freedom to see the result (I recommend using another Matlab session to do this so you don't mess up SMAC accidentally). If you like the results, you can go back to INITIAL CONDITIONS and **Restart Computation** which will incorporate the new controller when the Matlab code is recompiled.

Nothing to it.

## References

- [1] An, Yang, *et al.*, Optics Letters v.20 No. 9, p. 1068, May 1, 1995.
- [2] Gabriela Gonzalez's timetraces.m and velhist.m programs (`/home/ware/smac/LSC/MirrorVelocities`).
- [3] M. Regehr, thesis.
- [4] *et al.*, T970084
- [5] *et al.*, Preliminary Design Review (G 970192 III.4)
- [6] Nergis, LSC Detection Mode Controls Design, 2/23/98
- [7] Sievers, *et al.*, SMAC Manual, Fig. 25, pg. 45, 1/16/98
- [8] R. Abbott, T970115, Infrared Pre-stabilized Laser Electronics Design Requirements, pg. 14, Sec. 3.1.1.1.2, 9/25/97
- [9] Email from Jay Heefner, March 26, 1998.
- [10] D. Coyne, Test Mass Transmissibility, T970191, 2/8/98.
- [11] K. Blackburn, L970042, 1/27/97.
- [12] S. Kawamura, T970158.
- [13] Email from Peter Fritschel, March 31, 1998.